Least-Squares Fit For Points Measured Along Line-Profiles Formed From Line And Arc Segments

by

Samir Savaliya

A Thesis Presented in Partial Fulfillment
of the Requirements for the Degree
Master of Science

Approved January 2013 by the
Graduate Supervisory Committee:

Joseph Davidson, Chair
Jami Shah
Veronica Santos

ARIZONA STATE UNIVERSITY

May 2013

ABSTRACT

Tolerances on line profiles are used to control cross-sectional shapes of parts, such as turbine blades. A full life cycle for many mechanical devices depends (i) on a wise assignment of tolerances during design and (ii) on careful quality control of the manufacturing process to ensure adherence to the specified tolerances. This thesis describes a new method for quality control of a manufacturing process by improving the method used to convert measured points on a part to a geometric entity that can be compared directly with tolerance specifications. The focus of this paper is the development of a new computational method for obtaining the least-squares fit of a set of points that have been measured with a coordinate measurement machine along a line-profile. The pseudo-inverse of a rectangular matrix is used to convert the measured points to the least-squares fit of the profile. Numerical examples are included for convex and concave line-profiles, that are formed from line- and circular arc-segments.

DEDICATION

This research work is dedicated to my dear parents for their hardship in making my dreams possible and believing in my aspirations. I also dedicate this work to my wife for her never ending support and love. This is also dedicated to my caring brother and sister whose affection I always treasure.

ACKNOWLEDGEMENTS

My most sincere appreciation goes to my committee chair, Dr. Davidson, for his never-ending patience, guidance and support. Without his contribution this research work would not have been possible.

I would like to thank Dr. Jami Shah and Dr. Veronica Santos, for their valuable suggestions and time serving as part of my advisory committee.

I would like to thank Yifie He for his valuable advice on T-Map for line profiles. I would also like to thank to my colleagues Prabath Vemulapalli, Lupin Niranjan, Austin Pezzella and Ian Kubik for their respective help in my research. They were helpful sources of information and always willing to discuss my ideas. Also I would like to thanks my friends, Maryam Khorshidi, Prashant Mohan, Shyam Rao, Payam Haghighi, Mahmoud Dinar, Sumit Narsale, Valeriy Khaldarov, Zihan Zhang, Xiang Ke for their great time spent in Design Automation Lab.

I would like to thank former students Neelakantan Mani, Shrinath Balaji, Yadong Shen and Maneekandan Mohan for their research advices and helpful supports.

I wish to acknowledge the financial support for this work provided by the National Science Foundation Grant #CMMI-0969821.

TABLE OF CONTENT

PAGE

CHAPTER PAGES

CHAPTER PAGES

LIST OF TABLES

TABLE PAGE

LIST OF FIGURES

FIGURE PAGE

FIGURE PAGE

CHAPTER 1

INTRODUCTION

A statement made by Lord Kelvin regarding metrology describes the motivation for this thesis:

"When you can measure what you are speaking about and express it in numbers, you know something about it; and when you cannot measure it, when you cannot express it in numbers, your knowledge is of a meager and unsatisfactory kind. It may be the beginning of the knowledge, but you have scarcely in your thought advanced to the stage of a science."

In this thesis, inspection means measuring dimensions that determine geometric shape of a manufactured part for conformance to dimensional and geometric tolerance specifications on a drawing. A drawing of a part specifies relative location of nominal geometric features, such as planes, cylinders, profiles etc., dimensions and tolerance specifications and it also contains other information such as, desired material requirement, and it provides a medium of communication between all departments of a manufacturing industry, from design to metrology. Tolerance specifications on a feature determine limits for manufacturing variations that are permissible for a feature. Coordinate measurement machines (CMMs) are used to record the coordinates for a large number of points, a point-cloud, of one or more features on a part. Then conversion softwares are used to reduce the measured data to feature parameters, such as thickness of a plate, diameter of a cylinder and its location. This research

is concerned about the development of a method to convert measured data in coordinate form on a line profile, made of line and arc segments, to parameters that represent a manufactured profile with respect to nominal feature.

1.1. Background

Geometric imperfections exist in every manufacturing process that is used to produce a mechanical product or part. Since there is always finite error in a manufactured part, a tradeoff is necessary between acceptable quality part and available manufacturing facility. Tolerance is defined as acceptable limit of dimensional variation allowed on a feature of the part. Application of tolerances on a part can make it interchangeable in an assembly so that any one chosen at random from a batch of these parts will fit successfully. Tolerances determined in the design stage influence the product life as well as its manufacturing process. However, a part with tighter tolerances requires better precision manufacturing processes and more deliberate measurement processes that cause higher production time and cost.

As per conventional practice, a dimensional tolerance means limiting the range of a dimension, such as the range in diameter of a cylinder. However, due to requirement of more complex parts, geometric variations were acknowledged and new geometric tolerance scheme introduced to control feature's variations based on part's functionality. Guidelines for specifying geometric dimensions and tolerances are documented in GD&T standards. Two standards popular in industries are the ASME Y14.5M standard [1] and the ISO standard. The ISO standards provide GD&T guidelines in several volumes as shown in Table 1.1.

Table 1.1. ISO standards related to GD&T specifications

ISO 128	Technical Drawings
ISO 1101	Geometrical Product Specifications (GPS) - Geometrical tolerancing -- Tolerances of form, orientation, location and run-out
ISO 1660	Technical drawings -- Dimensioning and tolerancing of profiles
ISO 2692	Geometrical product specifications (GPS) – Geometrical tolerancing -- Maximum material requirement (MMR), least material requirement (LMR) and reciprocity requirement (RPR)
ISO 2768-1	General tolerances – Part 1: Tolerances for linear and angular dimensions without individual tolerance indications
ISO 2768-2	General tolerances – Part 2: Geometrical tolerances for features without individual tolerance indications
ISO 5458	Geometrical Product Specifications (GPS) – Geometrical tolerancing -- Positional tolerancing
ISO 5459	Technical drawings -- Geometrical tolerancing -- Datums and datum-systems for geometrical tolerances
ISO 5460	Technical drawings -- Geometrical tolerancing -- Tolerancing of form, orientation, location and run-out -- Verification principles and methods -- Guidelines

1.2. Dimensional Metrology

The objective of dimensional metrology is to make measurement on the features of a manufactured part and to reduce the data to a form that presents an assessment of whether or not all the features are within tolerance zones described in the drawing. Conventional inspection methods are made using hard inspection gauges and simple non-automated measuring instruments such as a vernier caliper, micrometer etc. Though the inspection time for gauges is less, each is expensive and measures only the dimension for which it is designed. Moreover, since a gauge only provides a “Go-No Go” result, trends in a manufacturing process cannot be learned. A simple non-automated measuring instrument provides measurement value over large range of dimensions; but cannot measure complex features such as turbine blades. Non-conventional measuring instrument

like Coordinate Measuring Machine (CMM) provides precise measurement of complex of geometries that are difficult to measure by conventional instruments.

A typical CMM machine is a versatile measuring device, which assesses and records the coordinates of the measuring probe as it is brought against any type of feature of a part mounted within the machine working space (Figure 1.1). Higher accuracy than the conventional measuring instruments can be achieved by proper calibration and inspection setting. In addition, the automated inspection process on CMM provides consistent measurements and reduces human errors. The fundamental difference between CMM and conventional measuring instruments is that the CMM measures sets of coordinates of a large number of points on the part to provide a 'point cloud'.

There are two methods to confirm the acceptance of a part: soft-gauging and regression. Soft-gauging or functional gauging is to just check whether all the

Figure 1.1. Typical types of CMM machines: Portable CMM (left) and gantry type (right)

points in the cloud are within the specified tolerance zone or not. Like the hard inspection gauges, this method is computationally fast and gives "Go-No Go" decisions without determining feature parameters' values such as, size, location and orientation of the feature. It is mostly used when parameterization of the part or feature is difficult, such as turbine blades. Another method, regression, is to reduce the amount of the data points to a small number (usually seven or less) of feature parameters (i.e. three locations, three orientations and a size) that identify the nominal location, orientation, and size of a feature of the manufacture part. For example, points measured on a cylindrical surface can be reduced to the diameter of a maximum inscribed cylinder. Now the question is which one is better, soft-gauging or regression? For just an inspection point of view the soft-gauges are used. But for a broader perspective, when one wants to follow the trend in the manufacturing process, the method of data reduction is useful. The trend in the manufacturing process helps to recognize process parameters that are causing manufacturing variations. For example, consistently bigger sizes of drilled holes may be a sign of tool wear. However, Regression methods require considerable amount of computation to obtain the seven or less feature parameters that can be used to assess a feature. Moreover, parameters' values can be quite different for different methods (e.g. least squares, maximum inscribed, minimum zone etc.) of converting the cloud of measured points [3].

1.3. Geometric Dimensioning & Tolerancing

The objective of GD&T is to control geometric variations of features so that a part assembles appropriately and functions as per design intention. The

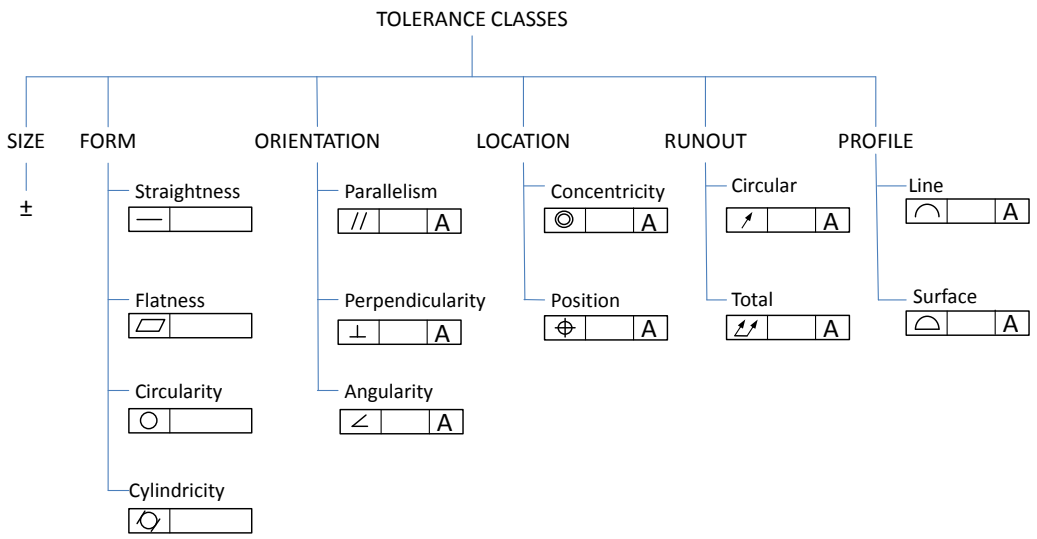

Figure 1.2. Tolerance classification as per the tolerance standard ASME Y 14.5M

tolerance standard ASME Y14.5M (1994 & 2009) [1,2] describes definitions of the geometric variations permitted by the different geometric tolerances. The symbolic representation of the tolerance classes, datums, material conditions etc. provides a language for clear communication between designer, process planner, manufacturing engineer and inspection engineer.

The ASME standard tolerances are classified into six classes: five geometric tolerances and the dimensional tolerance for size. As shown in Figure 1.2, the geometric tolerance classes are then further divided into subclasses based on the form of control. Each tolerance specification contains a tolerance type symbol, tolerance value, and optional information, such as datum references and condition. Datums are required for the orientation, location, runout and profile tolerance classes, and material condition may be applied when size of the feature is also being controlled together with orientation, location or profile tolerance.

The specifications in a feature control frame (FCF) define two boundaries around the nominal geometry; together they form a tolerance zone that limits all acceptable possible geometric manufacturing variations of the feature. The shape of the tolerance zone depends on the class of tolerance and the feature to which the tolerance is applied. Since this research is aimed at line profiles, an example of a line profile tolerance is demonstrated for further description.

1.3.1. Profile tolerance

The ASME Y14.5M Tolerance Standard [1] defines a line profile as a two dimensional outline of an object. Profile tolerances in general are used to control features like turbine blade that cannot be controlled by other geometric tolerances. Profile tolerances are used to control form or combinations of form, orientation,

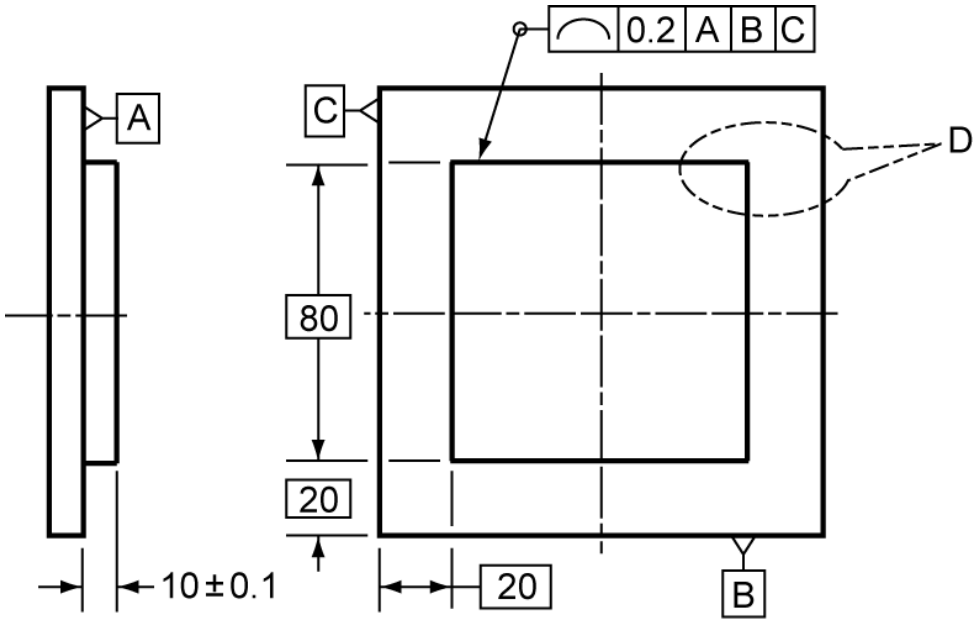

Figure 1.3. Specification of a line profile on a square boss, raised from a plate [23].

and location of a feature relative to its true profile. For certain features, it also can be interpreted to control size. A true profile is a profile defined with basic dimensions i.e. without any tolerances. If the datum is not specified, the tolerance specified controls form of the profile only.

The feature control frame for profile tolerance typically contains tolerance symbol ⌒ (line profile), or ⌓ (surface profile), a tolerance value, and optional datum information. Datums are required when orientation and location are required to control. A line profile is a 2D element. The line profile tolerance defines a tolerance zone an area on one or both sides of the true profile. A surface profile is made of surfaces. Hence, surface profile tolerance defines a volumetric tolerance zone.

A description of line and surface profile tolerance zones is given here by an example. As shown in Figure 1.3**,** the line profile tolerance is applied on the raised square boss. The small circle on the leader indicates that the profile tolerance is applied all around the (square) profile feature. The dome shaped symbol ⌒ is used in feature control frames for line profile tolerances. At each cross section, the shape of the square is controlled by the profile tolerance $t = 0.2$ mm relative to the Datums A, B, and C. This specification establishes a tolerance zone between two boundary squares. One is 0.1 mm larger along every line normal to the surface, and the other is 0.1 mm smaller. The Datums B, and C in the specification provide orientation and position constraint to the two squares. Moreover, Datum A controls orientation of the cross sectional plane on which the

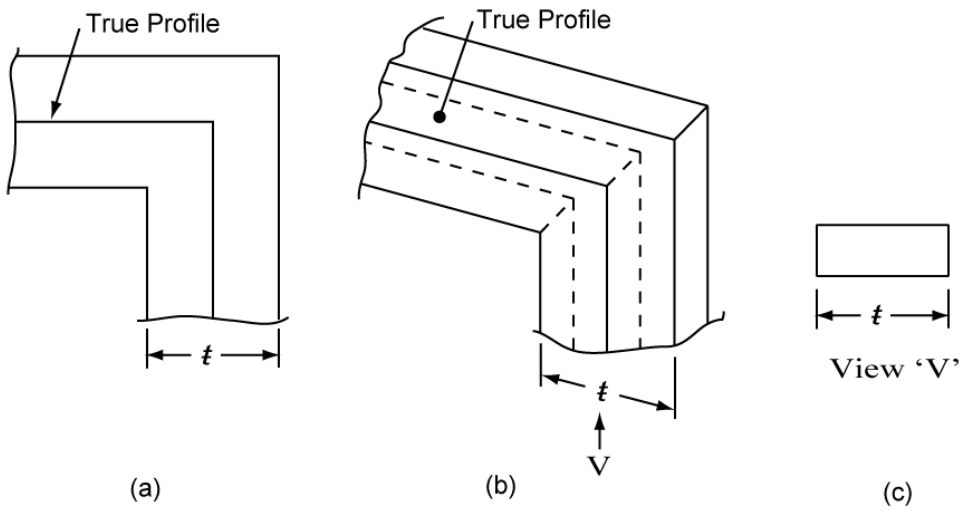

Figure 1.4. Portion of tolerance zones (Detail D) for line- and surface-profile of the boss in Figure 1.3; (a) 2D tolerance zone for the line profile, (b) 3D tolerance zone if the specification in Figure 1.3 were for surface profile, (c) A rectangular cross section of the 3D tolerance zone viewed from 'V'.

line profile is being considered instantaneously. For a line profile, a 2D tolerance zone at a cross section is shown in Figure 1.4(a). For surface profiles, the symbol is dome the same shape but with a line at bottom ⌓. As shown in Figure 1.4(b) the tolerance zone is a volume, the 2D tolerance zone raised (extruded) along the height of the square boss. This controls all four surfaces, on which feature control frame is applied, within the 3D tolerance zone.

An alternate approach to defining the tolerance zone, as described in the ISO Standard [4], requires the boundaries to be formed as the inner and outer envelopes of a roller of size t having its center traversing the true profile (Figure 1.5). Although either construction always will yield rounded corners for the outer boundary (the ISO roller becomes stationary at a corner), the ASME Standard [1] permits a relaxation of the parallel-boundary requirement at discontinuities in slope (sharp corners) so that the tolerance-zone may extend to the *intersection* of

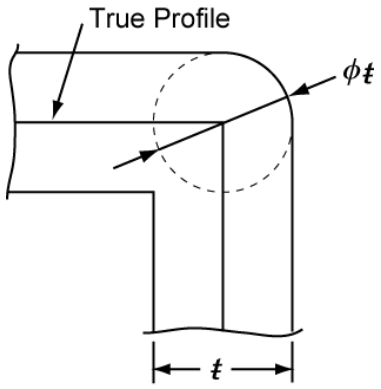

Figure 1.5. Tolerance zone boundaries formed by traversing roller of size t having its center on true profile.

the boundary lines (Figure 1.3(a)). We have included such extensions for the tolerance-zone at the four sharp corners depicted in Figure 1.3. Throughout the thesis, the same practice is followed while defining the tolerance zones for line profiles.

1.4. Problem Statement

Data reduction methods in CMM softwares are limited to lines, planes, circles, cylinders, and spheres. This research is focused on extending the capability of the CMM software in terms of handling type of geometry. A new computational method is developed for obtaining the least-squares fit of a set of points that have been measured on a line-profiles that are C^1 and C^2 discontinuous. Though the method is general in terms of type of geometry, examples are established for convex or concave line profiles with line and arc segments. The results will be a 'regression profile', i.e. a perfect form profile of different size and location.

CHAPTER 2

LITERATURE REVIEW

2.1. Feature Fitting - An optimization problem

Fitting a substitute geometry on measured points can be considered as an optimization problem. The objective is to minimize distances between measured points and the substitute geometry to determine feature parameters. Many fitting objectives can be represented as specific case of a general criterion L_p norm [5]. In fitting problem, objective is to find the parameters of feature that minimizes the L_p norm:

$$\left[\frac{1}{n}\sum_{i=1}^{n}|d_i|^p\right]^{\frac{1}{p}}.$$

Where d_i is the shortest distance between i^{th} point and the substitute geometry, n is number of points in the measured data and p defines objective criterion and its value varies from 0 to ∞. The parameters of the substitute geometry are the variables available for minimizing the objective function. To make computationally simpler, reduced form of the L_p norm can be defined as,

$$\sum_{i=1}^{n}|d_i|^p.$$

Two types of fitting problems are popular in the CMM fitting softwares, the least-squares fit and the Chebyshev fit. The L_p norm gives least squares solution when the value of p is 2. And Chebyshev fit can be obtained by

substituting the value of p as ∞. Of course, any p value between 0 to ∞ gives a unique substitute geometry. Nassef and ElMaraghy [6] demonstrated that the optimal value of p to obtain the best fit may vary from 1 to ∞, depends on number of points measured on the feature. Here the best fit means the substitute feature having minimum averaged error. They pointed out that despite popularity of the least-squares fit and the Chebyshev fit, they cannot be generalized for all geometric variations. For example, as shown in Table 2.1, their study shows that for a line feature with 60 or less number of points the best p value is 1. Whereas, for 80 or higher number of points, the best p value is 2 or higher. Furthermore, when a cylinder is tested, the best p values are different than that of the case of line for approximately same number of points. Hence, the best fitting function depends on the number of measured points relative to number of point required to represent the manufacture profile reasonably.

Table 2.1 Best p values for features line, cylinder and five sided polygonal profile for different number of measured points. Taken from [6].

Line		**Cylinder**		**Five sided polygonal profile (Car Door example)**	
No. of measured points	**Best p value**	**No. of measured points**	**Best p value**	**No. of measured points**	**Best p value**
20	1	4 × 2	20	10	4
40	1	4 × 4	30	20	6
60	1	8 × 4	40		
80	2	16 × 4	40		
100	5				

The least-squares fits is widely used in commercial CMM softwares to determine substitute geometry. The method is computationally faster as compared to Chebyshev fit. Moreover, since all measured points contribute to the fit, the method is less sensitive to outliers.

The Chebyshev fit is further classified into two types: the two-sided fit and the one-sided fit. The objective of the two-sided fit is to obtain complete form variation of the feature, i.e. minimize the maximum distance between two parallel features that bound all measured points. An example of a two-sided fit is the two nearest parallel planes between which all measured points are located. Since the zone between two parallel features is minimized, the method is also called the minimum zone fit.

The one-sided fit is used for fitting a feature on one side of the measured points. The substitute feature lies on one or more points such that the distance between the farthest measured point and the substitute feature is minimized. A feature of size such as a circle, a cylinder, or a sphere requires a one-sided mating envelope (maximum inscribed or minimum circumscribed) fit to confirm the feature to location and orientation tolerances. For planes, a one-sided fit can be used to simulate one plane of a datum reference frame that is made of three planes mutually perpendicular to each other. Depending upon constraints applied to the feature defined in the tolerance specification, the parameters of the substitute feature can vary. For example, an unconstrained (primary datum) plane requires

three points for one-sided fit, while the secondary datum constrained by the primary datum requires two points.

The Chebyshev fits are very sensitive to outliers, some of which may be inaccurate measurements, but the tolerance practice suggests to use them because the method best describes the tolerance zone [1, 7]. Despite its importance, it is not used in commercial softwares for all types of geometries because the objective function becomes nonlinear and introduces many challenges, such as solution getting stuck in local minima [8], requirement of much more computational power than the least squares fits.

Recent CMMs softwares claim capabilities of assessing lines, planes, circles, spheres, airfoils, gears, 2D contours and free form surfaces for conformance to tolerance specifications. NPL report [9] on review of recent CMMs capabilities shows that, for 2D contour and 3D freeform surface the CMM softwares evaluate deviations of the measured points from the nominal geometry. They do not reduce the measured data to number of parameters (usually seven or less) for assessment of the manufactured feature. The method proposed in this thesis reduces the measured points on line profile to four parameters: rotation, two displacements and size, such that the distances from the measured points and the nominal profile are minimized in least-square sense. As mentioned §§ 1.2, these parameters are useful to learn drift in manufacturing process.

2.2. Feature Fitting Methods

Several optimization algorithms are used to fulfill different fitting objectives and different geometry. Mani [3] describes the practice of feature fitting methods that are consistent with the GD&T standards. The types of tolerances considered are form, orientation and size. He also demonstrated that, CMM softwares supplied by different vendors use different feature fitting algorithms that lead to inconsistent results. Moreover, depending upon the algorithm used, the result may or may not be Chebyshev fit that is consistent with the ASME standard.

Murthy and Abdin [10] suggest three optimization methods for minimum zone evaluation, Monte-Carlo, Simplex search and Spiral search. The types of geometries used are planar, cylindrical and spherical. The effectiveness of each method varies based on type of geometry considered for fitting. In general, computational requirement of such methods increases rapidly as number of feature parameters increases. They suggest, as used by many researchers, to use normal least square fit as best initial guess for those iterative methods.

A minimum zone fit is difficult to achieve because of non-linearity in the problem formulation. Iterative methods are computationally expensive and still do not guarantee the exact solution. Carr and Ferreira [11, 12] solve the non-linear optimization problem by sequence of linear programs that converges to non-linear optimization. The term that makes the optimization problem non-linear in the formulation is equality constrain $||\mathbf{T}|| = 1$ or $T_x^2 + T_y^2 + T_z^2 = 1$. Where, $\mathbf{T}$ is direction vector of the solution i.e. minimum zone. For example, for flatness

problem, **T** is normal vector of mid-plane of the two parallel planes departed as close as possible, enclosing all points between them. Now consider a rigid body transformation matrix that transforms the solution and the point data in first quadrant. Hence, for $T_x \geq 0$, $T_y \geq 0$ and $T_z \geq 0$, the equality constraint implies inequality constrain $T_x + T_y + T_z \geq 1$. The method is applied to lines, planes, axes, and circular features for form assessment.

Another method dealing with nonlinear optimization is *Levenberg-Marquardt* method described in a technical report by Madsen et al [13]. It is combination of gradient method and Gauss-Newton method to exploit benefits of both, and minimizes the objective function in least-square sense. When the current iteration is far from the solution, gradient method is utilized, for good convergence. But, when it is close to the optimum point, gradient method becomes very slow. Hence, Gauss-Newton method is applied, which provides close to quadratic solution when the current iteration is close to the final solution.

Shakarji [8] presents Chebyshev algorithms developed at the National Institute of Standard and Technology (NIST). Parameterizations for a line, a plane, a circle, a sphere, a cylinder, and a cone are given to solve the optimization problem. Simulated annealing is used that not only search a non-linear function in downhill direction but also allows occasional uphill moves to avoid arriving at local minima.

The number of sampling points plays a significant role in precise assessment of the manufactured profile. On the other hand, the inspection time

and cost increases as the number of sampling points increases. Barari et al [14] propose a sampling method that uses error density function that guides for further sampling locations on the surface in order to achieve desired accuracy. An example of form variation assessment using minimum zone fit is demonstrated for a sculptured surface. Recently Shakarji and Srinivasan [15] presented weighted least-squares method, which can be utilized to complement measurements done on the feature are not uniform. They formulated a singular value decomposition (SVD) problem with weight assigned to each measured point. Higher weights are applied to the area from where less sampling points are collected as compared to the points in denser sampling area. Also if values of all the weights are equal to one then it becomes unweighted least-squares.

Polini et al [16] introduce a new approach of least squares fit for specific class of profiles, revolute profiles, i.e. a profile that is invariant about an axis. A homogeneous transformation matrix is determined to transform measured data in order to minimize distance between the measured points and the surface in least squares sense. For revolute surface the transformation parameters are reduced to five: two rotations and three translations. The method is divided in two steps. In first step, four transformation parameters are determined to align the axis of the measured point-cloud and that of the theoretical surface. In second step, the fifth parameter, translation along the axis, is determined. Levenberg-Marquardt method is used for the minimization problem. The results are similar to those in [14, 15]. However, those results were for a minimum zone fit instead of least squares. Polini et al [16] claim that the method may be used for any type of

surface profile. However, the formulation and examples are presented only for revolute profiles.

Choi and Kurfess [17] present a method to determine whether a point cloud, by homogeneous transformation, can fit into the tolerance zone for any kind of profile. Then the method is extended for minimum zone fit around measured points for profiles in [18]. The objective function is a truncated square function, which does not include the points between the minimum-zone boundaries of the current iteration. In other words, it minimize the sum of squares of distances between the points, that are beyond the outer boundary, and the outer boundary itself, and distances between points, that are inside the inner boundary, and inner boundary itself. A gradient-based iterative optimization method is used for this minimization problem. The authors claim that the method works for all types of profile. Examples used for demonstration are plane surface, and truncated cone. For the truncated cone, minimum zone is evaluated on the entire surface: two planar ends and the truncated cone between.

In recent studies, the method of moving least-square (MLS) is become popular for surface approximation. The method involves fitting a polynomial of small degree (usually 2 or 3) for each point in a cloud in least square sense using neighboring points. However, good approximation depends on selection of neighboring points. Lipman et al [19] propose a method to determine neighboring points that assures minimal approximation error. In another paper Lipman et al [20] presents fitting continuous non-smooth functions to set of data points. From

the metrology point of view, the method may be useful for free form surfaces. However, it may not be suitable for fitting a geometry that is not free form, such as square boss (Figure 1.3). From the metrology point of view, a profile fitted over points measured around the sides of square boss should be a square but can be bigger or smaller than the true profile.

2.3. Tolerance Map (T-Map)

This research is closely related to the Tolerance Map (T-Map) model for representing design limits to geometric manufacturing variations. Davidson and Shah [21] introduced the T-Map, a new mathematical model for geometric tolerances consistent with the ASME standard. The benefit of using this model is that it provides clear distinction between all the geometric tolerances, and, when multiple tolerances are applied to the same feature, it represents the coupling of variations permitted by the standard [1]. A T-Map is a hypothetical Euclidean point-space, the shape and size of which represents all allowable variations of a feature within its tolerance-zone. It is made of points; each point is obtained by one-to-one mapping from all the possible variations of a perfect form feature within its tolerance zone. The T-Map can be a closed area, a volume or a hypervolume of *n*-dimensions depending on the allowable degrees of freedom of the feature within its tolerance zone. For line profiles, geometric variations can be represented by a true profile, profiles parallel to it, and all of these displaced and within the tolerance zone. Each such parallel profile represents a point the T-Map for the line profile and tolerance specifications. Areal coordinates are used to build the point space of a T-Map. A brief description about areal coordinates

followed by T-Map for square line profiles (Figure 1.3), from [23], is given in following sub sections.

2.3.1. Areal Coordinates

Areal coordinates of a point is specified by center of mass of masses placed at vertices of a simplex, the ratios of which determine the position of the point. Areal coordinates can be formed for *n*-dimensional space with *n*+1 basis points of a simplex. Consider an example of 2-D space, in which the areal coordinates are based on a triangle of reference as shown in Figure 2.1. The basis is set by the three vertices ψ_1, ψ_2 and ψ_3 of the triangle. Consider that masses λ_1, λ_2 and λ_3 are located at these vertices, respectively, such that $\lambda_1 + \lambda_2 + \lambda_3 \neq 0$. The values of masses λ_1, λ_2 and λ_3 determine position of any point ψ such that ψ is centroid of the masses. The masses λ_1, λ_2 and λ_3 are also known as barycentric coordinates. A negative value for one or more of the coordinates shows that the point ψ is outside of the triangle. The position of the point ψ is uniquely determined by the linear combination

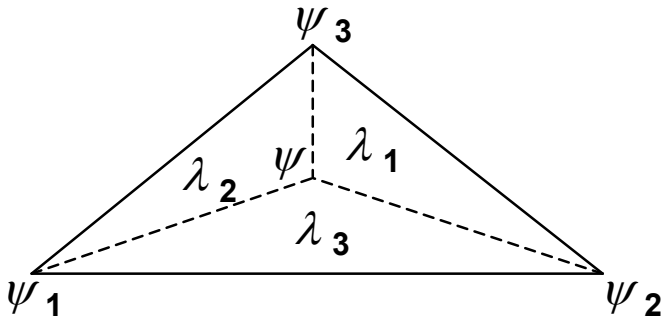

Figure 2.1. Two-simplex for areal coordinates in 2D space.

$$(\lambda_1 + \lambda_2 + \lambda_3)\ \psi = \lambda_1\ \psi_1 + \lambda_2\ \psi_2 + \lambda_3\ \psi_3.$$

Since the position of ψ depends only on two independent ratios of these coordinates, the coordinates are redundant. Hence an additional expression $\lambda_1 + \lambda_2 + \lambda_3 = 1$ can make the system determinant. The ratios of coordinates can also be regarded as ratios of areas of triangles formed by connecting the point ψ to the vertices ψ_1, ψ_2 and ψ_3 as shown in Figure 2.1; hence they often are named as areal coordinates.

2.3.2. T-Map for square Line profiles

In this section, development of T-Map of square line profiles is described. The text in this section is a short summary of the developments presented in [22], and Figure 2.3 (a), Figure 2.3 (b), Figure 2.4 and Figure 2.4 are taken from, [22].

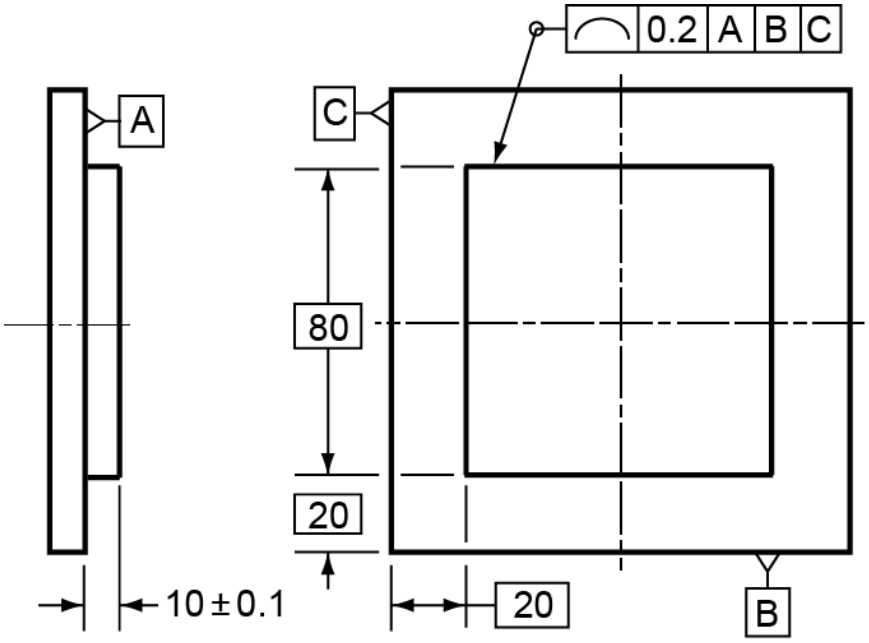

Figure 1.3 (Repeated from §§1.3.1). Specification of a line profile on a square boss, raised from a plate [23].

A Tolerance-Map (T-Map) represents the freedom of a feature in its tolerance-zone. For line-profiles, the manufacturing variations will be represented with the true profile and profiles parallel to it. These parallel profiles may be displaced from the true profile. Each point in the T-Map corresponds to any one of these parallel profiles or to any one of them that is displaced, yet remains within the tolerance-zone. Four degrees of freedom are required to specify the manufacturing variations of a line-profile, such as any one cross-section of the square boss in Figure 1.3 (repeated here for convenience). Four degrees of freedom, two displacements, a rotation and a size change with respect to its true profile correspond to four dimensions of four-dimensional (4-D) T-Map. Therefore, it becomes necessary to choose five of the parallel and/or displaced profiles as basis profiles and to define the T-Map by placing five corresponding basis points $\psi_1 \ldots \psi_5$ to form the vertices of a basis simplex. Five barycentric coordinates $\lambda_1 \ldots \lambda_5$, each one at its basis point ψ_i, then identify any point ψ in the T-Map, and each such point corresponds to one manufacturing variation (one profile) in the tolerance-zone.

Of the five basis-profiles required, two will be: ψ_1, the smallest-sized profile, and ψ_2, the largest-sized profile, i.e. the inner and outer boundaries to the tolerance-zone, respectively. These are both locked in place and cannot displace. The remaining basis-profiles are based on displacements of the *middle-sized* square profile, even though the true profile in the design specification may lie at one boundary of the tolerance-zone or be unevenly positioned between both boundaries [1]. Each middle-sized square is represented by its components of

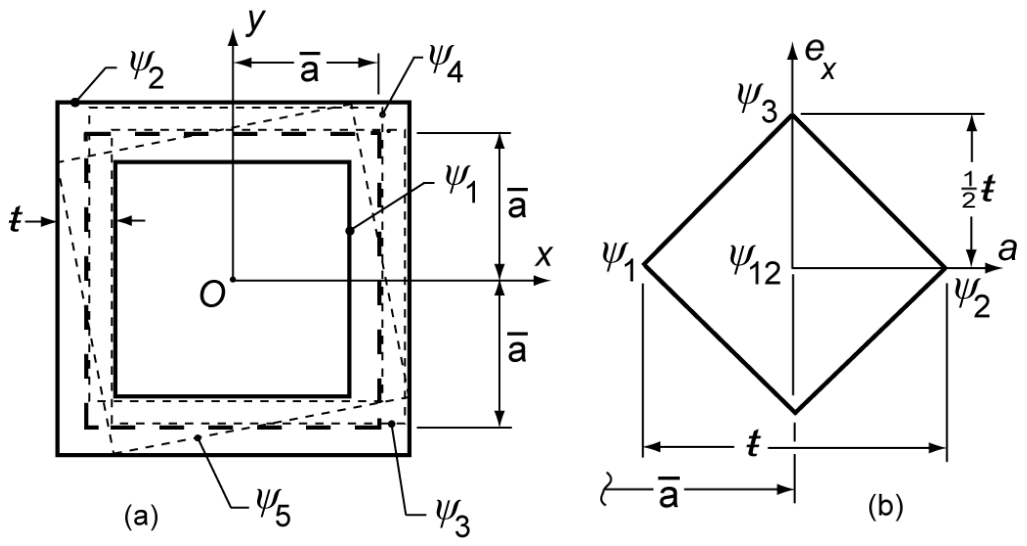

Figure 2.2 (a) The middle-sized profile (dashed-lined square) in the (exaggerated) tolerance-zone that is specified with the profile tolerance t; five variational possibilities are labeled, three with dotted lines; (b) One 2D cross-section of the corresponding T-Map that is confined to all size variations and displacements e_x only in x-direction. Taken from [22] with minor modifications.

eccentricity (translations), e_x and e_y, and its rotational displacement θ. The basis-profiles displaced to the limits $e_x = t/2$ and $e_y = t/2$ in the x- and y-directions are labeled ψ_3 and ψ_4, respectively, and the one rotated counterclockwise the maximum amount $\theta = t/2\bar{a}$ is ψ_5 (Figure 2.3 (a)).

Consider just two geometric variations of the square profile in Figure 2.3(a): its size and displacement e_x in x-direction. The smallest and largest sized profiles ψ_1 and ψ_2 respectively are regarded as two points on horizontal line in T-Map point space, as shown in Figure 2.3(b). Similarly consider ψ_3 as middle sized profile translated in x-direction to extreme rightward by $t/2$, and then isosceles triangle $\psi_1\psi_2\psi_3$ in Figure 2.3(b) establishes areal coordinates for 2D T-Map space. Since the dashed square in Figure 2.3(a) can displace leftward by $t/2$ also, the

boundary to this 2-D cross-section of the T-Map is a square of side-length $\mathbf{t}/\sqrt{2}$. Notice that the middle sized profile shown in dashed line in Figure 2.3(a), corresponds to origin ψ_{12} of T-Map shown as at midpoint of line segment $\psi_1\psi_2$ in Figure 2.3(b). This square profile is shown in Figure 2.3 (a) with the dashed line.

The 3-D T-Map for all the middle-sized square profiles is established with the four basis-points ψ_{12}, ψ_3, ψ_4, and ψ_5 shown in Figure 2.4. Basis-points ψ_3, ψ_4, and ψ_5 are placed at the same distance $\mathbf{t}/2$ from the origin along the three axes of a rectangular Cartesian frame of reference with axes e_x, and e_y, and θ'. Note that the angular limit $\theta=\mathbf{t}/2\,\bar{a}$ is multiplied by the length $\bar{a}$, i.e. $\theta'=\bar{a}\,\theta$ so that the units along all axes are the same, i.e. a length [L]. Consistent units on all the axes permit the T-Map to be used for metric computations.

Square profiles that are larger or smaller than the middle-sized one are more limited in their allowable displacements e_x, e_y, and θ, and the limits diminish

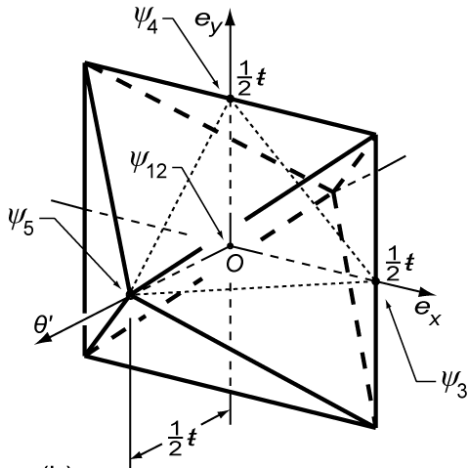

Figure 2.3 The T-Map for all the middle-sized squares in the sharp-cornered tolerance-zone of Figure 2.3 (a). Taken from [22].

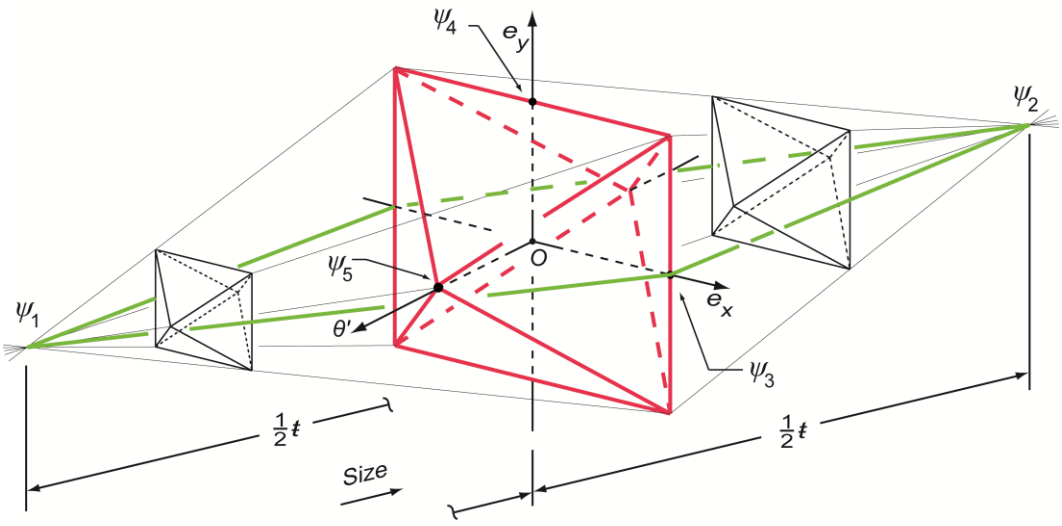

Figure 2.4 The 4-D T-Map for the square tolerance-zone in Figure 2.3 (a) and showing all five basis-points $\psi_1,\ldots,\psi_5$. The 3-D base in red is 3-D T-Map for middle sized profile (Figure 2.4) and 2-D cross section in green is 2-D T-Map for considering two variations: size and displacement e_x in x-direction. For clarity of the graphics, the scale in the direction of size ($\psi_1\psi_2$) is exaggerated. Taken from [22] with a minor modification.

linearly with change in size. Therefore, the full T-Map for the square tolerance-zone in Figure 2.3 (a) is a double hyperpyramid in 4-D that is depicted in Figure 2.4. The base for each single hyperpyramid is the 3-D octahedron from Figure 2.3 (b), and every other section (two are shown) at right angles to the direction of size is a smaller and geometrically similar octahedron. The combined basis-point ψ_{12}, shown in Figure 2.3 (b), has been replaced with the individual basis points ψ_1 and ψ_2.

There now is another way to view the objective of this research: reduce the measured points on one line-profile to a set of small-displacement coordinates that locate a single point within the T-Map of Figure 2.4. The result is an *i*-Map, that displays the quality of manufacturing relative to tolerance specifications.

2.4. Inspection Map (*i*-Map)

An inspection map (*i*-Map) of a feature is a reduction of the coordinates of measured points on a feature on a manufactured part, or a sample of several parts, to a small number of parameters that corresponds to those in the T-Map for the feature. For all parts meeting the design specifications, an *i*-Map of a feature is subset of T-Map of the same feature. For parts not meeting the design specifications, the *i*-Map or portion of the *i*-Map lies outside the boundary of the T-Map of the same feature. As discussed in Chapter 1, a cloud of points measured on a feature is reduced to few parameters by feature fitting methods. These parameters represent the manufacturing distortions of the feature in each possible degree of freedom of the feature within its tolerance zone. Since the *i*-Map is established in the same coordinate frame as the T-Map, the size and location of an *i*-Map represents the degree of conformance of a sample to the design specifications. Consistent variations in position and size of the *i*-Map provide useful information about stability or change in manufacturing processes.

Depending on the types of fit (see section 2.1) applied on a point-cloud, an *i*-Map can be a point or a higher dimensional geometry of the same dimension as that of the T-Map. For example, a two-sided fit on a point cloud produces two parallel boundaries within which all the measured points are located. The location and specification of these two boundaries forms a zone, transformed with respect to true profile, but enclosing all the measured points inside it. The one-to-one mapping of all possible variations of the feature within this zone to the point space forms an *i*-Map. The dimension of this *i*-Map is same as that of the T-Map

for the feature, but it resides within the T-Map. On other hand, a least squares fit and one-sided fit provide a single substitute feature rather than a zone. The substitute feature represents only one variation out of many possible variations within the tolerance zone. Hence, the least squares fit becomes a point in the T-Map of all possible variation in the tolerance zone.

CHAPTER 3

MOORE-PENROSE INVERSE AND REGRESSION LINE

Chapters 3 and 4 establish the mathematical foundation for the least squares fit. Introduction of the Moore-Penrose inverse and its properties is provided in this chapter. Chapter 4 establishes relationships between metrology problem and robotics to form system of equations that is solved using the Moore-Penrose inverse. §§3.2 is reproduced from [23].

3.1. Moore-Penrose Inverse (from [26])

For any system of equations $[\mathbf{b}] = [\mathbf{K'}][\mathbf{x}]$, there could be unique solution if coefficient matrix $[\mathbf{K'}]$ is square and nonsingular. But for rectangular matrix $[\mathbf{K'}]_{mxn}$, the inverse of the matrix $[\mathbf{K'}]^{-1}$ is indefinite. Penrose showed that, for every finite matrix $[\mathbf{K'}]_{mxn}$, where $m > n$, there exists unique matrix $[\mathbf{K}]^{\#}$ that satisfies the four equations,

$$\begin{aligned} &[\mathbf{K}]\,[\mathbf{K}]^{\#}[\mathbf{K}] = [\mathbf{K}], \\ &[\mathbf{K}]^{\#}\,[\mathbf{K}]\,[\mathbf{K}]^{\#} = [\mathbf{K}]^{\#}, \\ &([\mathbf{K}]\,[\mathbf{K}]^{\#})^{*} = [\mathbf{K}]\,[\mathbf{K}]^{\#}, \text{ and} \\ &([\mathbf{K}]^{\#}\,[\mathbf{K}])^{*} = [\mathbf{K}]^{\#}\,[\mathbf{K}]. \end{aligned} \qquad 3.1$$

Where $[\mathbf{K}]^{*}$ denotes the conjugate transpose of $[\mathbf{K}]$. The matrix $[\mathbf{K}]^{\#}$ called *Moore-Penrose inverse*, named after Moore and Penrose who presented the conditions (in Eqs.3.1). Uniquely *Moore-Penrose inverse*,

$$[\mathbf{K}']^{\#} = \{([\mathbf{K}']^{\mathsf{T}}\,[\mathbf{K}'])^{-1}\,[\mathbf{K}']^{\mathsf{T}}\},$$

For an inconsistent set of equations $[\mathbf{b}] = [\mathbf{K'}][\mathbf{x}]$ minimizes $([\mathbf{b}] - [\mathbf{K'}][\mathbf{x}])^2$. This unique property of *Moore-Penrose inverse* used, in this thesis, to calculate least

squares fits for line profile. The next section of the chapter is taken from a recent paper [23].

3.2. Regression Line using Moore-Penrose Inverse

To understand better the meaning of the Moore-Penrose inverse, which is used later in the paper, we undertake a straight-line fit of n identified points in a plane. Considering the solution-line to be of the form $y = mx + b$, there are n linear equations that relate the x_i- and y_i-values. From the Gauss-Markov Theorem [25], the least-squares fit is obtained by minimizing the sum

$$\sum \{y_i - (mx_i + b)\}^2 \qquad 3.2$$

for $i = 1 \ldots n$. As one example, apply simple linear regression to the five points in Table 3.1 which are symmetrically disposed about the line $y = 1 + x/2$ in the $x_j y_j$-

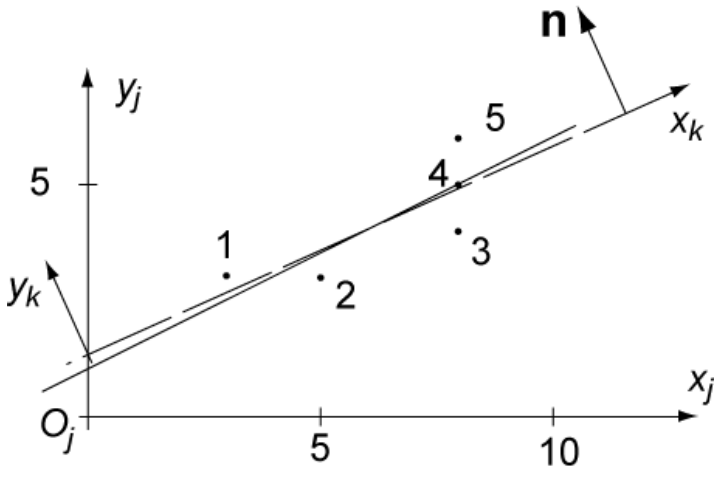

Figure 3.1 Five points equally disposed about a line $y = 1 + x/2$ (solid line) in the $x_j y_j$-frame and the standard regression line (dashed line) for them.

frame in Figure 3.1. When standard software (e.g. MAPLE) for linear regression is applied to these five points, the result is $m = 24/53$ and $b = 69/53$. It is shown as the line with long dashes in Figure 3.1.

Table 3.1. Coordinates of points for the example of least-squares fit for a line

Point	**1**	**2**	**3**	**4**	**5**
x	3	5	8	8	8
y	3	3	4	5	6

The set of n equations, which relate the n points to the linear regression line, may also be written

$$[\mathbf{y}_i] = [\mathbf{K}'][\$] = \begin{bmatrix} x_1 & 1 \\ x_2 & 1 \\ \vdots & \vdots \\ x_n & 1 \end{bmatrix} [\$], \qquad 3.3$$

where $[\mathbf{y}_i] = [y_1 \ \ldots \ y_n]^{\mathsf{T}}$, $[\$] = [m \ b]^{\mathsf{T}}$, and $[\boldsymbol{K}']$ is an $n \times 2$ rectangular coefficient matrix. The n linear equations are, of course, inconsistent. However, they may be solved for the unknowns m and b in $[\$]$ by using one of several *generalized inverses*; these give an *array* of inverse matrices and corresponding solutions for $[\$]$ [26]. Further, a special one of those inverses, the Moore-Penrose inverse $[\boldsymbol{K}']^{\#}$, ensures that the values m and b contained in $[\$]$ correspond to a minimization of the sum of the squares of all the differences $y_i - (mx_i + b)$. The set of y_i-values reside in matrix $[\mathbf{y}_i]$ and the corresponding set of directions for their measurement resides in the rows of $[\boldsymbol{K}']$. For an overconstrained (and

inconsistent) set of linear equations, $[\boldsymbol{K}']^{\#}$ is formed [26] as implied in the second of the equations

$$[\$] = [\mathbf{K}']^{\#}\,[\mathbf{y}_i] = \{([\mathbf{K}']^{\mathsf{T}}\,[\mathbf{K}'])^{-1}\,[\mathbf{K}']^{\mathsf{T}}\}\,[\mathbf{y}_i]. \qquad 3.4$$

When coordinates for the five points in the example above are introduced into matrices $[\boldsymbol{K}']$ and $[\mathbf{y}_i]$ of Eq 3.3, the Moore-Penrose inverse, $[\boldsymbol{K}']^{\#}$, of $[\boldsymbol{K}']$ gives the same values $m = 24/53$ and $b = 69/53$ that arose from the solution using linear regression. For what follows in §4.2, it is helpful to note here that, when every y_i is increased (or decreased) by the same value ΔF, Eq. 3.3 produces an unchanged slope m and a value for b that is increased exactly by ΔF.

Equations 3.3 and 3.4 apply to *any* overconstrained set of linear equations and *any* geometric shape. However, to be useful in the setting of manufacturing variations and tolerance-zones, matrix $[\mathbf{y}_i]$ must contain values that are measured with respect to a reference location of the given geometric shape, the rows of matrix $[\boldsymbol{K}']$ must represent the corresponding directions in which the measured y_i-values (deviations) are made, and matrix [**$**] then contains values that describe the location of the least-squares fit of the geometric shape relative to the same reference location that was used when measuring the deviations y_i. Therefore, in *any* geometric setting for which such equations might arise, Eq 3.4 relates the deviations of the y_i-values from the least-squares location of the geometric shape. For the special case of linear regression in the plane of Figure 3.1, (*i*) the geometric shape is a line, (*ii*) its reference location is the x-axis, (*iii*) its least-

squares fit is the regression line, (*iv*) the coordinates *m* and *b* in matrix [**$**] give the relative location of the regression line and the reference line, and (*v*) all the y_i-values are measured at right angles to the (reference) *x*-axis.

The computed values *m* = 24/53 and b = 69/53 for the least-squares line in Figure 3.1 are not very close to the theoretical values of 1/2 and 1 because the reference direction for error measurement was not made at right angles to the theoretical geometric shape. However, a second iteration may be undertaken from a new reference $x_k y_k$-frame that has its x_k-axis aligned with the first solution (dashed line in Figure 3.1). When the matrix [$\mathbf{y}_i$] in Eqs 3.3 and 3.4 is then formed from the y_k-values that are computed from this new reference direction, and when the results are transformed from the $x_k y_k$-frame to the $x_j y_j$-frame, a revised least-squares solution for best-fit of the points emerges: $m = 0.496$ and $b = 1.024$. Further, when the reference direction *is* the theoretical line $y = 1 + x/2$ in the $x_j y_j$-frame in Figure 3.1, Eq 3.4 produces values $m = 1/2$ and $b = 1$.

CHAPTER 4

METHOD OF ROBOTICS AND LEAST-SQUARES FIT FOR POINTS MEASURED AROUND A PROFILE

This chapter introduces the method of robotics to obtain a regression line profile for the measured points. §§4.1 establishes coordinates to represent line profile, convenient in robotics. In §§ 4.2, method of determining the minimum distance from a line, a segment of the line profile envelope, to a measured point is developed. Then §§4.3 introduces the system of in-parallel robot; linear actuators are applied at each measured point applying forces on the platform etched by the line profile. The displacement of each actuator is set inward and normal to the line segment. For a large amount of measured points, representation with an in-parallel robot forms a set of inconsistent equations. For static equilibrium to occur, the platform must be displaced by a small amount, which is obtained using the Moore-Penrose inverse. §§ 4.1, 4.2, 4.3, 4.4 and 4.5 are reproduced from [24].

4.1. Profile segments as envelopes

Given values for *p, q, r* and *s*, the equation

$$px + qy + rz + s = 0 \tag{4.1}$$

identifies all combinations of coordinates (*x, y, z*) of a point in a Cartesian frame of reference so that everyone lies on a single plane. Therefore, the coordinates $\varpi \equiv (p,q,r,s)$ define the specific plane that is identified in the same Cartesian frame. The location of the plane may be established with the three points where the coordinate axes pierce it (Figure 4.1). By setting, say, *y* and *z* to zero in Eq.

4.1, the pierce-point for the *x*-axis is seen to be $-s/p$. In two dimensions, the coordinates $(p,q,s) \equiv \varpi_{xy}$ are sufficient because $r = 0$ for every plane, each plane is parallel to the *z*-axis (Figure 4.1), and, when viewed from its intersection point (at infinity) with the *z*-axis, each one appears as a line in the *xy*-plane, such as ℓ in Figure 4.1. Coordinates *p* and *q* are the direction ratios of a normal line that is directed from the origin and at right angles to the given line, and $s/\sqrt{p^2+q^2}$ is the directed normal distance from the given line to the origin.

The coordinates (*p* , *q* , *s*) are homogeneous for every line in the *xy*-plane, i.e. they may be scaled up or down proportionately without changing the location of the line (see e.g. [28]). Therefore, coordinates ρ(*p* , *q* , *s*), where ρ is any real number, represent the same line as (*p* , *q* , *s*). However, for metric computations, such as determining the shortest distance from a line (*p*, *q*, *s*) to any point, the line

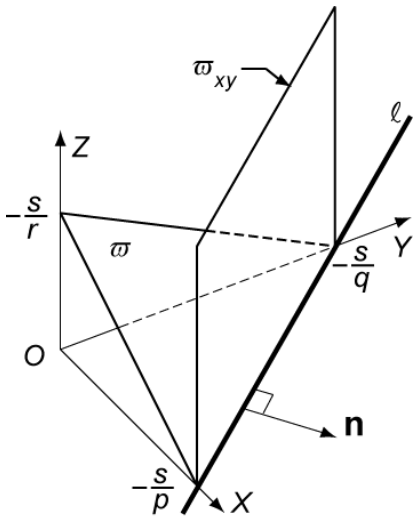

Figure 4.1. A plane ϖ in 3D, a plane ϖ_{xy} in 2D, and a line ℓ in the *xy*-plane defined by the 2D coordinates (p,q,s) of ϖ_{xy}.

coordinates must be *normalized*, i.e. ρ is chosen so that $1/\rho = \sqrt{p^2 + q^2}$. When ρ is negative, the sense of the unit normal is reversed, thereby providing a way to identify that side of a profile which faces inward. For example, the point equations for the two lines in Figure 4.2 are $x + 2y \pm 2 = 0$, the upper and lower signs, respectively, applying to lines *A* and *B*. If these were opposite sides of a closed line-profile, an appropriate choice at each line for the sign and magnitude of its normalizing factor ρ would make the signs and magnitudes of its *p*- and *q*-coordinates identical to the coordinates for the inward unit normals $\mathbf{n}_A$ or $\mathbf{n}_B$ and make the shortest distance from each line to the origin be equal to *s*. This procedure gives the normalized coordinates for line *A* to be $(p, q, s) = (1, 2, 2)/\sqrt{5}$ and those for line *B* to be $(-1,-2,2)/\sqrt{5}$, and both distances to the origin become $+s = 2/\sqrt{5}$, the positive sign indicating that the sense of each measurement is consistent with that for its unit normal.

Note that there is no significance of mechanics or geometry to the normalizing factor ρ. This is in contradistinction to a similar-looking set of three

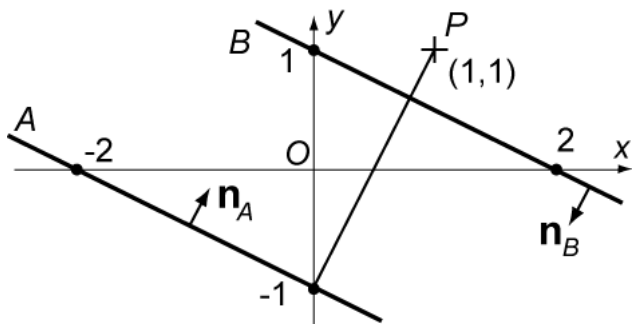

Figure 4.2 A point *P* and two lines *A* and *B* in the *xy*-plane, each with its inwardly directed normal $\mathbf{n}_i$.

(screw) coordinates that will be used in §4.3 to locate a line. For those coordinates, the normalizing factor will represent either a force or the amplitude of a small displacement that acts along the line [28].

4.2. Minimum distance between an envelope and a measured point

Given a point (*x, y*) and a line (*p, q, s*), both in a planar *xy*-frame, the equation ensuring that the point lies on the line is $px+qy+s=0$. Further, when the point does not lie on the line, its minimum (normal) distance from the line is [28]

$$d = px+qy+s; \tag{4.2}$$

this distance will be in the same units as those for *x* and *y* of a measured point whenever coordinates (*p, q, s*) are scaled so that $p^2 + q^2 = 1$, i.e. when the coordinates are normalized. For instance, the (directed) distance from line *A* in Figure 4.1 to point *P* is $(1\cdot 1+2\cdot 1+2)/\sqrt{5}=+\sqrt{5}$, and from line *B* it is $-1/\sqrt{5}$.

Assessing minimum distances at the corners of a profile can be problematic because the envelope tangent-lines are not *segments;* instead, each line (*p, q, s*) is of infinite extent. For example, point #3 in Figure 4.3 lies *on* vertical line segment located at right of the line profile, yet lies closest to the true profile at top most envelope-line of the profile that is horizontal. This matter will be resolved by assessing minimum distances from a *reference-envelope* that is a parallel curve larger than the middle-sized profile (Figure 4.3). A larger parallel curve is generated easily from the envelope description of a middle-sized profile

by increasing the value of coordinate s by the same amount for every tangent-line. For purposes of the profile and measured points shown in Figure 4.3, the outer boundary to the tolerance-zone is an acceptable reference-envelope ($\Delta s = t/2 =$ 0.1mm), although a value of $\Delta s = 2t$ or $3t$ is surely better in a practical measurement setting to allow for some measured points to lie outside of the tolerance-zone. Once the correct minimum-distance direction $\mathbf{n}_i$ and a corresponding distance d from the reference envelope are established for each point, it is easy to subtract Δs from every distance value.

4.3. Least-squares fit of a square line-profile to measured points

In Figure 4.3, the middle-sized square profile (dashed line) and the boundaries of its tolerance-zone are shown drawn on the platform of a planar in-parallel robot that is guided with three linear actuators that lie on the normalized screws $\$'_1$, $\$'_2$, and $\$'_3$. The actuators are attached to the platform at three of the measured points, i.e. at A, B, and C, and the directions of the corresponding $\$'_i$ are the same as for the inward unit normals $\mathbf{n}_i$ from the closest side of the square to the (enlarged) reference envelope for the profile. For what follows in developing formulation for least-squares fit in this section, it is necessary to align coordinate frame of the measured points and coordinate frame of the geometry from which their deviations are measured. Each of the three linear actuators exerts a force of magnitude F_i' and causes a velocity of magnitude v'_i at the measured point where it is attached to the platform. Since speed and time are of no importance in measurement reduction, each v'_i will be replaced with a differential displacement d'_i of the measured point in the direction of $\mathbf{n}_i$. The corresponding deviation torsor

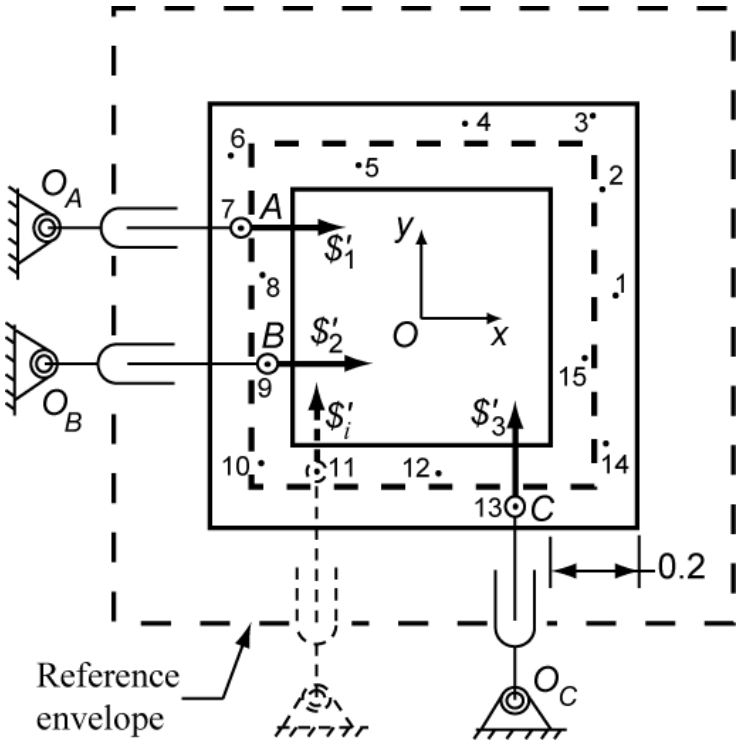

Figure 4.3. The line-profile (dashed line) of Figure 1.3, its tolerance-zone boundaries (with an exaggerated scale), and 15 measured points, all lying on the platform of a planar in-parallel robot which is guided by three linear actuators lying on the screws $\$'_1$, $\$'_2$ and $\$'_3$ at points *A*, *B*, and *C;*

for the platform body is represented by [**$**] ≡ (0, 0, $\delta\theta$; δx, δy, 0). Since displacements are confined to the *xy*-plane, the three zero-coordinates may be omitted.

Each of the actuator forces in the *xy*-plane is represented with wrench coordinates, i.e. $F_i'\ \$'_i \equiv (\mathbf{F}'_i; \mathbf{T}'_i) \equiv (\mathcal{L}'_i, \mathcal{M}_i', 0; 0, 0, \mathcal{R}'_i)$, where $\mathcal{L}'_i$ and $\mathcal{M}_i'$ are the *x*- and *y*-components of actuator-force $\mathbf{F}'_i$ and $\mathcal{R}'_i$ is the moment of $\mathbf{F}'_i$ about the origin, i.e. $\mathcal{R}'_i = -y_i\mathcal{L}'_i + x_i\mathcal{M}_i'$. Since all forces will lie in the *xy*-plane, the three zero-coordinates may be omitted, just as for [**$**]. Also, the geometry may be isolated from the statics by normalizing the wrench coordinates, i.e.

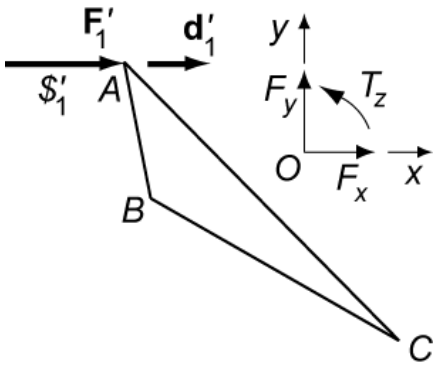

Figure 4.4. The free-body diagram of the platform carrying the profile. The external loads are the force $\mathbf{F}'_1$ acting along the screw $\$'_1$ at point A and the equilibrium wrench ($\mathbf{F}_1$;$\mathbf{T}_1$) exerted on the platform from the environment and represented with the coordinates (*Fx, Fy; Tz*). Also shown is the differential displacement vector $\mathbf{d}'_1$ that is aligned with $\$'_1$ at A. The shape of the platform ABC, and the relative location of the *xy*-frame are together congruent to those same features in Figure 4.3

$$F'_i\$'_i \equiv (\mathcal{L}'_i,\ \mathcal{M}'_i\ ;\ \mathcal{R}'_i) \equiv F'_i\,(L'_i,\ M'_i\ ;\ R'_i), \qquad 4.3$$

this making $(L'_i)^2 + (M'_i)^2 = 1$. The normalized coordinates L'_i, M'_i, and R'_i for each $\$'_i$ are the scalar *screw* coordinates for the actuator-wrench $F'_i\$'_i$; they contain only geometry, i.e. direction and location of $F'_i\$'_i$.

A free-body diagram of the platform in Figure 4.3 contains the three forces $\mathbf{F}'_i$ (i = 1, 2, 3) and an equilibrium wrench, composed of a force and a couple, exerted on the platform from the environment. The force and couple are represented with the wrench ($\mathbf{F}$; $\mathbf{T}$). Consider now that all of the actuated joints have no force applied and are free to move except one, say $\$'_1$, shown in Figure 4.4. Then, the only additional loads on a free-body diagram of the platform are those *portions* of the equilibrium wrench reacting back on it from the environment

which are required to equilibrate $F_1'\$'_1$, i.e. the force and couple $(\mathbf{F}_1 ; \mathbf{T}_1)$ shown in Figure 4.4 with the components F_x, F_y, and T_z. Since the virtual work of all forces and moments on the free body must be zero for a kinematically admissible displacement of the platform arising from $\mathbf{d}'_i$, the system of forces and couples for the special case in Figure 4.4 leads to

$$F_1'd'_1 + [T_z \;\; F_x \;\; F_y][\delta\theta \;\; \delta x \;\; \delta y]^{\mathsf{T}} = 0, \qquad 4.4$$

in which the order of the coordinates in $(\mathbf{F}_1 ; \mathbf{T}_1)$ has been changed to $(\mathbf{T}_1 ; \mathbf{F}_1)$ and the zero-coordinates again have been omitted. The term $F_1'd'_1$ represents the virtual work of force $\mathbf{F}'_1$ with virtual displacement $\mathbf{d}'_1$, both in the direction of $\$'_1$, at point A on the platform, and the product $[T_z \;\; F_x \;\; F_y][\delta\theta \;\; \delta x \;\; \delta y]^{\mathsf{T}}$ represents the virtual work from the equilibrium-wrench acting on the platform whose deviation torsor is $[\$] \equiv [\delta\theta \;\; \delta x \;\; \delta y]^{\mathsf{T}}$.

It is helpful to shift attention to the wrench $-(\mathbf{T}_1 ; \mathbf{F}_1)$ exerted on the environment and *produced* at the platform by the force $F_1'\$'_1$ at A. Since the platform in Figure 4.4 is a two-force (two-wrench) member, with each wrench intensity of equal magnitude, $-(\mathbf{T}_1 ; \mathbf{F}_1) \equiv -(T_z ; F_x , F_y) \equiv (\mathcal{R}'_1 ; \mathcal{L}'_1, \mathcal{M}_1') \equiv F_1'(R'_1; L'_1, M_1')$. Making this substitution in Eq. 4.4 gives

$$F'_1d'_1 = F'_1[R'_1 \;\; L'_1, \;\; M'_1][\delta\theta \;\; \delta x \;\; \delta y]^{\mathsf{T}} \qquad 4.5$$

for the virtual work expression when force is exerted only at $\$'_1$. Two more Eqs. 4.5, with subscripts $_2$ and $_3$, occur when force is applied only at $\$'_2$ and only at $\$'_3$.

The force-amplitude at each actuated joint may be removed from each term, and all terms on the right come from the product of a row matrix and a column matrix of three elements each. When the three equations are ordered sequentially, then the rows of screw coordinates, when taken together, comprise a matrix [$\boldsymbol{K}'$] that is formed entirely from the (normalized) coordinates for $\$'_1$, $\$'_2$ and $\$'_3$, and the three equations may be written

$$\begin{bmatrix} d'_1 \\ d'_2 \\ d'_3 \end{bmatrix} = \begin{bmatrix} R'_1 & L'_1 & M'_1 \\ R'_2 & L'_2 & M'_2 \\ R'_3 & L'_3 & M'_3 \end{bmatrix} \begin{bmatrix} \delta\theta \\ \delta x \\ \delta y \end{bmatrix} \quad \text{or} \quad [\mathbf{d}'_i] = [\boldsymbol{K}'][\$]. \tag{4.6}$$

The reader familiar with robotics will recognize [$\boldsymbol{K}'$] as a Jacobian for the actuators of the robot platform in which the normalized coordinates have been rearranged. (For those interested in a more detailed treatment of the principles involved, the notation here has been made nearly consistent with that in Davidson & Hunt [28], §§1.6, 6.11, 8.5, and 9.6.)

So long as the screws $\$'_1$, $\$'_2$ and $\$'_3$ are independent for the three measured deviations d'_1, d'_2, and d'_3 at locations A, B, and C around the profile, the solution to Eq. 4.6 for [$], i.e. [$] = [$\boldsymbol{K}'$]$^{-1}$[$\mathbf{d}'_i$], is unique and all three scalar Eqs. 4.6 are satisfied exactly. This solution ensures that d'_1, d'_2, and d'_3 are kinematically consistent with the platform (profile) displacement [$]. However, in practical situations, there are many more measured points around a line-profile than three. For instance, in Figure 4.3 there are 15 points. For every additional point, there would be an added, and redundant, linear actuator with its normalized

screw $\$'_i$ exerting a force of amplitude F_i' on the platform. One example is shown with dashed lines at Point 11 in Figure 4.3. Each of these additional points adds a row to the matrices [$\mathbf{d}'_i$] and [$\boldsymbol{K}'$] in Eq. 4.6, so that, for all the measured points,

$$[\mathbf{d}'_i] = \begin{bmatrix} d'_1 \\ d'_2 \\ \vdots \\ d'_n \end{bmatrix} = [\boldsymbol{K}'][\$] = \begin{bmatrix} R'_1 & L'_1 & M'_1 \\ R'_2 & L'_2 & M'_2 \\ \vdots & \vdots & \vdots \\ R'_n & L'_n & M'_n \end{bmatrix} [\$]. \qquad 4.7$$

Solution to Eqs. 4.7 provides [**$**], rigid body displacements ($\delta\theta$, δx, δy) of the platform in plan. However, in metrology size is also an important measure of dimensional variation. In next section, Eqs 4.7 are modified to accommodate size variation.

4.4. Adding the 4th dimension for metrology

The coordinates ($\delta\theta$, δx, δy) of [**$**] appear only in a 3-D cross-section of the T-Map (Figure 2.3(b)), such as in the base of the 4-D double hyperpyramid in Figure 2.4; they do not represent the *size* of the least-squares envelope, i.e. the fourth dimension of the T-Map. The values for displacements d'_i, then, may all contain a constant value ΔF that represents the change in feature size between that of the middle-sized profile and the least-squares profile, and they *must* contain a value Δs that was introduced artificially in §§4.2 to establish the correct proximity of a measured point to the profile. For reduction of CMM data, then, each generic Eq 4.8 must be augmented to

$$\left.\begin{aligned} d'_i &= [\boldsymbol{R}'_i\ \boldsymbol{L}'_i\ \boldsymbol{M}'_i][\delta\theta\ \ \delta x\ \ \delta y]^{\mathsf{T}} + (\Delta s - \Delta F) \\ &= [\boldsymbol{R}'_i\ \boldsymbol{L}'_i\ \boldsymbol{M}'_i\ 1][\delta\theta\ \ \delta x\ \ \delta y\ \ (\Delta s - \Delta F)\ ]^{\mathsf{T}} \end{aligned}\right\} \qquad 4.8$$

(compare to $y_i = mx_i + b$ in §3.2). The scalar relation in Eq 4.8 forms the transition between the setting of in-parallel robotics and the setting of reducing CMM data to geometric variables related to Tolerance-Maps. Now the least-squares fit is obtained by minimizing the sum

$$\sum[\ d'_i - \{\ \boldsymbol{R}'_i\delta\theta + \boldsymbol{L}'_i\delta x + \boldsymbol{M}'_i\delta y + (\Delta s - \Delta F)\}\ ]^2 \qquad 4.9$$

for $i = 1\ldots n$. Matrix [$] in Eq 4.7 is augmented to contain the *four* components $\delta\theta$, δx, δy and $(\Delta s - \Delta F)$, and the matrix [$\boldsymbol{K}'$] in Eq 4.7 is augmented on the right with a column of ones so that the n Eqs 4.8 (for the n measured points) produce the matrix equation

$$[\mathbf{d}'_i\ ] = \begin{bmatrix} d'_1 \\ d'_2 \\ \vdots \\ d'_n \end{bmatrix} = [\boldsymbol{K}'][\$] = \begin{bmatrix} \boldsymbol{R}'_1 & \boldsymbol{L}'_1 & \boldsymbol{M}'_1 & 1 \\ \boldsymbol{R}'_2 & \boldsymbol{L}'_2 & \boldsymbol{M}'_2 & 1 \\ \vdots & \vdots & \vdots & \vdots \\ \boldsymbol{R}'_n & \boldsymbol{L}'_n & \boldsymbol{M}'_n & 1 \end{bmatrix}[\$] \qquad 4.10$$

The Moore-Penrose solution to Eq. 4.7 for [$], i.e. [$] = $[\boldsymbol{K}']^{\#}[\mathbf{d}'_i]$ (see Eq. 3.4), produces the least-squares location ($\delta\theta$, δx, δy) and size-adjustment ($\Delta s - \Delta F$) for the profile, i.e. that location and size for a profile which minimizes the sum in Eq 4.9. (Compare the pair of Eqs 3.2 and 3.3 to the pair 4.9 and 4.10.)

Note that coordinates ($\delta\theta$, δx, δy) correspond to coordinates (θ, e_x, e_y) in the T-Map of Figure 2.4.

4.5. An Example of least-squares fit for square line profiles

As one example, consider the measured points that are shown around the middle-sized profile in Figure 4.3. The points represent an imperfectly manufactured square profile. The coordinates (L'_1, M_1'; R'_1) for the actuator screws at each point, and the deviations d', are presented in Table 4.1 for each of the measured points; the deviations are all measured from the outer boundary of the tolerance-zone, so Δs = 0.1 mm (Figure 2.3). The values in Table 4.1 are used to build matrices [$\boldsymbol{K}'$] and [$\mathbf{d}'_i$] in Eq. (4.10). The Moore Penrose solution of [$\boldsymbol{K}'$] produces the least-squares solution

$$[\$] = [\delta\theta \;\; \delta x \;\; \delta y \;\; (\Delta s - \Delta F)]^{\mathsf{T}} = [0.000562 \;\; 0.011858 \;\; 0.013294 \;\; 0.092828]^{\mathsf{T}}.$$

Table 4.1. Coordinates of measured points around a manufactured square profile

Points	L'_i	M_i'	R'_i, mm	d_i', mm
1	–1	0	5	0.05
2	–1	0	30	0.08
3	0	–1	–40	0.02
4	0	–1	–10	0.05
5	0	–1	15	0.15
6	1	0	–38	0.05
7	1	0	–20	0.08
8	1	0	–10	0.12
9	1	0	11	0.14
10	1	0	35	0.12
11	0	1	–25	0.14
12	0	1	4	0.13
13	0	1	22	0.05
14	–1	0	–30	0.08
15	–1	0	–10	0.11

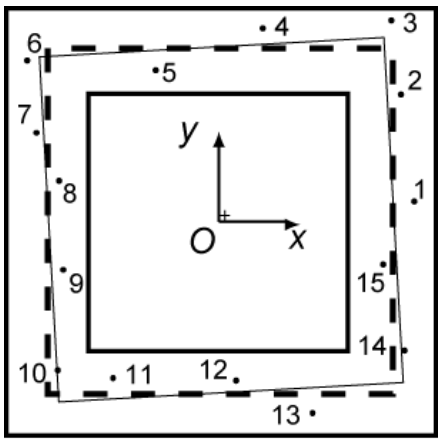

Figure 4.5 The resultant least-squares profile shown with the thin line. Its displacement from origin *O* is shown with the '+' mark.

The resultant least-squares profile of this solution is shown as the profile with the thin line in Figure 4.5. Note that the scale of the tolerance-zone is enlarged by a factor of 10 in Figure 4.3 and Figure 4.5, and the scale for the profile dimensions is diminished by a factor of 10. Consequently, the least-squares profile is drawn at $\delta\theta$ = 0.0562 rad = 3.22° in the counterclockwise direction. Further, to make the appearance of the displaced origin '+' in Figure 4.5 be consistent with the displayed points, its coordinates δx = 0.011858 mm and δy = 0.013294 mm have been scaled up by a factor of 10 with respect to the middle-sized profile. The corresponding size adjustment from the middle-sized profile is ΔF = 0.1 – 0.092828 = 0.007172 mm, i.e. a small growth in size.

4.6. Exact least-squares by invoking further iterations

As discussed in §§3.2, the least squares solution depends on initial condition used to determine matrices [$\mathbf{d}_i'$] and [$\boldsymbol{K}'$] in Eqs. 4.10. For the example of the linear regression in §§3.2, three iterations required to obtain solution close

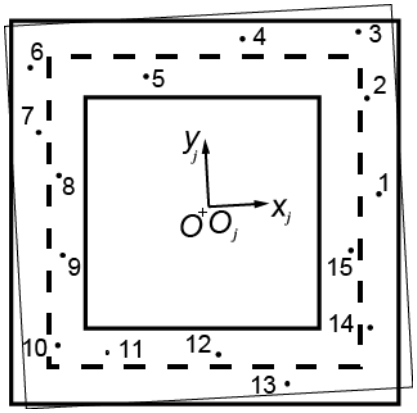

Figure 4.6 The displaced O_j-frame and the outer envelope lying on it. The outer envelope is displaced by the amount of least square solution of the previous iteration.

to theoretical solution. Hence to check whether the solution §§4.5 converged, further iterations are carried out for the example of the square profile.

As shown in Figure 4.6, consider the reference envelope is lying on a movable lamina, which contains reference frame O_j. The lamina displaces during each iteration by the amount of solution of the previous iteration. The same procedure as in §§4.2, 4.3 and 4.4 can be applied for next iterations, provided that the displaced outer envelope and measured points are in j-frame. The reference envelope is transformed by least square solution of the previous solution ($\delta\theta \;\; \delta x \;\; \delta y$). Coordinates of the measured points in j-frame (of the *current* iteration) can be obtained by,

$$\begin{bmatrix} x_j \\ y_j \\ 1 \end{bmatrix} = [A]^{-1} \begin{bmatrix} x \\ y \\ 1 \end{bmatrix} = \begin{bmatrix} \cos\delta\theta & -\sin\delta\theta & \delta x \\ \sin\delta\theta & \cos\delta\theta & \delta y \\ 0 & 0 & 1 \end{bmatrix}^{-1} \begin{bmatrix} x \\ y \\ 1 \end{bmatrix}. \qquad 4.11$$

Where, [A] is transformation matrix, and (x, y, 1) are homogenous coordinates of the measured point in the frame of the *previous* iteration.

The minimum distances [$\mathbf{d}_i'$] and the coordinates (L'_i, M_i'; R'_i) are obtained based on the new configuration of the reference envelope and the measured points in j-frame. Results of two further iterations are shown in Table 4.2.

Table 4.2 Coordinates of measured points with respect to the latest least squares solution

	Iteration-2				***Iteration-3***			
Points	L'_i	M_i'	R'_i, **mm**	d_i', **mm**	L'_i	M_i'	R'_i, **mm**	d_i', **mm**
1	-1.000	0.000	4.964	0.066	-1.000	0.000	4.964	0.066
2	-1.000	0.000	29.964	0.082	-1.000	0.000	29.964	0.082
3	0.000	-1.000	-40.011	0.063	0.000	-1.000	-40.011	0.063
4	0.000	-1.000	-10.011	0.076	0.000	-1.000	-10.011	0.076
5	0.000	-1.000	14.989	0.162	0.000	-1.000	14.989	0.162
6	1.000	0.000	-38.009	0.067	1.000	0.000	-38.009	0.067
7	1.000	0.000	-20.009	0.087	1.000	0.000	-20.009	0.087
8	1.000	0.000	-10.009	0.121	1.000	0.000	-10.009	0.121
9	1.000	0.000	10.991	0.129	1.000	0.000	10.991	0.129
10	1.000	0.000	34.991	0.096	1.000	0.000	34.991	0.096
11	0.000	1.000	-25.034	0.148	0.000	1.000	-25.034	0.148
12	0.000	1.000	3.966	0.122	0.000	1.000	3.966	0.122
13	0.000	1.000	21.966	0.032	0.000	1.000	21.966	0.032
14	-1.000	0.000	-30.036	0.116	-1.000	0.000	-30.036	0.116
15	-1.000	0.000	-10.036	0.135	-1.000	0.000	-10.036	0.135
	$\delta\theta$ =	0.1296 e–8			$\delta\theta$ =	0.3121 e–14		
	δx =	–0.7470 e–5			δx =	–0.2848 e–14		
	δy =	0.6657 e–5			δy =	–0.2852 e–13		
	ΔF =	–0.6325 e–5			ΔF =	–0.1545 e–13		

Deviations of the new least square line profiles are shown at bottom of the table. It is observed that, the values of the least-squares solution are not significant even for second iteration. Notice that the practical manufacturing variations (d_i' values) in Eq. 4.10 are typically two orders of magnitude less than

the nominal dimension of the profile. Hence, having small range of variation, the method is linear for tolerance problems.

4.7. *i*-Map representation of the least-squares solution

Now the manufactured line profile can be evaluated based on the tolerance specifications given in Figure 1.3. The four deviations ($\delta\theta\ \delta x\ \delta y\ \Delta F$) obtained in §§4.5 can be modeled in the T-Map for the square line profile (Figure 2.4). The least squares line profile will represent as a point in the T-Map. The coordinates of the point in T-Map are

$$(\theta'\ ex\ \ ey\ \Delta F) = (\ \bar{a}\ \delta\theta\ \ \delta x\ \ \delta y\ \Delta F) = (\ 0.02284\ \ 0.0119\ \ \ 0.0133\ \ 0.0072).$$

The *i*-Map is drawn in the T-Map as a point as shown in Figure 4.7 using coordinates (0.02284, 0.0119, 0.0133, 0.0072). The 3D hyper volume with thick

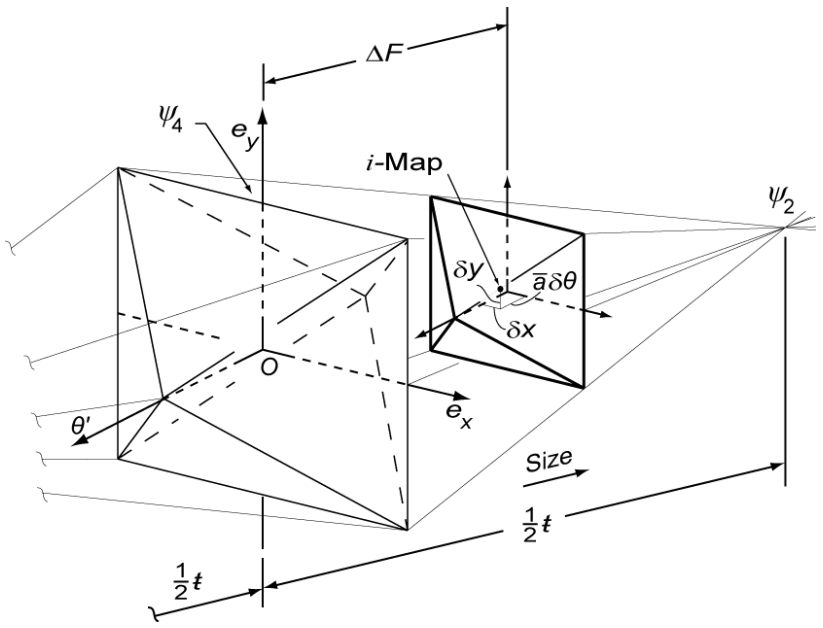

Figure 4.7 *i*-Map for the solution obtained in §§4.5; it is a point in 4D T-Map of square profile shown in Figure 1.3. Coordinates of *i*-Map are scaled for clarity.

lines is the T-Map of the square profile at size ΔF.

4.8. Minimum zone – form error assessment

Form variation, based on the least-square fit, can be determined by distance between two parallel boundaries, at the orientation and location as those of the least-squares solution, but separated by minimum distance such that all the measured points are in between. The method to find the two boundaries that form the minimum zone is described in this section.

As shown in Figure 4.6, consider a movable lamina with origin O_j on which the reference envelope is lying. The lamina is displaced by the amount of the least-squares solution. Now the inverse transformation, as in Eq. 4.11, is applied to the measured points, to transform the measured points into the *j*-frame. The shortest distances, $[\mathbf{d}'_i]$, from the measured points (on *j*-frame) and the reference envelope (in *j*-frame) are calculated using Eq. 4.2. Then the minimum

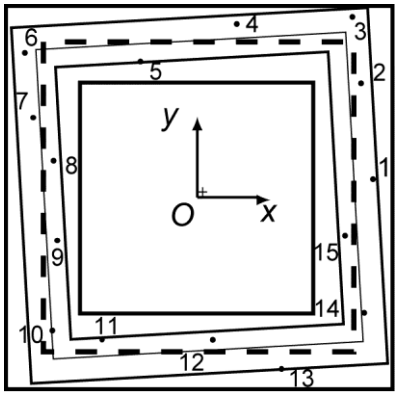

Figure 4.8 The resultant minimum zone, based on the least-squares solution, shown as two parallel square boundaries. One is located on point farthest outward from the least-squares fit and the other is on point farthest inward.

zone is calculated by,

$$Z = \max[\mathbf{d}'_i] - \min[\mathbf{d}'_i]. \qquad 4.12$$

For the problem of the square profile, the values of $[\mathbf{d}'_i]$ are,

$[\mathbf{d}'_i]^{\mathsf{T}} = [0.066, 0.082, 0.063, 0.076, 0.162, 0.067, 0.087, 0.121, 0.129,$

$0.096, 0.148, 0.122, 0.032, 0.116, 0.135]$

And the value of the minimum zone is,

$Z = 0.162 - 0.032 = 0.13$ (Figure 4.8).

4.9. Orientation zone

It would be interesting to analyze situation when orientation of the minimum zone in §§4.8 is constrained with respect to Datums. Orientation zone can be defined by zone between two parallel curves that are separated by minimum distance such that all the measured points are in between, and orientation of the zone is constrained with respect to Datums.

Solution to orientation zone is simplification to the least-squares fit. It can be obtained by reducing the $[\boldsymbol{K}']$ matrix in Eq. 4.10 by substituting zeros in first column, which cause orientation change of the platform (Figure 4.3) due to application of the linear actuator. Corresponding changes result no orientation change in displacement torsor [$], i.e. $\delta\theta$ = 0.0 rad. Hence to determine orientation zone for the points measured around line profile can be obtained by solving simplified form of Eq. 4.10,

$$[\mathbf{d}'_i] = \begin{bmatrix} d'_1 \\ d'_2 \\ \vdots \\ d'_n \end{bmatrix} = [\boldsymbol{K}'][\$] = \begin{bmatrix} L'_1 & M'_1 & 1 \\ L'_2 & M'_2 & 1 \\ \vdots & \vdots & \vdots \\ L'_n & M'_n & 1 \end{bmatrix} [\$] \quad , \qquad 4.13$$

where $[\$] = [\delta x \;\; \delta y \;\; (\Delta s - \Delta F)]^{\mathsf{T}}$. And then fitting a minimum zone based on the solution [$] obtained from Eq. 4.13.

For the example of points measured around the square profile, the location of the solution is $[\delta x \;\; \delta y \;\; (\Delta s - \Delta F)]$ = [0.011, 0.016, 0.091]. Further, to obtained minimum zone distances of points from the solution are,

$[\mathbf{d}'_i]^{\mathsf{T}}$ = [0.070, 0.100, 0.046, 0.076, 0.176, 0.048, 0.078, 0.118, 0.138,

0.118, 0.133, 0.123, 0.043, 0.100, 0.130]

Hence, orientation zone can be defined as

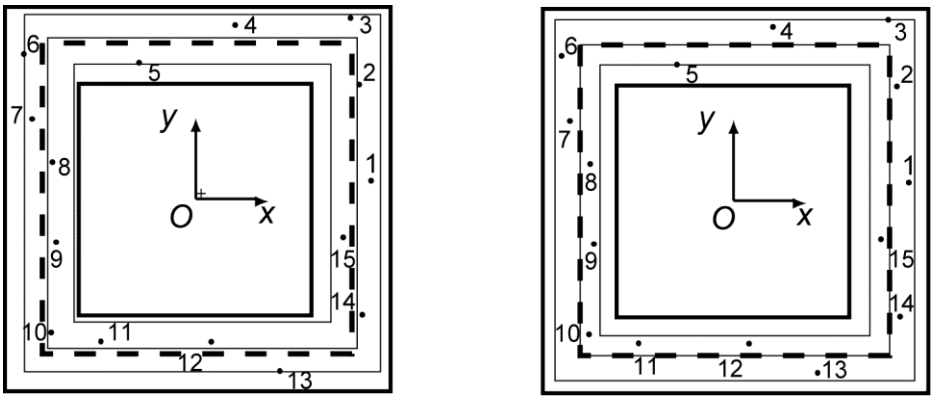

Figure 4.9 (a) The resultant orientation zone. Orientation of the solution is constrained; (b) The resultant positional zone. Position and orientation of the solution is constrained.

$Z = \max[\mathbf{d}'_i] - \min[\mathbf{d}'_i] = 0.176 - 0.043 = 0.133$ mm.

The resultant orientation zone in Figure 4.9(a) is displaced from the origin *O* by (0.011, 0.016). And the two boundaries parallel to the solution are 0.133 mm apart, locked by two points farthest extreme inside and outside.

4.10. Positional zone

For determining positional zone both, position and orientation, of the minimum zone is constrained with respect to Datums. While constraining position and location of the solution, positional zone is defined by determining difference between farthest and nearest point from reference envelope (Figure 4.3), which is parallel to the MSP. Hence form the $[\mathbf{d}'_i]$ values in the Table 4.1, the positional zone is,

$Z = \max[\mathbf{d}'_i] - \min[\mathbf{d}'_i] = 0.15 - 0.02 = 0.13.$

As shown in Figure 4.9(b), positional zone for the point measured around the square profile has not displacements. The positional zone is between two boundaries parallel to MSP are 0.13 mm apart.

CHAPTER 5

LINE PROFILES MADE OF LINE AND ARC SEGMENTS

In this chapter, one more difficulty is added to the problem of least-squares shown in Chapter 4. Extending the method in Chapter 4, envelope equation for arc segments is developed that enables to form matrices [$\boldsymbol{K}'$] and [$\mathbf{d}'_i$] (in Eqn. 4.10) to determine least-squares fit for profiles made of line and arc segments. T-Map for nonsymmetrical line profile (as shown in Figure 5.1), made of line and arc segments, is developed in §§5.1. Envelope equation for arc segment and minimum distance from measured points to it is developed. Envelope equation for line segment is developed in Chapter 4. Example of least-squares fit demonstrated for points measured around the line profile. §§5.1 – 5.5 are reproduced from [24]

The specifications for a sample profile (raised boss) used in this chapter are shown in Figure 5.1. The shape of the boss is controlled by the line-profile tolerance $t = 0.2$ mm relative to the Datums A, B, and C. The specification establishes two parallel curves, the boundaries to the tolerance-zone, at each cross-section of the profile (Figure 5.2). One is 0.1 mm larger along every line normal to the surface, and the other is 0.1 mm smaller, according to the ASME Standard [1].

5.1. T-Map for the sample line profile

The purpose of this section is to supplement, and to briefly introduce, the developments presented in [22] to produce the Tolerance-Map (T-Map) for the

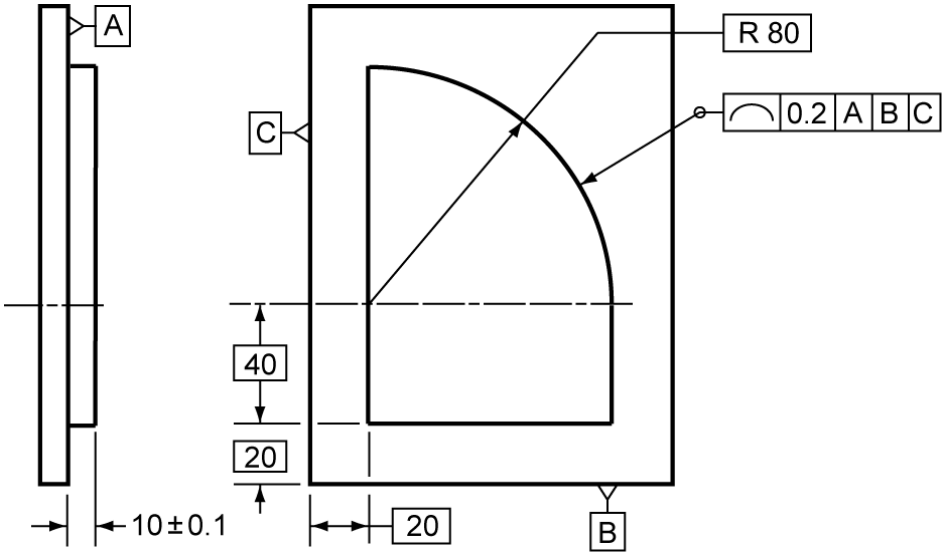

Figure 5.1. Specification for a sample raised profile having sharp corners. Its shape is controlled by the profile tolerance $t = 0.2$ mm relative to Datums A, B, and C.

line-profile specified in Figure 5.1. With this T-Map it will be possible to make a direct comparison of a manufactured profile, as represented with a set of measured points, with the tolerance specifications for it.

As mentioned in §§ 2.3, a Tolerance-Map represents the freedom of a feature in its tolerance-zone. For line-profiles, four independent variables are required to specify the manufacturing variations of a line-profile, such as any one cross-section of the raised boss in Figure 5.1: two translations, one rotation, and change in size. Correspondingly, its T-Map will be four-dimensional (4-D). Therefore, it becomes necessary to choose five of the parallel and/or displaced profiles as basis profiles and to define the T-Map by placing five corresponding basis points $\psi_1 \ldots \psi_5$ to form the vertices of a basis simplex.

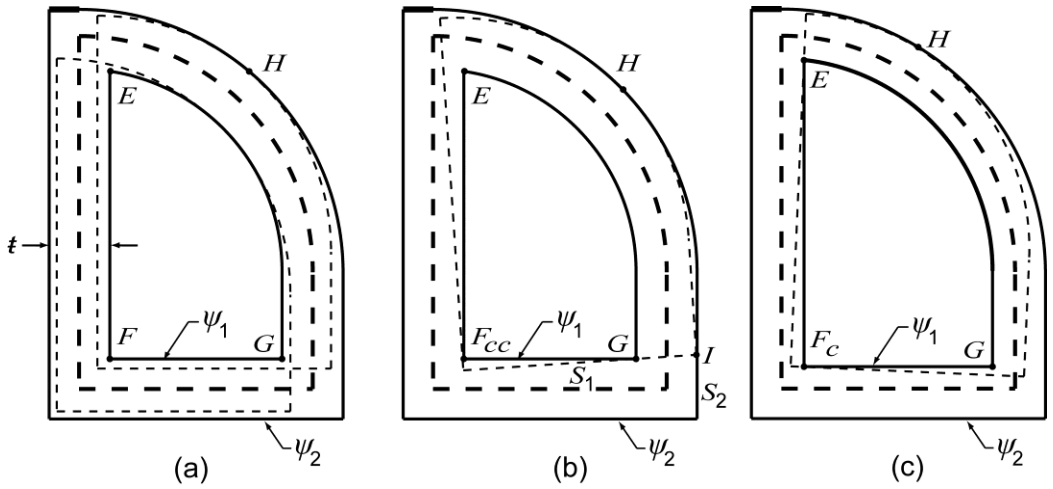

Figure 5.2 Selected displaced locations for the middle-sized profile (dashed-line) in the (exaggerated) tolerance-zone that is specified with the profile tolerance t = 0.2mm from Figure 5.1. (a) Two of its fully translated possibilities (dotted lines) at 45°. (b) Constrained at three points of the boundary and rotated counterclockwise. (c) Also constrained, but rotated clockwise.

The construction of the complete T-Map for the profile specified in Figure 5.1 occurs in four stages: produce the T-Map for the 3-D section of a *square* profile, truncate it with a rhombic prism, truncate that result with opposite 90-deg shells taken from the same oblique circular cylinder to account for the rounded corner, and lastly expand to the fourth (size) dimension.

5.1.1. T-Maps for Square and Rectangular Line-Profiles

The first stage of 3D T-Map for square line profiles is described in §§ 2.3.2. The second stage in development is to account for the rectangular shape of the profile in Figure 5.1 and Figure 5.2. As can be seen with Figure 5.3 and Figure 5.4, a fully rotated middle-sized profile still has freedom to translate in the longer direction, and the limit to rotations is based on the longer length $\bar{b}$. Four of the faces of the octahedral T-Map in Figure 2.3(b) have a steeper slope than

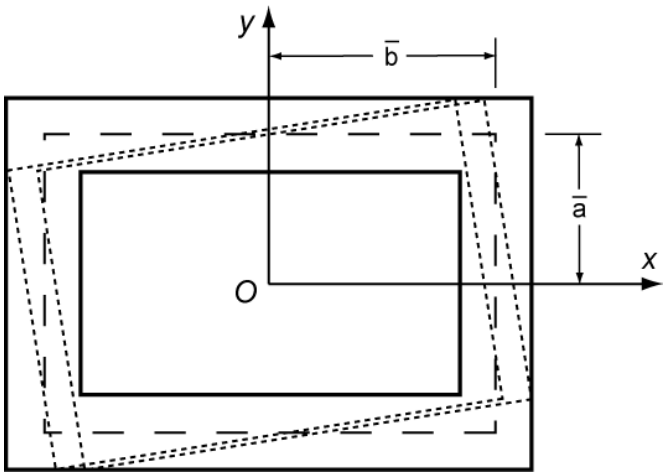

Figure 5.3. The middle-sized profile (dashed-lined rectangle) in the (exaggerated) tolerance-zone that is specified with the profile tolerance t, and two of its fully rotated variational possibilities (dotted lines). From [22].

they did for the square [22]. Hence, the T-Map in Figure 5.4 can be obtained by truncating the T-Map in Figure 2.3(b) with a rhombic prism that has its central axis along e_x and has diagonal dimensions t and t/δ, where $\delta = \bar{b}/\bar{a} > 1$, the aspect ratio for the rectangle. When the same foundations (basis-tetrahedron ψ_{12}, ψ_3, ψ_4, and ψ_5 and scales for overlain Cartesian coordinates) for constructing Figure 2.3(b) are used to construct the 3-D T-Map for the middle-sized *rectangular* profiles, the result is the shape shown in Figure 5.4 in which ψ_5 now lies beyond the boundary of the T-Map. The added two edges in the $e_x\theta'$-plane correspond to the allowable translations of middle-sized profiles that have been rotated to a limit of the tolerance-zone. For instance, the two rotated profiles (dotted lines) in Figure 5.3 show the limits to this translation; they correspond to the two vertices (heavy dots) at the front of the T-Map in Figure 5.4. More detail for this construction can be found in [22].

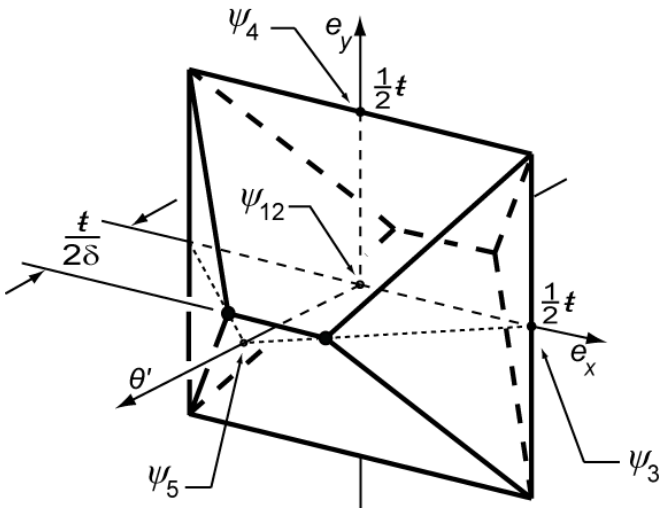

Figure 5.4. That portion of the T-Map for a sharp-cornered rectangular profile which represents the middle-sized rectangles in the tolerance-zone of Figure 5.3. The two vertices at the front (with dots) correspond to the two rotated profiles shown in Figure 5.3. Taken from [22].

Eight of the 10 surfaces forming the 3-D T-Map for the middle-sized profile in Figure 5.2 are obtained by combining the constructions for Figure 2.3(b) and Figure 5.4: truncate the shape in Figure 2.3(b) with the same rhombic prism that has diagonal dimensions t and t/δ. Now, however, its central axis lies along the e_y-axis because the y-axis in Figure 5.1 and Figure 5.2 parallels the longer line-segment of the profile. This completes the second stage, and the results are the 8 planar faces of the T-Map boundary shown in Figure 5.5.

5.1.2. The Invariant Point (Pole) of the Profile

It is helpful to view the displacements e_x, and e_y, and θ of the profile to be the same as those of a moveable lamina on which the middle-sized profile (MSP) is etched. For both the square and rectangular profiles, the undisplaced location, ψ_{12}, is shown with a dashed line (Figure 2.3(b) and Figure 5.4). Additionally, in

Figure 2.3(a) for the square profile, one fully rotated location (CCW) is ψ_5. For two such locations of a lamina, there is a unique point that does not displace. In classic kinematics literature (see e.g. [29] or [30]) this point is called the 'pole' of the two locations. For line-profiles, it is the point to which the eccentricities e_x and e_y apply in the associated T-Map, and it is this point that *must be used* later in the paper as the origin of the reference frame $O_j x_j y_j$ in which all geometric quantities are represented: the measured points, the geometry of the profile, the associated screws, and the regression (least-squares) line-profile. For the square and rectangular profiles in Figure 2.3(a) and Figure 5.3, the pole is at the geometric center O. However, for the rectangular profile, there is not one fully rotated location of the lamina that is locked in place. Of the linear array of possibilities shown in Figure 5.3, we choose the one that is mid-way between the two dotted ones at the limits. Note that, for both the square and rectangular profiles, the fully rotated lamina, which is used in defining the pole and its associated origin of the required coordinate system, corresponds to one of the two points in the T-Map where the θ'-axis pierces the boundary. See Figure 2.3(b), Figure 5.4, and Figure 5.5.

5.1.3. The T-Map for the Middle-Sized Profile in Figure 5.2

The 3-D T-Map for the middle-sized profile in Figure 5.1 and Figure 5.2 is shown in Figure 5.5. This stage is proposed by Yifie He, a graduate student at Design Automation Lab at ASU, and working on development of T-Map for line profiles. The third stage of development is about producing the specific geometry of the curved portions. Their shape may be found analytically by using the

homogeneous coordinate transformation [A] that locates the displaced lamina (carrying the dotted MSP in all parts of Figure 5.2) relative to the fixed (dashed) MSP; it transforms homogeneous coordinates of points *from the displaced frame to the fixed frame*. From any good book on robotics, e.g. [31],

$$[A] = \begin{bmatrix} \cos\theta & -\sin\theta & e_x \\ \sin\theta & \cos\theta & e_y \\ 0 & 0 & 1 \end{bmatrix} \approx \begin{bmatrix} 1 & -\theta & e_x \\ \theta & 1 & e_y \\ 0 & 0 & 1 \end{bmatrix} \qquad 5.1$$

where the small displacements e_x, and e_y, and θ locate the dotted frame relative to the fixed one and the origins of both frames are at the geometric centers of the unrounded rectangles. The second form of [A] in Eq. 5.1 arises because angle θ is always very small (<0.2/80 for the profile in Figure 5.1) and only first-order small quantities need to be retained.

Table 5.1 contains the coordinates of superimposed points in both the displaced and fixed laminae; each row represents a constraint between the laminae. For instance, the third and fourth ones constrain the left and lower line-segments to touch corners F and G, respectively, of the *inner* boundary (Figure 5.2(b)). The last row in the table contains the coordinates of the arc-center corresponding to the contact of a point H on the arc of the dotted MSP with the arc of the *outer* boundary (fixed) of the tolerance-zone (Figure 5.2(b) and Figure 5.2 (c)). The coordinates in Row 5 of Table 5.1 are related by $[x_{Hc}\ y_{Hc}\ 1]^{\mathsf{T}} = [A][-40\ -20\ 1]^{\mathsf{T}}$. As a consequence of the contact at point H, the displaced arc-center

(x_{Hc}, y_{Hc}) lies on a circle of radius $t/2 = 0.1$ mm (Figure 5.1) and with the fixed center $(x,y)=(-40,-20)$, i.e.

$$(x_{Hc}+40)^2+(y_{Hc}+20)^2 = (t/2)^2. \qquad 5.2$$

Table 5.1 Coordinates of contacts in Figure 5.2(b) and Figure 5.2(c)

Point	Coordinates (x, y), mm	
	In Displaced Frame	In Fixed Frame
E	$(-40, y_E)$	$(-39.9, 59.9)$
F_c	$(x_F, -60)$	$(-39.9, -59.9)$
F_{cc}	$(-40, y_F)$	$(-39.9, -59.9)$
G	$(x_G, -60)$	$(39.9, -59.9)$
Arc-center	$(-40, -20)$	(x_{Hc}, y_{Hc})

When the transformed coordinates $x_{Hc} = -40+20\theta+e_x$ and $y_{Hc} = -40\theta-20+e_y$ are combined with Eq. 5.2, and the substitution $\theta' = \overline{a}\ \theta = 40\theta$ (see §3.1) is made, the expression for the curved portion of the T-Map boundary for the line-profile in Figure 5.1 arises:

$$\left(e_x+\frac{1}{2}\theta'\right)^2+(e_y-\theta')^2=(0.1)^2. \qquad 5.3$$

Equation 5.3 is seen to represent an oblique circular cylinder of radius $\mathbf{t}/2$ and with its axis both passing through the origin and having the direction ratios $e_x : e_y : \theta' :: -1/2 : 1 : 1$, so giving an $e_x\, e_y$-section for the T-Map consistent with Fig. 9(d) in [22]. The curved portion of the T-Map boundary is a segment of the first-quadrant 90° shell cut from this cylinder; with one adjacent planar surface, it blends with continuities C^0 and C^1. The short line-segment on the top surface of Figure 5.5(a), and its counterpart opposite in the T-Map, identify the points having C^2-discontinuity (curvature) with the blended planar face.

We now see that each of the contact constraints at points *E*, *F*, *G*, and *H* in Figure 5.2(b) and Figure 5.2 (c) may be formalized by relating the coordinates in one row of Table 5.1. These formalizations, together with Eq. 5.3, may be used to confirm all the surfaces that form the right half of the boundary shown in Figure 5.5(a). For the Rows 1-4 of Table 5.1, it is convenient to use the inverse of transformation [*A*], i.e.

$$[A]^{-1} \approx \begin{bmatrix} 1 & \theta & -e_x \\ -\theta & 1 & -e_y \\ 0 & 0 & 1 \end{bmatrix}, \qquad 5.4$$

in which only first-order small quantities have been retained. Taken together, the matrix equations are

$$\left.\begin{array}{l} \begin{matrix} E & F_c & F_{cc} & G \end{matrix} \\ \begin{bmatrix} -40 & x_F & -40 & x_G \\ y_E & -60 & y_F & -60 \\ 1 & 1 & 1 & 1 \end{bmatrix} = \\ \quad\underbrace{\qquad}_{cw}\quad\underbrace{\qquad}_{ccw} \\ \begin{matrix} \qquad\qquad\qquad\qquad\qquad\qquad E & \qquad F_c & \qquad F_{cc} & \qquad G \end{matrix} \\ \begin{bmatrix} 1 & \theta & -e_x \\ -\theta & 1 & -e_y \\ 0 & 0 & 1 \end{bmatrix} \begin{bmatrix} -39.9 & -39.9 & -39.9 & 39.9 \\ 59.9 & -59.9 & -59.9 & -59.9 \\ 1 & 1 & 1 & 1 \end{bmatrix} \\ \qquad\qquad\qquad\qquad\qquad\qquad\underbrace{\qquad\qquad}_{cw}\qquad\underbrace{\qquad\qquad}_{ccw} \end{array}\right\} \qquad 5.5$$

The counterclockwise displacement in Figure 5.2(b) is constrained at points *G* and *H*, and also at point *F* with the coordinates in Row 3 of Table 5.1. From Eqs. 5.5, the constraints at F_{cc} and *G* lead respectively to

$$\left.\begin{array}{l} -40 = -39.9 - 59.9\theta - e_x \\ -60 = -39.9\theta - 59.9 - e_y \end{array}\right\}$$

or to

$$\left.\begin{array}{r} e_x + 1.5\,\theta' = \mathbf{t}/2 \\ e_y + \theta' = \mathbf{t}/2 \end{array}\right\} \qquad 5.6$$

The first and second of Eqs. 5.6 are seen to be algebraic representations for the right-front vertical face and the top-front face of the T-Map in Figure 5.5(a). When Eqs. 5.6 are combined with Eq. 5.3, the vertex at the front of the T-Map is identified (heavy dot in Figure 5.5(a)) with the coordinates $(e_x, e_y, \theta') = (0.07, 0.08, 0.02)$ mm. It is this vertex in the T-Map that represents the dotted MSP in Figure 5.2(b).

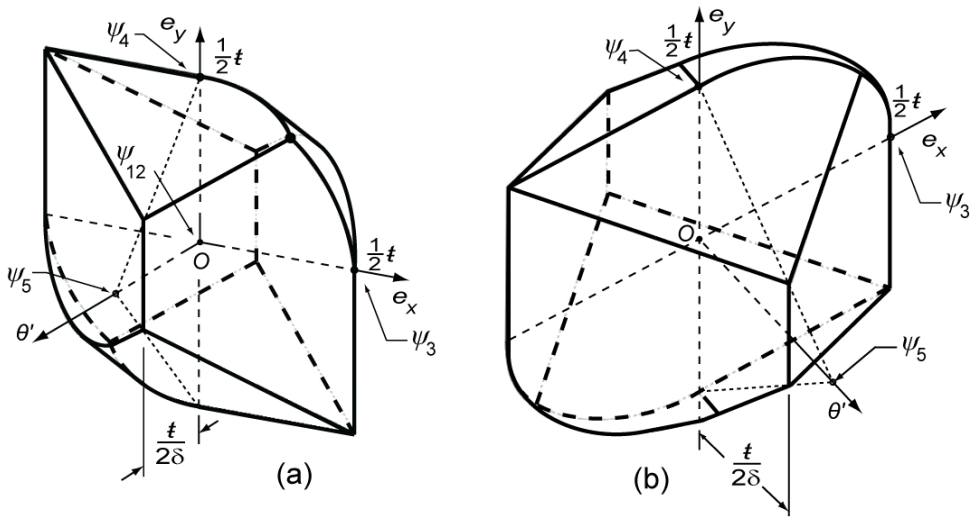

Figure 5.5. The 3-D T-Map for the middle-sized profile in Figure 5.1 and its tolerance-zone in Figure 5.2. (a) Aligned similarly to the T-Maps in Figure 2.3(b) and Figure 5.4. (b) At an orientation that makes the cylindrical portions more apparent.

Using the same procedure for points *E*, *F*, and *H*, *F* now represented with the coordinates in Row 2 of Table 5.1, algebraic forms for the two faces at the top-rear and the right-rear of the T-Map emerge for Figure 5.5(a), i.e.

$$\left.\begin{aligned} e_x - 1.5\,\theta' &= \mathbf{t}/2 \\ e_y - \theta' &= \mathbf{t}/2 \end{aligned}\right\} \qquad 5.7$$

(Note that, in Figure 5.2(c), the inner boundary of the tolerance-zone must be drawn closer to the MSP, i.e. the exaggeration reduced, so that the contacts of constraint are realistic.)

5.2. T-Maps for different sizes of the profile

Consider a case when the profile size is very close to the size of the outer boundary of the tolerance zone. Then, the displacements of the profile are

constrained only by the outer boundary; the profile never contacts with the inner boundary. In this section, the contacts between the profiles (of sizes $-t/2 < \Delta F < 0$ and $0 < \Delta F < t/2$) and boundaries of the tolerance zone are studied, and equations of surfaces for the corresponding T-Maps are constructed for each distinct range of these different sizes. The objective of this sub-section is to produce the morphological forms of the 3D hypersections of the 4-D T-Map over the full range of allowable profile size. I am grateful to Mr. Yifei He for his assistance in using his *intersection-of-primitive method*, a form of CAGD, to identify or confirm all of these morphological forms.

Consider a profile of arbitrary size with its each segment denoted by integers (1_m to 4_m) and vertices denoted by alphabets (a_m to d_m) in Figure 5.6(a).

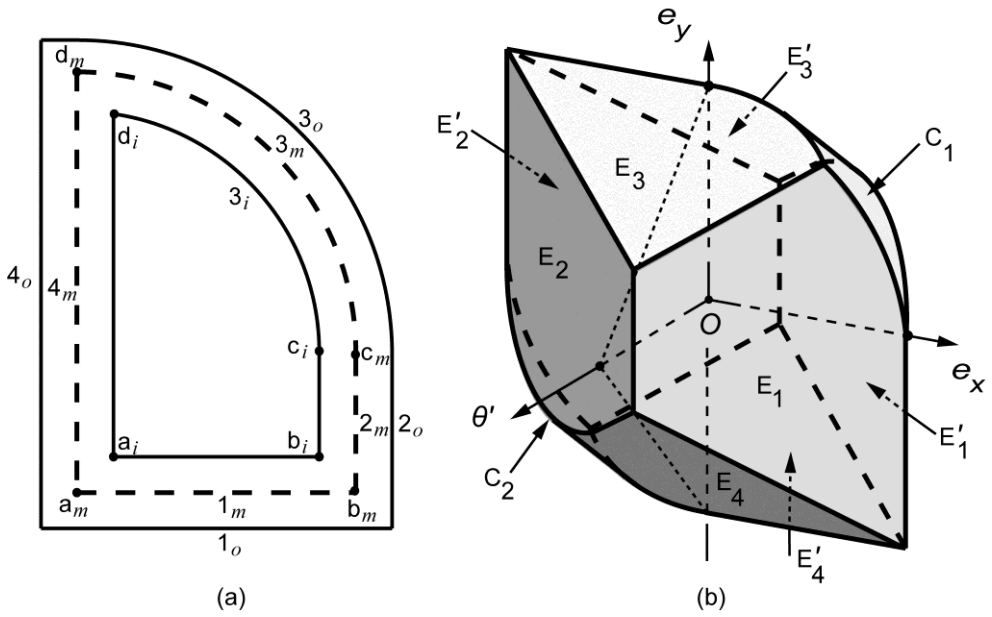

Figure 5.6. (a) The profile of arbitrary size (in dashed line) constrained between the two boundaries of the tolerance-zone. (b) Faces of the T-Map are formed due to contacts between the profile the boundaries of the tolerance zone.

For outer and inner boundaries of the tolerance zone, subscripts $_o$ and $_i$ are used to denote corresponding segments and vertices respectively. Also, as shown in Figure 5.6(b), the faces of the corresponding T-Map of the profile (in Figure 5.6(a)) are denoted by, E_i –for planar faces on front side, E'_i -for planar faces on rear side, and C_i -the cylindrical faces. Notice that the T-Map shown in Figure 5.6(b) is identical to 3D T-Map for the MSP (Figure 5.5), and we are interested to study variations of it while the size of the profile varies.

5.2.1. T-Maps for allowable profiles larger than the MSP

Any contact between the profile and the tolerance zone boundaries restrain the profile motion in the direction perpendicular to the boundary tangent, at the contact point. The corresponding point in the T-Map space lies on one surface of the T-Map; for example when the profile is displaced in the *x*-direction till extreme extents and rotated CCW, because of the contact between vertex b_m and line segment 2_o of outer boundary, the corresponding point in T-Map space lies on face E_1 (Shown in Figure 5.6(b)). Similarly, when two vertices of the displaced profile are in contact with boundaries simultaneously, the corresponding point in T-Map lies on an edge (intersection of two faces) of the T-Map; and for the three or more simultaneous contacts, the point lies at a vertex (intersection of three or more faces) of the T-Map. This subsection determines first, second and third contact, for the profiles larger than MSP, due to which the profile is constrained. Based on the contacts, the equations of surfaces of the T-Map are derived. This subsection is divided into four cases of extreme displacements in 45˚, 135˚, 225˚,

and 315˚ directions. In each case, rotations in the CCW and CW directions are applied to the profile until possible extent.

Case-1: Profile is displaced in extreme upper left direction (135˚)

Consider a profile larger than MSP ($\Delta F > 0$) is translated in 135˚ direction up to possible extent, as shown in Figure 5.7(a). The first contact occurs at vertex d_m with outer boundary segments 4_o and 3_o. For convenience, contacts are denoted as d_m4_o and d_m3_o. When the profile is rotated in CCW direction, two immediate contacts d_m4_o, 3_m3_o occurs. On the other hand, when the profile is rotated in CW direction, two immediate contacts are d_m3_o and a_m4_o.

First, consider the CCW rotation of the profile. Due to the two contacts the rotation of the profile is analogous to a very small double slider mechanism with sliders at contacts d_m4_o and 3_m3_o (Figure 5.7(b)), sliding along the tangents to the tolerance zone boundary. Since the profile is a part of the link connecting two sliders, the profile rotates about instantaneous center *P* of the mechanism. For very small possible displacements, *P* (approximately) overlaps with vertex d_m Figure 5.7(b). There are two possibilities of occurrence for the third contact during CCW rotation: contact 1_mb_i, and contact b_m2_o (shown in Figure 5.7(b)). For the occurrence of contact 1_mb_i, the shortest distance that the line segment 1_m requires to displace is $t/2+\Delta F-(t/2-\Delta F) = 2\Delta F$, in *y*-direction. Because of the rotation about *P*, the contact at 1_mb_i satisfies equation,

$$2\Delta F = 80\,\theta\,, \tag{5.8}$$

where θ is angle of rotation of the profile about instantaneous center P. Here the second order terms are neglected. Similarly, contact for vertex b_m requires to displaced by $t/2-\Delta F+(t/2-\Delta F) = t-2\Delta F$ in x-direction for contact $b_m 2_o$ to occur. And the equation that satisfies the contact is,

$$t - 2\Delta F = 120\,\theta\,. \tag{5.9}$$

From Eqs. 5.8 and 5.9, the size of the profile, at which both the contacts occurs, is $\Delta F = t/5$. It is apparent that the contact $1_m b_i$ limits angle θ when the size of the profile is $\Delta F \leq t/5$, and contact $b_m 2_o$ limits θ when $\Delta F \geq t/5$.

Now, we will further analyze each case for further possible rotations. For $\Delta F \leq t/5$ (when contact $1_m b_i$ occurs) further CCW rotation changes the kinematic configuration to that as shown in Figure 5.7(d). With rotation about the new instantaneous center P', contact $b_m 2_o$ occurs as shown in Figure 5.7(e) so that the three contacts are $1_m b_i$, $b_m 2_o$ and $d_m 4_o$. This identifies the upper end of the vertical edge at the front of the 3-D hypersection. When the size of the profile is $\Delta F \geq t/5$, rotation of the profile is constrained between three contacts $d_m 4_o$, $b_m 2_o$ and $3_m 3_o$, as shown in Figure 5.7(f), and the face E_3 (Figure 5.6 and Figure 5.15) has disappeared from the T-Map.

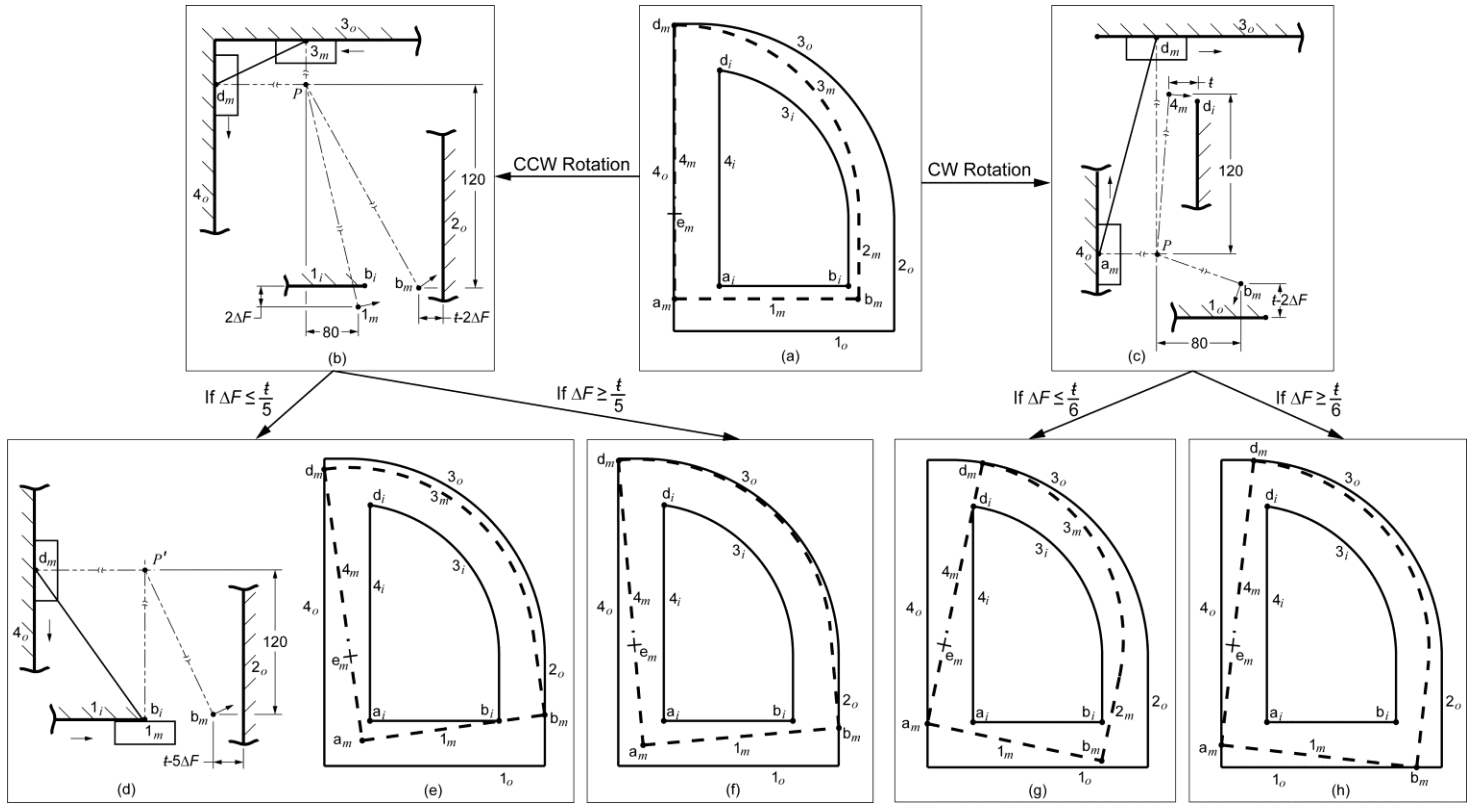

Figure 5.7. (a) The profile of size $\Delta F > 0$ is displaced in extreme upper left direction; (b) Double slider mechanism formed when the configuration in (a) rotated CCW; (c) Double slider mechanism formed when the configuration in (a) rotated CW; (d) contact-$1_m b_i$ occurs when profile size is $\Delta F \le t/5$. For clarity, line segment 1_m is represented as a point on the line segment, which will form contact$1_m b_i$; (e) For the configuration in (d), the profile slide at contact-$d_m 4_o$ and contact-$1_m b_i$, and new double slider mechanism occurs; (f) For $\Delta F \ge t/5$, the CCW rotation of the profile is constrained by contact-$d_m 4_o$ and contact-$b_m 2_o$; (g) CW rotation is constrained by contact-$4_m d_i$ for $\Delta F \le t/6$; (h) CW rotation is constrained by contact-$b_m 1_o$ for $\Delta F \ge t/6$.

When the profile is rotated in clockwise (CW) direction, based on contact a_m4_o and contact d_m3_o the configuration of double slider mechanism is formed as shown in Figure 5.7(c). When the profile rotates about instantaneous center *P*, the two possible candidates for the third contact are b_m1_o and 4_md_i. The equations satisfying the contact b_m1_o is,

$$\pi - 2\Delta F = 80\,\theta, \tag{5.10}$$

and contact 4_md_i is,

$$\pi = 120\,\theta. \tag{5.11}$$

Solving Eqs. 5.10 and 5.11, gives the critical size at which both the contacts occur as, $\Delta F = \pi/6$. As in Figure 5.7(g) and (h), it is apparent that for $\Delta F \leq \pi/6$, the third contact is 4_md_i, the place at the back of the 3-D hypersection where face E_1' intersects the negative θ'-axis. For $\Delta F \geq \pi/6$, the third contact is b_m1_o and, in this range of ΔF, the vertical line-segment at the back of the 3-D hypersection no longer intersects the θ'-axis. Instead, axis θ' pierce the face E_4'.

Case-2: Profile is displaced in extreme lower right direction (315°)

When the profile is larger than the MSP and displaced in lower right direction to extreme extent, the displacement is constrained by the contact between vertex b_m and line segments 1_o and 2_o, as shown in Figure 5.8(a). Again, for two possible rotation directions: CCW and CW, corresponding double slide mechanisms are shown in Figure 5.8(b) and (c) respectively. While the profile

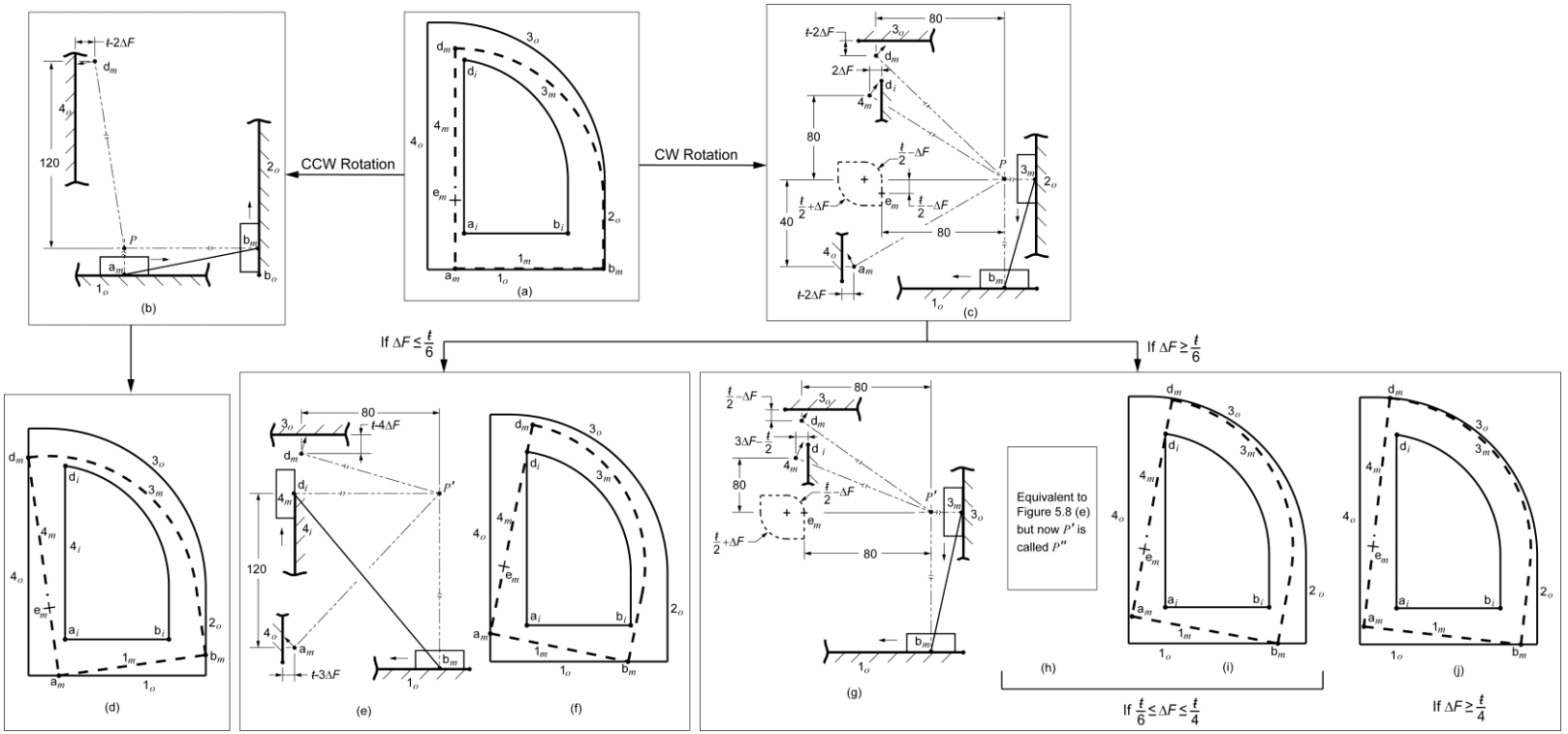

Figure 5.8. (a) The profile of size $\Delta F \geq 0$ is displaced in extreme lower right direction; (b) Double slider mechanism formed when the profile in (a) is rotated CCW; (c) Double slider mechanism formed when the profile in (a) rotated CW; (d) The CCW rotation is constrained by three contacts: contact-a_m1_o, contact-b_m2_o, contact-d_m4_o; (e) If $\Delta F \leq t/6$, the second contact occurs at $4_m d_i$; (f) Further rotation is constrained by the third contact a_m4_o; (g) If $\Delta F \geq t/6$, the profile rolls due to the contact between arc segments 3_m and 3_o. (h) If $t/6 \leq \Delta F \leq t/4$, the contact $4_m d_i$ occurs and the double slider mechanism is same as in (e) of this figure; (i) If $t/6 \leq \Delta F \leq t/4$, further rotation is constrained by the third contact d_m3_o; (j) If $\Delta F \geq t/4$, the profile is constrained by contact-d_m3_o and contact-b_m1_o.

rotates CCW, contacts represented as sliders, are a_m1_o and b_m2_o (Figure 5.8(b)). And the rotation of the profile will be constrained when contact d_m4_o occurs (Figure 5.8(d)). The contacts a_m1_o, b_m2_o and d_m4_o identify the lower end of the vertical edge at the front of the 3-D hypersection.

For CW rotation, contacts b_m1_o and 3_m2_o form a double slider mechanism. There are two possibilities for the third contact to occur: 4_md_i and 3_m3_o. Since the distance between line segment 4_m and vertex d_i is $\boldsymbol{t}/2 + \Delta F - (\boldsymbol{t}/2 - \Delta F) = 2\Delta F$, contact 4_md_i satisfies,

$$2\Delta F = 80\,\theta\,. \qquad 5.12$$

When the arc segment of the profile contacts tolerance zone boundaries, the arc center e_m lies on the dotted path shown in Figure 5.8(c). When it comes in contact with the arc segment of the outer boundary, the center e_m traces arc (dotted path in Figure 5.8(c)) with radius of $(80+\boldsymbol{t}/2) - (80+\Delta F) = \boldsymbol{t}/2-\Delta F$. Where $(80+\boldsymbol{t}/2)$ is radius of arc segment of outer boundary; and $(80+\Delta F)$ is radius of the arc segment of the profile of size (MSP+ΔF). Also, ΔF carries the sense of direction, i.e. ΔF is positive for the profiles larger than the MSP and negative for the profiles smaller than the MSP. Similarly, when the arc segment of the profile comes in contact with the arc segment of the inner boundary, the arc center e_m traces the arc with radius $(80+\Delta F) - (80-\boldsymbol{t}/2) = \boldsymbol{t}/2 + \Delta F$. For this case, the arc center e_m is displaced in the downward y-direction by $\boldsymbol{t}/2 - \Delta F$. Contact 3_m3_o

occurs when the arc center is lying on the upper right arc segment of the dotted path. Hence the contact 3_m3_o occurs when

$$\text{ŧ}/2 - \Delta F = 80\,\theta \tag{5.13}$$

is satisfied. From Eqs. 5.12 and 5.13, the critical size of the profile when both the contacts occur is $\Delta F = \text{ŧ}/6$. Contact $4_m\mathrm{d}_i$ occurs when the profile size is $\Delta F \leq \text{ŧ}/6$, and contact 3_m3_o occurs when $\Delta F \geq \text{ŧ}/6$.

Correspondingly, it is worth noting that the equation of cylinder for MSP represented in Eq. 5.3 changes based on its contact with the outer and inner boundaries. When the arc segment of the profile contacts the outer boundary, it forms a 90º cylindrical shell in first quadrant of equation,

$$\left(e_x + \frac{1}{2}\theta'\right)^2 + \left(e_y - \theta'\right)^2 = \left(0.1 - \Delta F\right)^2. \tag{5.14}$$

When the arc segment of the profile is in contact with the inner boundary, it forms a 90º cylindrical shell in the third quadrant of equation,

$$\left(e_x + \frac{1}{2}\theta'\right)^2 + \left(e_y - \theta'\right)^2 = \left(0.1 + \Delta F\right)^2. \tag{5.15}$$

These two equations are used to produce T-Map of different sizes along with equations of the planar faces developed later.

For $\Delta F \leq \ell/6$, when contact $4_m d_i$ occurs, the double slider mechanism configuration changes to as shown in Figure 5.8(e). When the profile rotates about new instantaneous center P', two possibilities of the third contact arises: $a_m 4_o$ and $d_m 3_o$. When contact $a_m 4_o$ occurs, it satisfies

$$\ell - 3\Delta F = 120\ \phi. \tag{5.16}$$

Here ϕ is the additional amount of rotation about the new instantaneous center P' for the contact to occur. And when contact $d_m 3_o$ occurs, it satisfies

$$\ell - 4\Delta F = 80\ \phi. \tag{5.17}$$

From Eqs. 5.15 and 5.16, both the contact occurs at the critical size $\Delta F = \ell/6$. While determining amount of rotation (ϕ) in equations 5.15 and 5.16 for different ΔF, it is found that the contact $a_m 4_o$ occurs when $\Delta F \leq \ell/6$ (Figure 5.8(f)), and $d_m 3_o$ occurs when $\Delta F \geq \ell/6$ (Figure 5.8(i) and (j)). However, there are some more details need to be address for $\Delta F \geq \ell/6$ that changes form of the T-Map.

Let's go back to the conclusion from Eqs. 5.12 and 5.13. For $\Delta F \geq \ell/6$, the second contact will be formed at $3_m 3_o$, as shown in Figure 5.8(g). The two possible candidates for the third contact are $4_m d_i$ and $d_m 3_o$. For contact $4_m d_i$ to occur, vertex 4_m must displace $2\Delta F - (\ell/2 - \Delta F) = 3\Delta F - \ell/2$ in the x-direction; where $(\ell/2 - \Delta F)$ is the displacement of the vertex during the rotation in previous kinematic setting. The contact satisfies equation,

$$3\Delta F - \mathbf{t}/2 = 80\ \phi. \qquad 5.18$$

Similarly, for contact $d_m 3_o$ the vertex d_m requires to displace $\mathbf{t} - 2\Delta F - (\mathbf{t}/2 - \Delta F) = \mathbf{t}/2 - \Delta F$. And the contact satisfies equation,

$$\mathbf{t}/2 - \Delta F = 80\ \phi. \qquad 5.19$$

Solving Eqs. 5.18 and 5.19, the critical size when both contacts occurs is $\Delta F = \mathbf{t}/4$.

For size $\Delta F \leq \mathbf{t}/4$, contact $4_m d_i$ occurs that leads to configuration similar to as shown in Figure 5.8(e), except the instantaneous center is now denoted as P'' for this third kinematic setting. From the conclusion of Eqs. 5.16 and 5.17, that corresponds to Figure 5.8(e), for $\mathbf{t}/6 \leq \Delta F$ and $\Delta F \leq \mathbf{t}/4$, further rotation about P'' constrains the profile by third contact at $d_m 3_o$ (Figure 5.8(i)). If the profile size is $\Delta F \geq \mathbf{t}/4$, the arc segment of the profile rolls and slide over the arc segment of the outer boundary, until the vertex d_m contacts arc segment 3_o, as shown in Figure 5.8(j). Figure 5.8(f) and (i) conclude that contact between line segment 4_m and vertex d_i occurs for the profiles of size $\Delta F \leq \mathbf{t}/4$.

When the MSP is displaced to the lower right corner of the tolerance-zone, its two vertical line-segments, 2_m and 4_m, coincide with vertical line-segments 2_o and 4_i of the tolerance-zone boundary, and segments 1_m and 1_o coincide; so that *all* allowable CW rotation is controlled in part by point d_i. However, when a profile only slightly larger than the MSP (e.g. $\Delta F = 0.02\mathbf{t}$), is displaced to the lower right corner, only segment 2_m coincides with 2_o (Figure 5.8(a)), so that CW

rotations from this location cannot at first be controlled by point d_i. Instead, they are controlled partially by arc-segment 3_m contacting boundary-segment 2_o. This explains the presence of the narrow face in the 3-D hypersection labeled $\Delta F = 0.02\boldsymbol{t}$ in Figure 5.15. Of course, with even more constrained CW rotation of the same profile ($\Delta F = 0.02\boldsymbol{t}$), constraint will shift from 3_m-2_o to 4_m-d_i (Figure 5.8(h)), so the corresponding relationships among T-Map coordinates produce an edge in the 3-D hypersection that is parallel to the edge formed as the intersection of faces E_1' and E_4'. in Figure 5.6(b). As ΔF increases even more, the width of the narrow face in the hypersection increases, and also its shape changes from a trapezoid to a triangle ($\Delta F = 0.25\boldsymbol{t}$ in Figure 5.15).

Case-3: Profile is displaced in extreme upper right direction (45˚)

The third case is when the profile is displaced at 45˚ to the greatest possible extent; the arc segment of the profile 3_m comes in contact with the arc segment of the outer boundary, as shown in Figure 5.9(a). For rotations in CCW and CW direction, arc segment 3_m at first rolls on arc segment 3_o, as shown in Figure 5.9(b) and (c).

There are three possibilities of occurrence of contacts: b_m2_o, 1_mb_i and d_m4_o (Figure 5.9(b)), while the profile rotates CCW. The contact b_m2_o will occur first, since the (shortest) distance for vertex b_m requires to travel is $\boldsymbol{t}/2-\Delta F - (\boldsymbol{t}/2-\Delta F)/\sqrt{2}$, which is smallest among the all three contacts. Moreover, the vertex b_m is farthest from the instantaneous center, hence, covers the largest distance during the profile rotation.

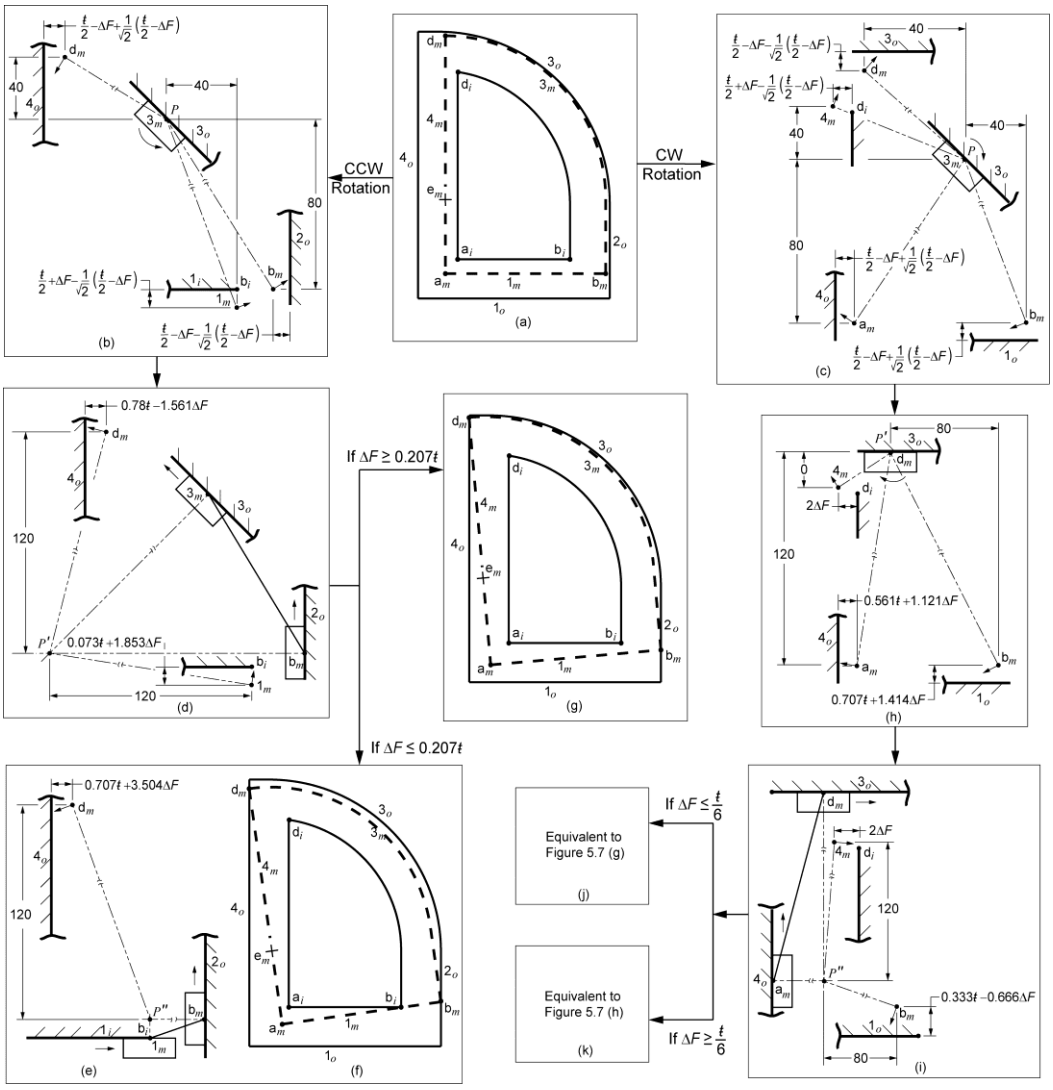

Figure 5.9. (a) The profile of size $\Delta F \geq 0$ is displaced in extreme upper right direction (45˚); (b) The profile rotates in CCW direction about P at contact 3_m3_o; (c) The profile rotates in CW direction about P at contact 3_m3_o; (d) For CCW rotation, second contact occur at b_m2_o; (e) If $\Delta F \leq 0.207t$, second contact 1_mb_i occurs; (f) The oration is constrained by contact d_m4_o, for the configuration in (e); (g) If $\Delta F \geq 0.207\ t$ contact 2_m2_o constrain rotation of the profile; (h) For CW, the arc segment of the profile rolls over the arc segment of the outer envelope that result into migration of the first contact from 3_m3_o to d_m3_o; (i) Second contact occurs when vertex a_m contact line segment 4_o; (j) If $\Delta F \leq t/6$, CW rotation will be constrained similar to in Figure 5.7(g); (k) If $\Delta F \geq t/6$, CW rotation will be constrained similar to in Figure 5.7(h).

The double slider mechanism formed due to the two contacts, 3_m3_o and b_m2_o, is shown in Figure 5.9(d). Contacts d_m4_o and 1_mb_i, are next candidates for occurrence of the third contact. Based on their distance from P, vertex d_m and a point on line segment 1_m travel $0.5(t/2-\Delta F-(t/2-\Delta F)/\sqrt{2})$, until contact b_m2_o occurs, in the direction normal to the tangents. After the occurrence of contact b_m2_o, the contact 1_mb_i occurs when,

$$0.073t + 1.853\Delta F = 120\phi \tag{5.20}$$

satisfies, and contact d_m4_o occurs when,

$$0.78t - 1.561\Delta F = 120\phi \tag{5.21}$$

satisfies. Solving equalities in Eqs. 5.20 and 5.21, critical size at which both the contacts occur is $\Delta F = 0.207t$. At this value of $\Delta F = 0.207t$, the edge between faces E_1 and E_3 reduces to a point so that faces E_1, E_2, and E_3 together with cylindrical shell C_1 have a common vertex. Of course, this corresponds to the result in *Case-1* ($\Delta F = 0.2t$) at which face E_3 vanishes with increasing ΔF. Although the two results $\Delta F = 0.207t$ and $\Delta F = 0.2t$ for the differential size at which Face E_3 vanishes appear inconsistence their difference arise because of second-order influence. Note that $\Delta F = 0.207t$ arose from an analysis using cylindrical surface C_1 along with two planar faces E_1 and E_3, but $\Delta F = 0.2t$ arose from two planar faces E_2 and E_3. As shown in Figure 5.9(e), for $\Delta F \leq 0.207t$ third contact occurs at 1_mb_i. Further rotation changes double slider mechanism

configuration, and the rotation of the profile constrained as shown in Figure 5.9(f). For $\Delta F \geq 0.207t$ third contact $d_m 4_o$ occurs and constrains the rotations as shown in Figure 5.9(g).

For CW rotation, the configuration is shown in Figure 5.9(c). Since two arc segments are in contact, the profile rolls until contact $d_m 3_o$ occurs (Figure 5.9(h)). Then it will rotate about the contact $d_m 3_o$ until the second contact $a_m 4_o$ occurs (Figure 5.9(i)). At this moment, two possible contacts for further CW rotation are $4_m d_i$ and $b_m 1_o$. Contact $4_m d_i$ occurs when it satisfies

$$2\Delta F = 120\beta. \tag{5.22}$$

Here β is further additional amount of rotation about the new instantaneous center P'' for the next contact to occur. Contact $b_m 1_o$ occurs when it satisfies,

$$0.333t + 0.666\Delta F = 80\beta. \tag{5.23}$$

Solving equalities in Eqs. 5.22 and 5.23, the critical size at which both the contacts occur is $\Delta F = t/6$. For $\Delta F \leq t/6$, the rotation of the profile will be constrained by the third contact $4_m d_o$, which is equivalent to Figure 5.7 (g). For $\Delta F \geq t/6$, the rotation of the profile will be constrained by the third contact $b_m 1_o$, which is equivalent to Figure 5.7 (h).

Case-4: Profile is displaced in extreme lower left direction (225˚)

For profiles larger than the MSP and displaced in 225˚ direction, there are two possibilities of the first contact as shown in Figure 5.10(a): contact $3_m 3_i$ when

two arcs are in contact, and contact $a_m a_o$ when vertex a_m is incident with vertex a_o. The critical size when both the contacts occurs satisfies,

$$80+\Delta F-(80-\boldsymbol{t}/2)=\sqrt{2}\,(\boldsymbol{t}/2-\Delta F)).$$

or 5.24

$$\Delta F+\boldsymbol{t}/2=\sqrt{2}\,(\boldsymbol{t}/2-\Delta F)).$$

Here, the terms in left hand side is distance covered by the profile when the arc segments are in contact, and the term in right hand side is distance covered by the profile when vertex a_m is incident with vertex a_o. Solving Eq. 5.24 provides the critical size $\Delta F = 0.0858\boldsymbol{t}$. It is apparent that for $\Delta F \leq 0.0858\boldsymbol{t}$ contact $3_m 3_i$ occurs, and contact $a_m a_o$ occurs when $\Delta F \geq 0.0858\boldsymbol{t}$.

For the case of $\Delta F \leq 0.0858\boldsymbol{t}$, when the profile is rotated in CCW, as shown in Figure 5.10(b) the profile rotates about instantaneous center *P*, located at contact $3_m 3_i$. Three vertices, d_m, a_m and b_m may come in contact with the outer envelope during CCW rotation. Notice that vertices d_m and a_m travels same distance to form contact. Moreover, they are at equal distances from *P*. Hence contacts $d_m 4_o$ and $a_m 1_o$ occurs, when it satisfies,

$$\boldsymbol{t}/2-\Delta F-\frac{1}{\sqrt{2}}\,(\boldsymbol{t}/2+\Delta F)=40\theta, \qquad 5.25$$

and contact $b_m 2_o$ occurs when it satisfies,

$$\boldsymbol{t}/2-\Delta F+\frac{1}{\sqrt{2}}\,(\boldsymbol{t}/2+\Delta F)=80\theta. \qquad 5.26$$

Solving Eqs. 5.25 and 5.26, the critical size when the profile is constrained by all three contact is $\Delta F = -0.179/t$. Contacts d_m4_o and a_m1_o occur when $\Delta F \geq -0.179/t$, and b_m2_o occurs when $\Delta F \leq -0.179/t$. But, for this case ($\Delta F > 0$), contacts d_m4_o and a_m1_o occur at same time and forms mechanism as shown in Figure 5.10(c). Such configuration makes the arc segment of the profile 3_m to depart from the arc segment of the inner envelope 3_i and allows further rotation of the profile. Hence as shown in Figure 5.10(c) and (e), with further rotation about new instantaneous center P', the profile will be constrained by third contact b_m4_o. On the other hand, for profiles of size $\Delta F \geq 0.0858t$, as shown in Figure 5.10(d), vertices d_m and a_m contact with line segments 4_o and 1_o respectively. The rotation of the profile about P forms third contact b_m1_o. This conclude that for this case, CCW rotation of all the profiles $\Delta F > 0$, are constrained by three contacts d_m4_o, a_m1_o and b_m2_o, which represents a vertex at lower end of the vertical edge at the front of the 3D hypersection..

For CW rotation, when profile size $\Delta F \leq 0.0858t$, as shown in Figure 5.10(f), the profile rotates about instantaneous center P at contact 3_m3_i. It is obvious that the second contact will occur when vertex a_m contacts line segment 4_o (Figure 5.10(g)). Now the profile will rotate about new instantaneous center P'', until contact b_m1_o occurs. Further rotation detach the arc segment 3_m from arc segment 3_o and forms double slider mechanism as shown in Figure 5.10(h). Further rotation about new instantaneous center P''', as shown in Figure 5.10(j), the profile will be constrained by three contacts a_m4_o, b_m1_o and 4_md_i.

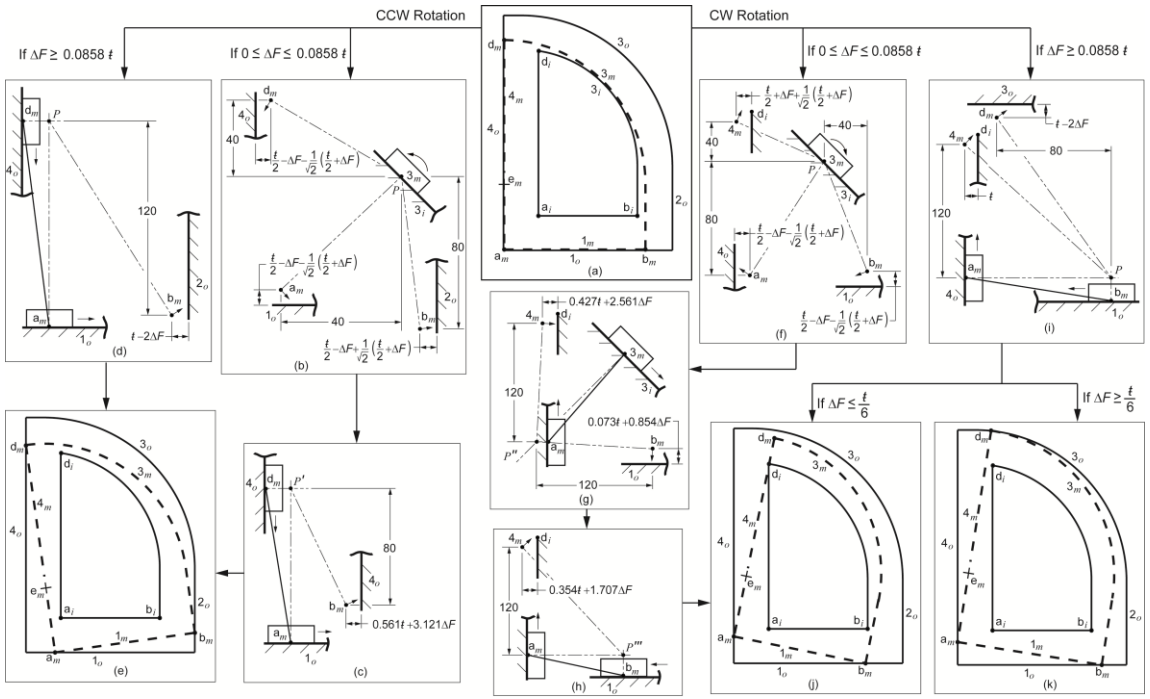

Figure 5.10. (a) The profile of size $\Delta F \geq 0$ is displaced in extreme lower left direction (225°); (b) If $\Delta F \leq 0.0858\ t$, CCW rotation occurs about contact 3_m3_i; (c) Next two contacts d_m4_o and a_m1_o occur simultaneously; (d) When the profile is of size $\Delta F \leq 0.0858t$ and rotated CCW, two contacts are d_m4_o and a_m1_o; (e) The CCW rotation is constrained by contacts d_m4_o and a_m1_o and b_m2_o; (f) If $\Delta F \leq 0.0858\ t$, CW rotation occurs about contact 3_m3_i; (g) For CW rotation, next immediate contact occurs when vertex a_m contacts line segment 4_o; (h) For further CW next contact b_m1_o occurs; (i) For the configuration in (h), CW rotation of the profile is constrained by the third contact 4_md_i; (i) If $\Delta F \geq 0.0858\ t$, CW contacts a_m4_o and b_m1_o occur; (j) The CW rotation for the configuration in (h), and for $\Delta F \leq t/6$ in configuration in (i), the profile is constrained by three contacts a_m4_o,b_m1_o and 4_md_i; (k) For the configuration in (i), if $\Delta F \geq t/6$, the CW rotation of the profile is constrained by a_m4_o,b_m1_o and d_m3_o.

For $\Delta F \geq 0.0858t$ and CW rotation of the profile, two vertices a_m and b_m contacts 4_o and 1_o as shown in Figure 5.10(i). The third contact may occur either when line segment 4_m contact vertex d_i or when vertex d_m contact arc segment 3_o. For contact $4_m d_i$ occurs when it satisfies,

$$t = 120\theta, \tag{5.27}$$

And contact $d_m 3_o$ occurs when it satisfies,

$$t - 2\Delta F = 80\theta, \tag{5.28}$$

From Eqs. 5.27 and 5.28, the critical size when both the contact $4_m d_i$ and $d_m 3_o$ occur is $\Delta F = t/6$. If the of the profiles is $\Delta F \leq t/6$, the rotation is constrained by three contacts $a_m 4_o$, $b_m 1_o$ and $4_m d_i$ (Figure 5.10(j)), and if $\Delta F \geq t/6$ the rotation is constrained by the three contacts $a_m 4_o$, $b_m 1_o$ and $d_m 3_o$ (Figure 5.10(k)).

Summary of the contacts:

From the four cases of profile size $\Delta F \geq 0$, contacts are summarized in Table 5.2. Notice that the two contact: $1_m b_i$ and $4_m d_i$ do not occurs after certain ΔF. Based on the contacts, equation of faces of the T-Maps are determined, using inverse transformation (Eq. 5.4), for the contacts $1_m b_i$ and $4_m d_i$, and forward transformation (Eq. 5.1) for the remaining contacts. Following the similar procedure as in 5.1.3, algebraic equations of planes on T-Map, corresponding to each contact, are obtained as shown in last column of Table 5.2.

[1]Table 5.2 Coordinates of contacts abstracted for profile size $\Delta F>0$, from Figure 5.7 to Figure 5.10.

Faces in Fig.5.6	Con-tact	Size limitation for contacts	Coordinates (x, y), mm		Refer Figure	Equation of planes/Cylinders
			In Displaced Frame	In Fixed Frame		
E_2	d_m4_o		$(-40-\Delta F, 60+\Delta F)$	$(-40.1, y_{dm4o})$	5.7(e),(f)	$e_x-1.5\theta' = t/2-\Delta F$
E_3'	d_m3_o		$(-40-\Delta F, 60+\Delta F)$	$(x_{dm3o},60.1)$	5.7(g),(h)	$e_y-\theta' = t/2-\Delta F$
E_2'	a_m4_o		$(-40-\Delta F, -60-\Delta F)$	$(-40.1, y_{am4o})$	5.7(g),(h)	$e_x+1.5\theta'=-t/2+\Delta F$
E_1	b_m2_o		$(40+\Delta F, -60-\Delta F)$	$(-40.1, y_{bm2o})$	5.8(d)	$e_x+1.5\theta' = t/2-\Delta F$
E_5'	3_m2_o		$(40+\Delta F, -20)$	$(40.1, y_{3m2o})$	5.8(c)	$e_x+0.5\theta' = t/2-\Delta F$
E_1'	4_md_i	$\Delta F\leq t/4$	$(-40-\Delta F, y_{4mdi})$	$(-39.9, 59.9)$	5.8(i)	$e_x-1.5\theta' = t/2+\Delta F$
E_4	a_m1_o		$(-40-\Delta F, -60-\Delta F)$	$(x_{am1o},-60.1)$	5.8(d)	$e_y-\theta' = -t/2+\Delta F$
E_4'	b_m1_o		$(40+\Delta F, -60-\Delta F)$	$(x_{bm1o},-60.1)$	5.8(i),(j)	$e_y+\theta' = -t/2+\Delta F$
E_3	1_mb_i	$\Delta F \leq 0.207t$	$(x_{1mbi}, -60-\Delta F)$	$(39.9, -59.9)$	5.9(f)	$e_y+\theta' = t/2+\Delta F$
C_1	3_m3_o					$\left(e_x+\frac{1}{2}\theta'\right)^2+(e_y-\theta')^2 = (0.1-\Delta F)^2$
C_2	3_m3_i	$\Delta F \leq 0.0858t$				$\left(e_x+\frac{1}{2}\theta'\right)^2+(e_y-\theta')^2 = (0.1+\Delta F)^2$

5.2.2. T-Maps for profiles smaller than the MSP

For profile size $\Delta F \leq 0$, all the possible contact are analyzed in four cases, same way as for the profile size $\Delta F \geq 0$. The Figures for the four cases are shown from Figure 5.11 to Figure 5.14. From these cases, contact and their coordinates,

[1]

in displaced frame and fixed frame, are shown in Table 5.3. The contacts are obtained from the cases such that, they occurs for largest variations of size.

Table 5.3 Coordinates of contacts abstracted for profile size $\Delta F<0$, from Figure 5.11 to Figure 5.14.

Faces ids in Fig.5.6	Con-tact	Size limitation for contacts	Coordinates (x, y), mm		Refer Figure	Equation of planes/Cylinders
			In Displaced Frame	In Fixed Frame		
E_3	$1_m b_i$		$(x_{1mbi}, -60-\Delta F)$	(39.9, –59.9)	5.11(g),(h)	$e_y+\theta' = t/2+\Delta F$
E_1	$4_m a_i$		$(-40-\Delta F, y_{4mai})$	(–39.9, –59.9)	5.13(g),(e)	$e_x+1.5\theta' = t/2+\Delta F$
E_2'	$2_m b_i$		$(40+\Delta F, y_{2mbi})$	(39.9, –59.9)	5.11(j)	$e_x+1.5\theta'=-t/2-\Delta F$
E_3'	$1_m a_i$		$(x_{1mai}, -60-\Delta F)$	(–39.9, –59.9)	5.11(j)	$e_y-\theta' = t/2+\Delta F$
E_5	$2_m 3_i$		$(40+\Delta F, y_{2m3i})$	(39.9, –20)	5.11(b)	$e_x+0.5\theta'=-t/2-\Delta F$
E_1'	$4_m d_i$		$(-40-\Delta F, y_{4mdi})$	(–39.9, 59.9)	5.12(g),(h)	$e_x-1.5\theta' = t/2+\Delta F$
E_2	$d_m 4_o$	$\Delta F \geq -t/4$	$(-40-\Delta F, 60+\Delta F)$	$(-40.1, y_{dm4o})$	5.11(d),(g)	$e_x-1.5\theta'=-t/2+\Delta F$
E_4'	$b_m 1_o$	$\Delta F \geq -0.207t$	$(40+\Delta F, -60-\Delta F)$	$(x_{bm1o}, -60.1)$	5.14(i)	$e_y+\theta' = -t/2+\Delta F$
E_4	$3_m d_i$		$(x_{3mdi}, 60+\Delta F)$	(–39.9, 59.9)	5.12(c),(d)	$e_y-\theta' = -t/2-\Delta F$
C_1	$3_m 3_o$	$\Delta F \geq -0.0858t$				$\left(e_x+\frac{1}{2}\theta'\right)^2+(e_y-\theta')^2 = (0.1-\Delta F)^2$
C_2	$3_m 3_i$					$\left(e_x+\frac{1}{2}\theta'\right)^2+(e_y-\theta')^2 = (0.1+\Delta F)^2$

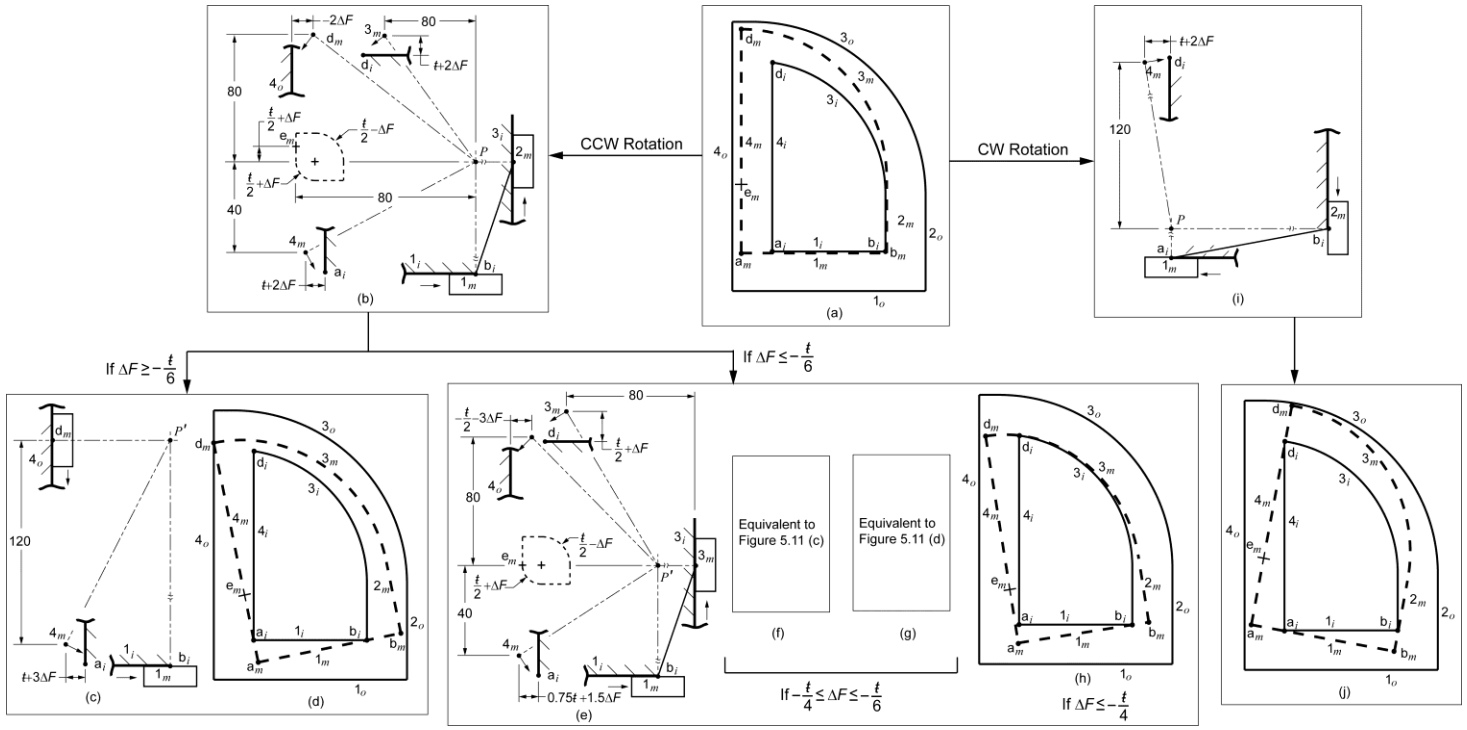

Figure 5.11. (a) The profile of size $\Delta F \leq 0$ is displaced in extreme upper left direction; (b) Double slider mechanism formed when the configuration in (a) rotated CCW. For clarity, line segments are represented as a point on that line segment that will form contact; (c) For $\Delta F \geq -t/6$ and CCW rotations, next contact occurs at $d_m 4_o$; (d) Further rotation constrain the profile when third contact $4_m a_i$ occurs; (e) For $\Delta F \leq -t/6$ and CCW rotations, contact $2_m 3_i$ migrate to $3_m 3_i$; (f) If $-t/6 \leq \Delta F \leq -t/6$ the double slider configuration will be same as in (c); (g) If $-t/6 \leq \Delta F \leq -t/6$, the CCW rotation will be constrained as in (d); (h) If $\Delta F \leq -t/4$, the contact $3_m 3_i$ migrate to $3_m d_i$ and constrained further CCW rotation; (i) Double slider mechanism formed when the configuration in (a) rotated CW; (j) Further CW rotation will be constrained when third contact $4_m d_i$ occurs.

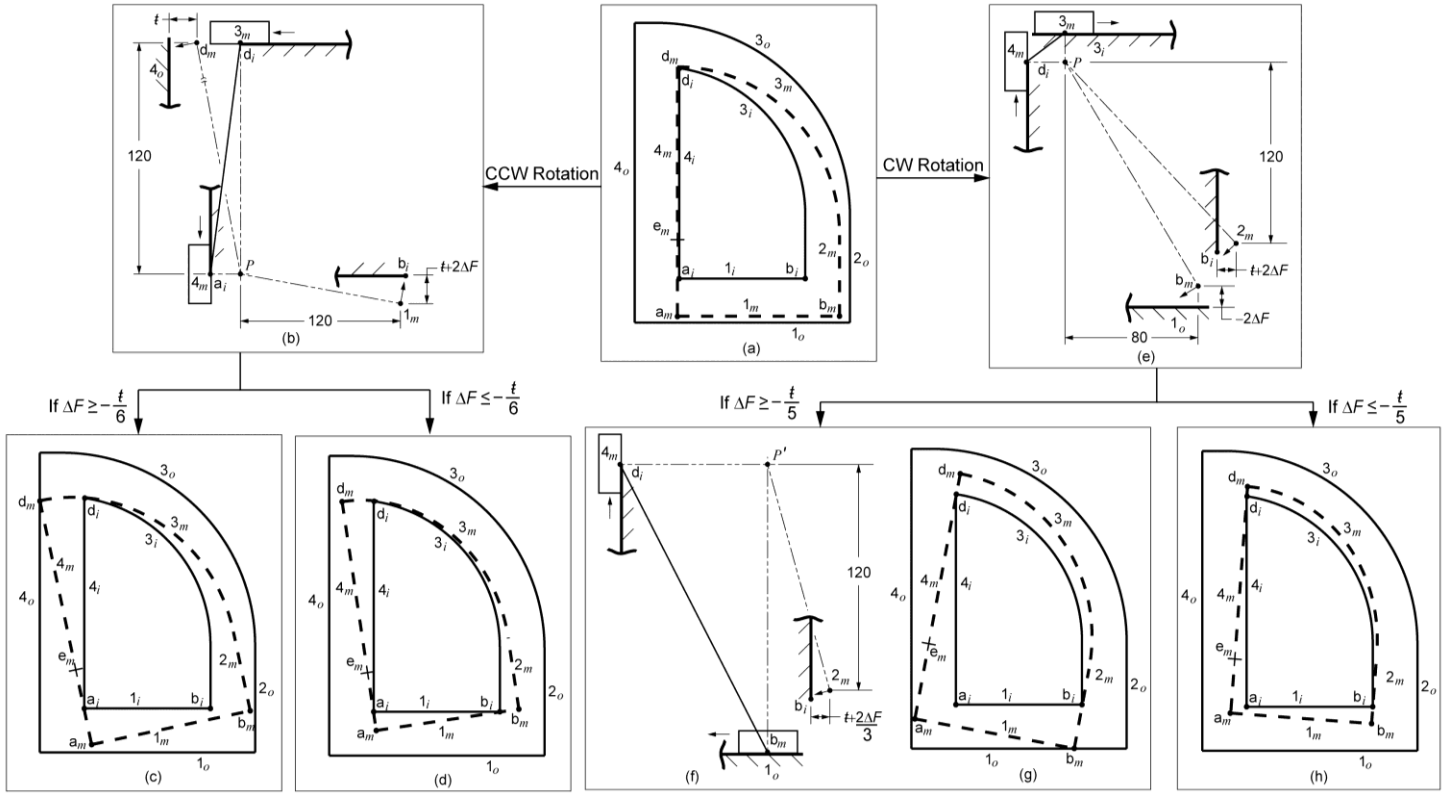

Figure 5.12. (a) The profile of size $\Delta F \leq 0$ is displaced in extreme lower right direction; (b) For CCW rotation, double slider mechanism is formed due to two contacts $4_m a_i$ and $3_m d_i$; (c) If $\Delta F \geq -t/6$, further rotation will be constrained by the third contact $d_m 4_o$; (d) If $\Delta F \leq -t/6$, further rotation will be constrained by the third contact $1_m b_i$; (e) For CW rotation two contacts, $4_m d_i$ and $3_m 3_i$, form double slider mechanism; (f) If $\Delta F \geq -t/5$, the contact $b_m 1_o$ and kinematic configuration changes; (g) The rotation is constrained for the configuration in (e), when contact $4_m d_i$ occurs; (h) If $\Delta F \leq -t/5$, the third contact occurs at $4_m d_i$ that constrains rotation of the profile.

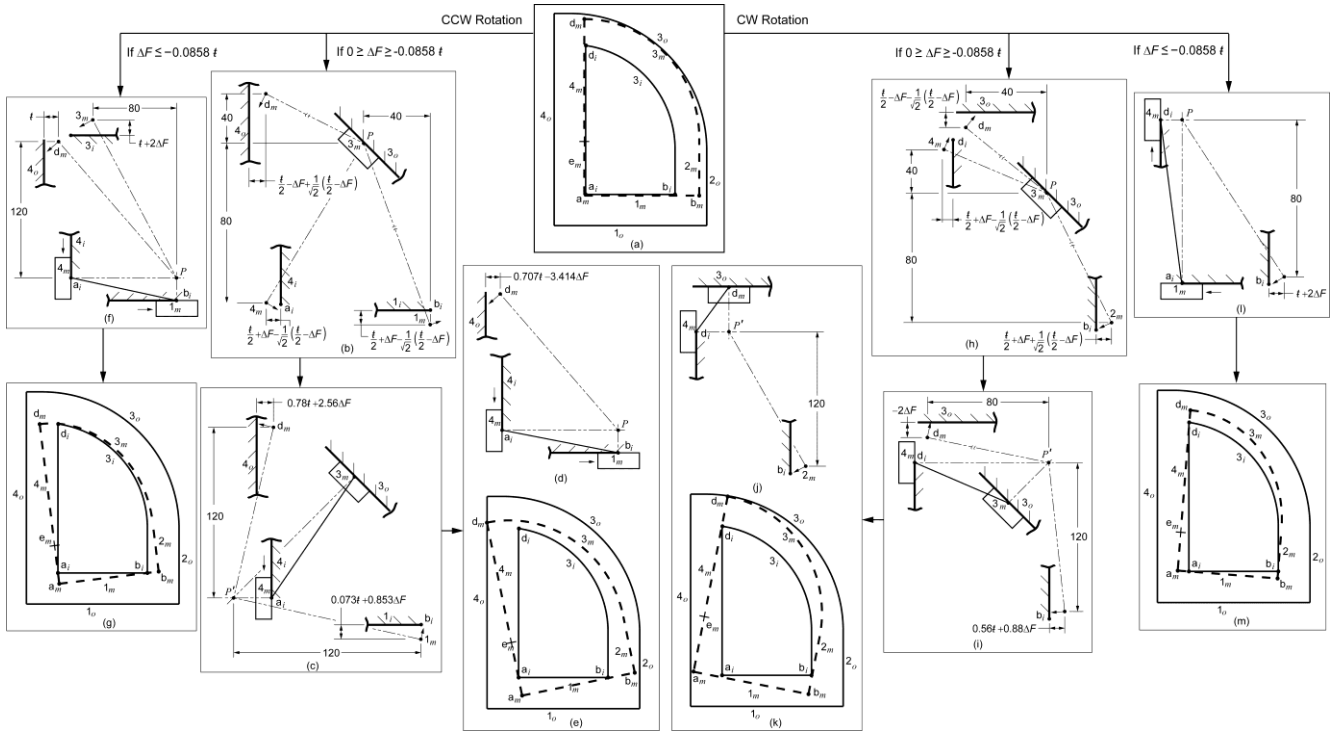

Figure 5.13 (a) The profile of size $\Delta F \leq 0$ is displaced in extreme upper right direction; (b) If $\Delta F \geq -0.0858\,t$, the arc segment of the profile contact the arc segment of the outer boundary; and the profile rolls in CCW direction; (c) Further rotation brings 4_m in contact with a_i; (d) When contact $1_m b_i$ occurs, the arc segment 3_m disconnect from arc segment 3_o; (e) When the third contact occurs, the rotation get constrained; (f) If $\Delta F \leq -0.0858\,t$, the CCW rotation forms contact $4_m a_i$ and $1_m b_i$; (g) Third contact $3_m d_i$ occurs when the profile rotated further; (h) If $\Delta F \geq -0.0858\,t$, the arc segment of the profile contact the arc segment of the outer boundary; and the profile rolls in CW direction; (i) The second contact $4_m d_i$ forms double slider mechanism; (j) The profile rolls until contact $d_m 3_o$ occurs; (k) The rotation of the profile constrained by the third contact $4_m d_i$; (l) If $\Delta F \leq -0.0858\,t$, the CW rotation forms contact $4_m d_i$ and $1_m a_i$; (m) Third contact $2_m b_i$ occurs when the profile rotated further.

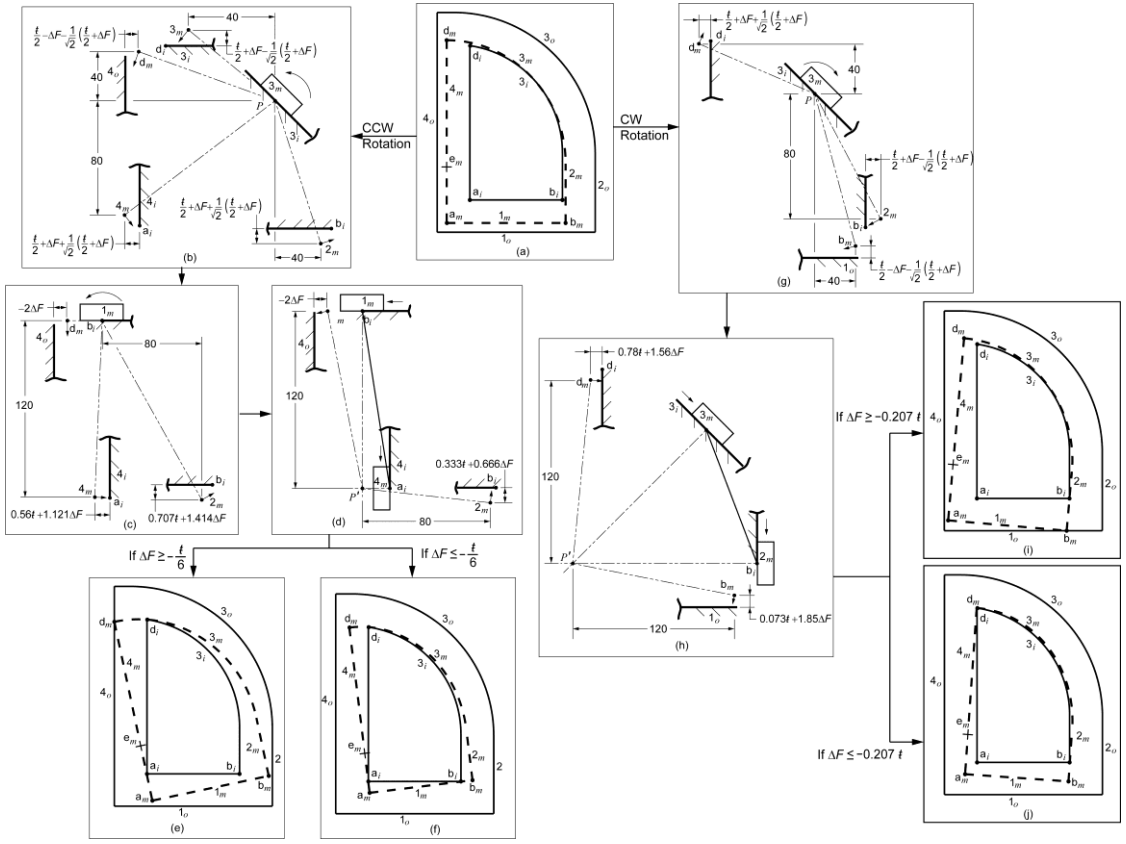

Figure 5.14 (a) The profile of size $\Delta F \leq 0$ is displaced in extreme lower left direction; (b) Due to the contact between arc segment of the profile and arc segment of the inner boundary, the profile rolls; (c) The profile rolls until contact $1_m b_i$ occurs; (d) Further CCW rotation forms third contact $4_m a_i$; (e) If $\Delta F \geq -t/6$, the third contact occurs at $d_m 4_o$; (f) If $\Delta F \leq -t/6$, the third contact occurs at $1_m b_i$; (g) The profile rolls in CW direction; (h) Second contact occurs at $3_m b_i$; (i) If $\Delta F \geq -0.207\,t$, the third contact occurs at $b_m 1_o$; (j) If $\Delta F < -0.207\,t$, the third contact occurs at $1_m b_i$

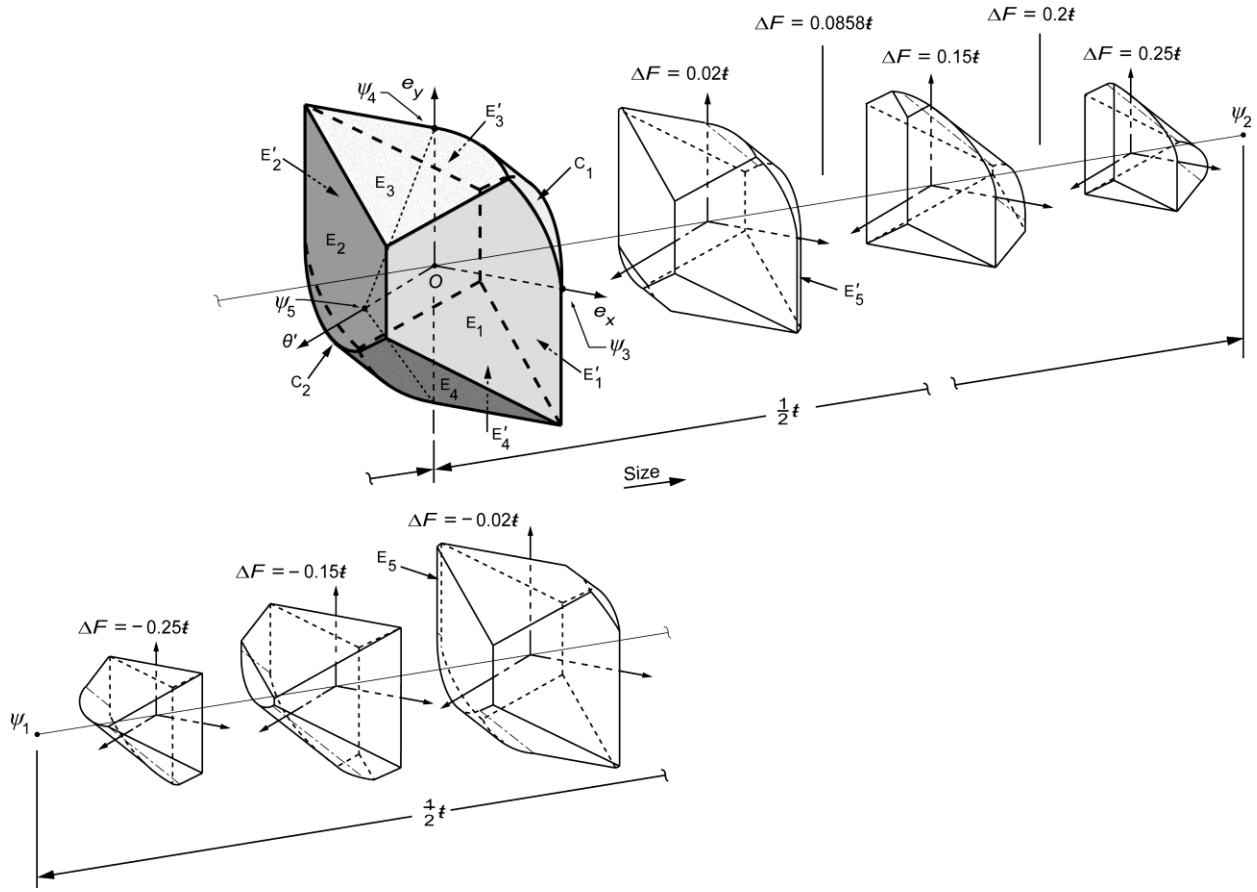

Figure 5.15. The different morphologies of the 3-D hypersections for the 4-D T-Map that is constructed for the tolerance-zone in Figure 5.2. The five basis-points are $\psi_1,\ldots,\psi_5$. For clarity of the graphics, the scale in the direction of size is both exaggerated and non-linear.

5.2.3. The 4-D T-Map for the profile specified in Figure 5.1

In the construction, line-profiles that are larger or smaller than the middle-sized one are more limited in their allowable displacements e_x, e_y, and θ. Based on the equations derived in Table 5.2 and Table 5.3, 3-D hyper sections of the 4D T-map are shown in Figure 5.15. The 3-D T-Map for MSP, shown in center, is largest among all the hyper sections. Others are smaller as the size grows (on right hand side in Figure 5.15) or as size diminishes (on left hand side in Figure 5.15).

Two types of faces are found from Table 5.2 and Table 5.3, one type of faces shrink as the profile size changes from zero, and other type of faces expand. Consider 3D T-Map as close convex shape made of many faces. Then the faces that are expanding disappear after certain sizes of the profile. Referring face notations in Figure 5.6, faces E_1', E_3 and C_2, which correspond to contacts $4_m d_i$, $1_m b_i$, $3_m 3_i$ in Table 5.2, vanish when the profile size grows (shown in Figure 5.15). Similarly faces E_2, E_4' and C_1, which correspond to contacts $d_m 4_o$, $b_m 1_o$, $3_m 3_o$ in Table 5.3, vanish when the profile size decreases.

Also, Notice the small face immerged, on 3-D T-Map for $\Delta F > 0$, on right hand side, and grows as the size increases. This face represents contact between arc segment of the profile (3_m) and line segment (2_o) of the outer boundary, during CW rotations, as shown in Figure 5.8(c). This face is not present in T-Map for MSP because on the other side the line segment 4_m comes in contact with vertex d_i as the profile rotates in CW direction.

5.3. Profile segments as an envelope

An easy way to establish the shortest distance between a point and a curve is to minimize the distance from the point to nearby tangents to the curve. Therefore, the subsections below establish the envelope equation for a circular arc anywhere in an *xy*-plane. Determining envelope coordinates for a line is described in §§4.1.

5.3.1. Envelope Equation for an Arc-Segment

Figure 5.16 shows a circle of radius *r*, three lines tangent to it, and two frames of reference. The circle has its center at the origin of the *k*-frame, but it is displaced from the origin of the *j*-frame. When every tangent to the circle is identified with its inward normal, the envelope-equation of the circle in the *k*-frame is $s_k^2 = r^2(p_k^2 + q_k^2)$; for normalized coordinates it specializes to $s_k = \pm r$. Adapting the homogeneous transformation in Eq. 5.1, the matrix

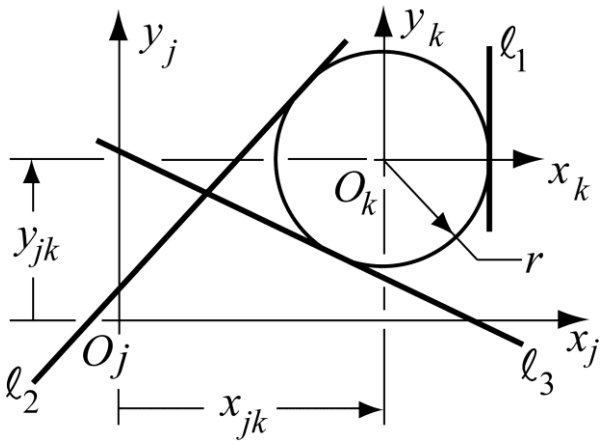

Figure 5.16 A circle with three tangent lines, and two distinct reference frames.

$$[A_{jk}] = \begin{bmatrix} 1 & 0 & x_{jk} \\ 0 & 1 & y_{jk} \\ 0 & 0 & 1 \end{bmatrix}$$

is used in the equation $[x_j \;\; y_j \;\; 1]^T = [A_{jk}]\,[x_k \; y_k \; 1]^T$ to transform the homogenous coordinates $(x_k, y_k, 1)$ of a point in the k-frame to their values in the translated j-frame. However, it also may be used in the matrix equation $[p_k \; q_k \; s_k] = [p_j \; q_j \; s_j][A_{jk}]$ to transform the homogeneous coordinates (p_j, q_j, s_j) of a line in the j-frame to the corresponding values in the k-frame [28]. The results are $p_k = p_j$, $q_k = q_j$, and $s_k = p_j x_{jk} + q_j y_{jk} + s_j$. Hence, presuming that the coordinates (p_j, q_j, s_j) are normalized, the envelope equation for any circle in the j-frame is

$$p_j x_{jk} + q_j y_{jk} + s_j = \pm r, \tag{5.29}$$

where the upper and lower signs, respectively, correspond to all unit normals pointing inward and outward. Further, for a circular arc that is identified by a range of polar angle about the origin of the k-frame (e.g. $0 \le \alpha \le \pi/2$, as in Figure 5.2), the corresponding ranges of p_k and q_k remain the same allowable ranges for p_j and q_j in the j-frame.

5.4. Minimum distance between an envelope and a measured point

Method of determining minimum distance between a measured point and a line segment is described in §§4.2. This subsection describes about how to determine minimum distance between a measured point and arc segment.

Given a point (x_j , y_j) and a line (p_j , q_j , s_j), both in a planar j-frame, the equation ensuring that the point lies on the line is $p_j x_j + q_j y_j + s_j = 0$, a reduced form of Eq. 4.1. Further, when the point does not lie on the line, its minimum (normal) distance from the line is [28]

$$d = p_j x_j + q_j y_j + s_j \,. \tag{5.30}$$

Distance d will be in the same units as those for x_j and y_j of a measured point whenever coordinates (p_j , q_j , s_j) are scaled so that $p_j^2 + q_j^2 = 1$, i.e. when the coordinates are normalized. For a circular arc, the minimum distance is obtained as an extreme value using Lagrange multipliers. The dependent variable to be minimized is d, the two independent variables are p_j and q_j, and one constraint function among p_j and q_j is $\phi = p_j^2 + q_j^2 - 1 = 0$. It is first helpful to combine Eqs. 5.29 and 5.30 to eliminate coordinate s_j. Then

$$d = p_j(x_j - x_{jk}) + q_j(y_j - y_{jk}) + r \,. \tag{5.31}$$

Following the procedure of Lagrange multipliers, the function $\mathcal{F} = d + \lambda\phi$ is formulated using d from Eq. 5.31. The two derivative expressions $\partial\mathcal{F}/\partial p_j = 0$ and $\partial\mathcal{F}/\partial q_j = 0$ lead to

$$\left.\begin{aligned} & x_j - x_{jk} + 2p_j\lambda = 0 \\ & \text{and} \\ & y_j - y_{jk} + 2q_j\lambda = 0 \,, \end{aligned}\right\} \tag{5.32}$$

these two equations ensuring that an extreme value of d is identified. The four equations; i.e. Eq. 5.31, the constraint $\phi=0$, and the two Eqs. 5.32; may be solved for the four variables d, p_j, q_j, and the Lagrange multiplier λ. The most important solutions are for the direction of the inward unit normal (p_j, q_j) and the minimum distance d of the measured point (x_j, y_j) from the circular arc. When arranged for sequential computation, these solutions are

$$\left.\begin{aligned} 2\lambda &= +\sqrt{\left(x_j - x_{jk}\right)^2 + \left(y_j - y_{jk}\right)^2}, \\ p_j &= \left(x_{jk} - x_j\right)/2\lambda, \\ q_j &= \left(y_{jk} - y_j\right)/2\lambda, \text{ and} \\ d &= r + \left(x_j - x_{jk}\right)p_j + \left(y_j - y_{jk}\right)q_j, \end{aligned}\right\} \qquad 5.33$$

where only the positive sign should be used for the square root. For those measured points lying inside the profile, Eqs. 5.33 produce a positive number for d, and for the points lying outside, d will be negative. When desired, the corresponding coordinate s_j for the tangent line may be obtained from Eq. 5.29.

As discussed in §§4.2, since envelope equation of the line profile treat line segments infinite length it may be problematic to assess minimum distances for points at the corners of a line profile. Hence, for convex profile an easy way is to assess minimum distances from a reference envelope that is a parallel curve larger than the true profile.

5.5. Fit of a line-profile to measured points by the least-squares method

The method of Moore-Penrose to obtain least-squares fit is general and can be used for any kind of profiles. Set up of Moore-Penrose inverse and robotics is built in §§4.4 and 4.5. Once minimum distances from measured points to the reference envelope, and corresponding inward normal vectors are calculated Eq. 4.10 can be used to determine least squares fit for measured point around line profile

As one example, consider the 17 measured points around the theoretical profile as shown in Figure 5.17. The points represent an imperfectly manufactured profile formed from a rectangle that has been modified with one rounded corner. The coordinates (R'_i ; L'_i , M_i') for the actuator screws at each point, and the deviations d'_i, are presented in Table 5.4 for each of the measured points. The deviations are all measured from the outer boundary of the tolerance-zone, so Δs

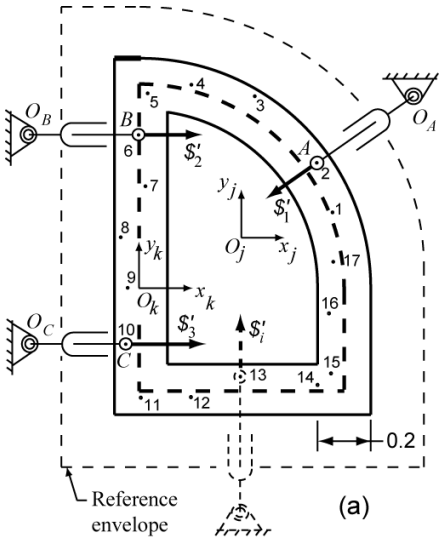

Figure 5.17. The line-profile (dashed line) of 5.1, its tolerance-zone boundaries (with an exaggerated scale), and 17 measured points, all lying on the platform of a planar in-parallel robot which is guided by three linear actuators lying on the screws $\$'_1$, $\$'_2$ and $\$'_3$ at points *A*, *B*, and *C;*

= 0.1 mm (Figure 5.17), and the screw coordinates are computed in the $O_j x_j y_j$-frame, in which origin O_j is at the pole for the middle-sized profile (§5.1.2). The values in Table 5.4 are used to build matrices [$\boldsymbol{K}'$] and [$\mathbf{d}'_i$] in Eq. (4.10). The Moore Penrose solution of [$\boldsymbol{K}'$] produces the least-squares result

$$[\$] = [\delta\theta \;\; \delta x \;\; \delta y \;\; (\Delta s - \Delta F)]^{\mathrm{T}}$$

$$= [-0.0006684 \;\; -0.0194883 \;\; 0.0228764 \;\; 0.0868641]^{\mathrm{T}}.$$

The resultant least-squares profile of this solution is shown as the profile with the thin line in Figure 5.18. Note that the scale of the tolerance-zone is enlarged by a factor of 10 in Figure 5.17 and Figure 5.18, and the scale for the profile dimensions is diminished by a factor of 10. Consequently, the least-squares profile is drawn at $\delta\theta = -0.06684$ rad that represents a rotation of 3.8^0 in the clockwise direction. Further, to make the appearance of the displaced origin '+' in Figure 5.18 be consistent with the displayed points at the exaggerated scale, its coordinates $\delta x = -0.0194883$ mm and $\delta y = 0.0228764$ mm have been scaled

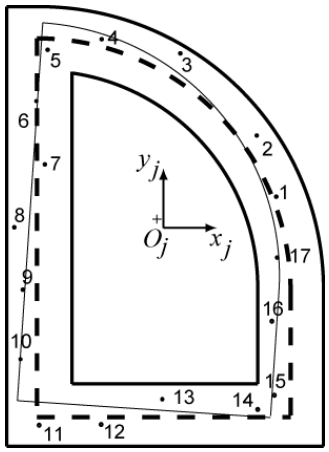

Figure 5.18 The resultant least-squares profile shown with the thin line. Its displacement from origin O is shown with the '+' mark.

up by a factor of 10 with respect to the middle-sized profile. The corresponding size adjustment from the middle-sized profile is ΔF = 0.1 – 0.08686 = 0.01314 mm., a small *growth* in size. And, finally, the coordinates $(e_x, e_y, \theta', \Delta F)$ of the *i*-Map point, corresponding to the above solution, are, respectively, –0.0195 mm, 0.0229 mm, –0.0267 mm, and 0.0131 mm, when rounded to three significant figures. Coordinate $\theta' = \overline{\alpha}\ \delta\theta = 40\,\delta\theta$ for the line-profile in Figure 5.1.

Table 5.4 Coordinates of measured points around manufactured line profile

Point	R'_i	L'_i	M'_i	d'_i
1	–3.916	–0.930	–0.367	0.083
2	6.853	–0.815	–0.579	0.054
3	23.842	–0.518	–0.855	0.020
4	33.955	–0.243	–0.970	0.075
5	–59.970	1	0	0.130
6	–40.000	1	0	0.100
7	–20.000	1	0	0.120
8	0.000	1	0	0.020
9	20.000	1	0	0.050
10	42.000	1	0	0.040
11	–40.000	0	1	0.070
12	–20.000	0	1	0.070
13	0.000	0	1	0.170
14	30.000	0	1	0.120
15	–53.000	–1	0	0.150
16	–30.000	–1	0	0.170
17	–14.611	–0.991	–0.130	0.133

5.6. Validation using known solution of circle from NIST

The method of least squares is verified with test cases for a circle published by National Institute of Standards and Technology (NIST) [32]. One of the datasets contains coordinates for 38 points, measured around a cylinder in a

plane perpendicular to its axis. As shown in Table 5.5 the coordinates of points in *k*-frame, are the data from NIST. NIST assessed the data in terms of location (in

Table 5.5 Coordinates of the measured points around circle, mm. For circle $\boldsymbol{R'_i=0}$.

Points	**Coord. in *k*-frame**		**Coord. in *j*-frame**				
	x_i	y_i	x_i	y_i	L'_i	M'_i	d'_i
1	-555.168	21.976	5.152	-12.264	-0.387	0.922	1.698
2	-553.188	22.943	7.131	-11.298	-0.534	0.846	1.640
3	-551.396	24.253	8.923	-9.988	-0.666	0.746	1.607
4	-549.864	25.847	10.455	-8.394	-0.780	0.626	1.593
5	-548.622	27.660	11.697	-6.580	-0.872	0.490	1.579
6	-547.754	29.683	12.566	-4.557	-0.940	0.341	1.633
7	-547.212	31.849	13.108	-2.391	-0.984	0.179	1.676
8	-547.083	34.028	13.236	-0.213	-1.000	0.016	1.762
9	-547.275	36.231	13.045	1.991	-0.989	-0.151	1.804
10	-547.803	38.303	12.516	4.063	-0.951	-0.309	1.841
11	-548.636	40.333	11.683	6.092	-0.887	-0.462	1.824
12	-549.791	42.172	10.528	7.931	-0.799	-0.602	1.819
13	-551.191	43.842	9.129	9.601	-0.689	-0.725	1.752
14	-552.870	45.264	7.449	11.024	-0.560	-0.829	1.695
15	-554.766	46.421	5.553	12.180	-0.415	-0.910	1.613
16	-556.826	47.201	3.493	12.961	-0.260	-0.966	1.577
17	-559.004	47.577	1.315	13.337	-0.098	-0.995	1.598
18	-561.220	47.615	-0.901	13.374	0.067	-0.998	1.595
19	-563.390	47.237	-3.071	12.996	0.230	-0.973	1.646
20	-565.454	46.493	-5.135	12.253	0.387	-0.922	1.715
21	-567.395	45.433	-7.075	11.193	0.534	-0.845	1.759
22	-569.088	44.082	-8.769	9.842	0.665	-0.747	1.818
23	-570.568	42.497	-10.249	8.257	0.779	-0.627	1.839
24	-571.799	40.689	-11.480	6.448	0.872	-0.490	1.833
25	-572.726	38.722	-12.407	4.482	0.941	-0.340	1.808
26	-573.377	36.626	-13.058	2.386	0.984	-0.180	1.726
27	-573.656	34.460	-13.336	0.220	1.000	-0.016	1.662
28	-573.533	32.239	-13.214	-2.001	0.989	0.150	1.635
29	-573.068	30.070	-12.749	-4.171	0.950	0.311	1.586
30	-572.214	28.059	-11.895	-6.181	0.887	0.461	1.595
31	-571.011	26.181	-10.692	-8.060	0.799	0.602	1.611
32	-569.511	24.585	-9.192	-9.656	0.689	0.724	1.668
33	-567.762	23.242	-7.443	-10.998	0.560	0.828	1.720
34	-565.818	22.200	-5.499	-12.040	0.415	0.910	1.764

35	-563.743	21.532	-3.423	-12.708	0.260	0.966	1.839
36	-561.629	21.145	-1.310	-13.096	0.100	0.995	1.839
37	-559.446	21.101	0.873	-13.139	-0.066	0.998	1.832
38	-557.274	21.345	3.046	-12.895	-0.230	0.973	1.750

plane) and size of the circle that represents least square fit to the measured points. To be consistent with the data and the solution provided by NIST, the size for a circle can be represented as absolute parameter, i.e. radius or diameter, unlike the size for profiles as in §§4.5 and 5.5. Also, it is obvious that the orientation is invariant for a circle.

As shown in Figure 5.19, the measured points provided by NIST are located in *k*-frame (Table 5.5), which is far from approximate center of the circle at O_j, where we wish to place the origin of the *j*-frame. The best guess of location of the *j*-frame with respect to the *k*-frame (x_{jk}, y_{jk}), is the geometric center (arithmetic mean) of the measured points in *k*-frame i.e. (–560.31927 mm, 34.24053 mm). The coordinates of the measured points in *j*-frame are also shown

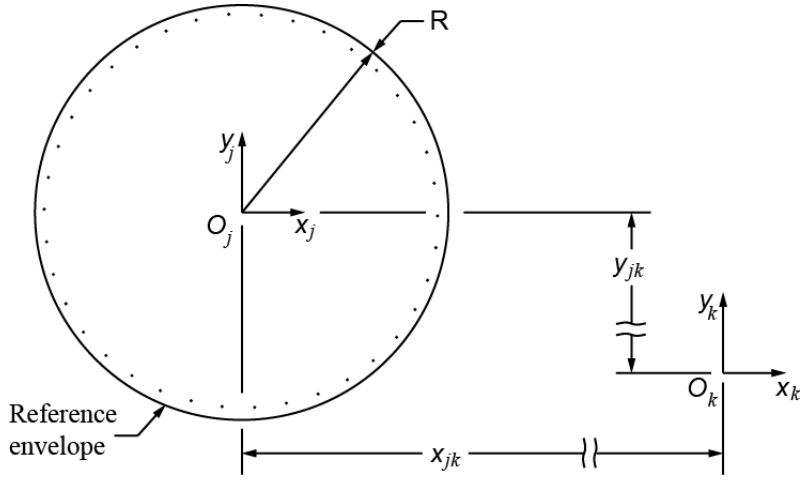

Figure 5.19 The measured points in *k*-frame. The *j*-frame is formed at the geometric center (arithmetic mean) of the measured points.

in Table 5.5. To ensure that the size of the reference envelope bounds all the measured points inside, its radius is assume to be R = 15.00 mm and its center coincides with O_j. With inward deviations all measured from this reference envelope, the least squares solution obtained by Moore-Penrose inverse is

$$(\delta\theta\ \delta x\ \delta y\ \Delta F) = (0,\ \ 0.00154 \text{ mm},\ \ -0.00151 \text{ mm},\ \ -1.70922 \text{ mm}).$$

Considering the initial position and size of the reference envelope the center of the least squares circle is located in k-frame at $(x_{jk} + \delta x, y_{jk} + \delta y)$ = (−560.31773 mm , 32.23902 mm). And diameter of the circle is 2*(R + ΔF) = 26.58156 mm. The corresponding results reported by NIST for, the coordinates of the center of the least squares fit circle are (−560.31773 mm, 34.23902 mm), and the diameter is 26.58155 mm. It is apparent that the results of the proposed method are quite consistent with the NIST results.

CHAPTER 6

PARTITIONING METHOD FOR LINE PROFILES WITH CONCAVITY

In this chapter, more general forms of line-profiles are considered. In addition to the methods used in Chapters 4 and 5 for convex profiles, this chapter introduces a way to treat concave profiles by partitioning the measured points in order to choose the correct tangent line among several parallel ones, this way, the correct minimum distance is obtained from a measured point to the reference envelope.

The search algorithm for determining the shortest distance (shown in §§4.2 and §§5.4) between every measured point and the envelope profile works for convex profiles. The envelope equation (Eq. 4.2) treats every tangent as infinitely long. Concave profiles contain at least one bitangent or tangent that intersects the profile. Hence, as per the envelope representation, one or more envelope tangents intersect with segments other than neighbors. If proper care is not taken, the measured points that are closest to a particular segment may be detected in proximity of another segment. Hence, a method is developed to partition both the envelope representation of the profile and the measured points to handle such problem for line profiles with concavity.

Two examples that illustrate the problem are shown in Figure 6.1. The tangents to line segments S_3 and S_5 intersect with the line segment S_8. Due to the intersection, some of the points that belong to S_8 may be detected in proximity of S_3 or S_5. Further, when two parallel segments are separated by a small value

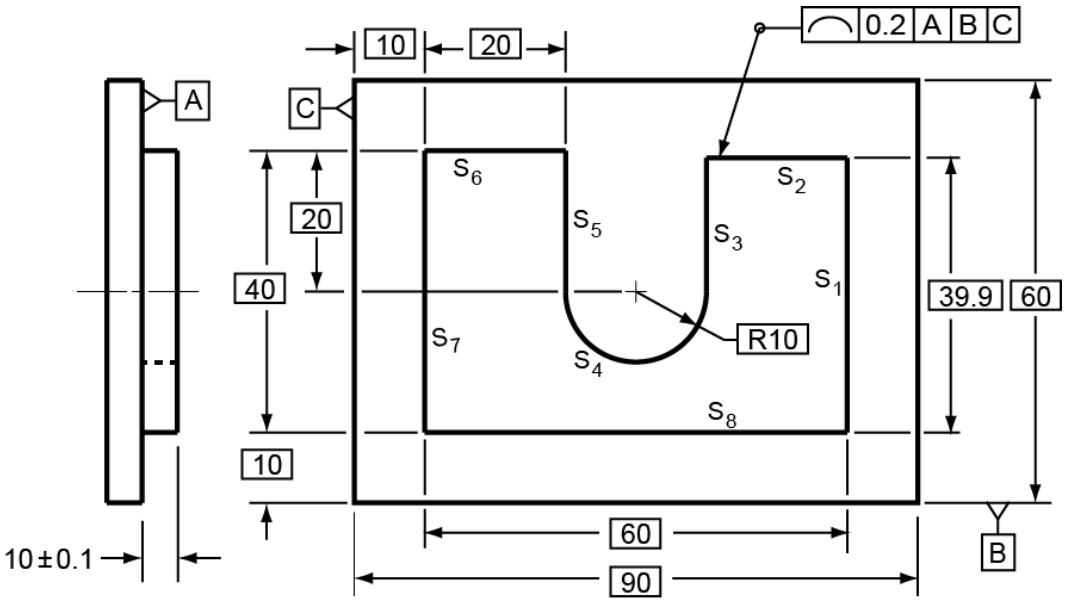

Figure 6.1 Specification of a profile with concavity.

(tolerance t), such as segments S_2 and S_6 in Figure 6.1, the same problem occurs. As per the dimensions in the drawing, S_2 is 0.1 mm offset inwards with respect to S_6. In addition, the tolerance zone is offset by 0.1 mm on both sides of the nominal profile. Hence, the envelope representation of the middle-sized profile (MSP) for S_6 is collinear with the outer tolerance-zone boundary at S_2. The points measured at S_2 that are far from middle-sized profile (near the outer envelope) could be recognized in proximity of S_6.

6.1. Partition zone for a profile segment

To handle concave profiles, a partition zone is formed around each segment of the MSP such that partition zones of any two segments never overlap. In addition, no measured point should lie outside the total area formed by the partition zones of all the segments. In other words, each measured point lies in

one of the partition zones, and is considered closest to the segment associated with that partition zone.

Typically, a partition zone is made of four sides. Two sides are parallel to the MSP segment, but further away than the boundaries to the tolerance zone. One is outside of MSP and another is inside such that, all the points corresponding to the segment are between them. Hopefully, the offset value of tolerance t is enough to capture all the points. However, $2t$ or $3t$ can also be used until the partition zone does not overlap with other partition zones. The other two sides are lines that bisect the angles formed between each end of the profile segment and the adjacent segment. These four sides produce a bounded partition zone. Such partition zones for segments S_4 and S_5 are shown in Figure 6.2(a) and (b) respectively. For an arc segment, the partition zone is made of both lines and arcs.

6.2. Points interior to the partition zone

Once partition zones for all profile segments have been formed, each point

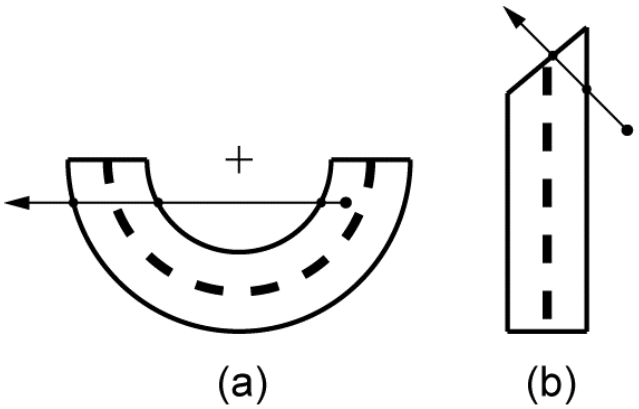

Figure 6.2 Partition zones for arc segment S_4 in (a) and line S_5 in (b).

is checked for within which partition zone it is lying. The point interior to a partition zone is determined by ray tracing method. If any arbitrary ray originating from a point intersects the boundary segments of the partition zone an odd number of times, then the point lies inside the zone, else it is outside the zone [33]. For example, a ray originating from a point inside the partition zone in Figure 6.2(a) intersects the boundary thrice. The intersection between a ray and partition zone boundary is formulated in the following subsections. Since the profiles considered here are made of lines and arcs, the Ray-Line intersection and the Ray-Arc intersection is derived.

6.2.1. Ray-Line intersection:

Any line passing through a point can be defined in parametric form as,

$$\mathbf{P}(s) = \mathbf{u} + s\mathbf{v} \quad . \tag{6.1}$$

where, **u** is position vector of the point on the line, **v** is unit vector and determines direction of the line, and *s* is line parameter. For line segment of length L, *s* varies from 0 to L. While for a ray, **u** is regarded as origin of the ray, and *s* varies from 0

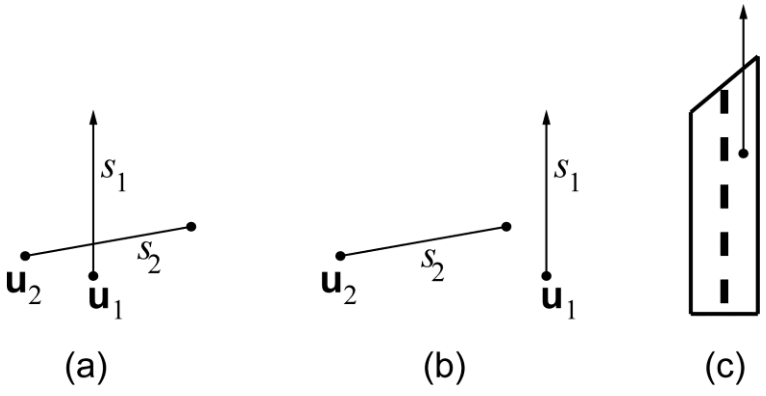

Figure 6.3 (a) Ray intersects line segment; (b) Ray does not intersect line segment; (c) Ray direction is parallel to the profile tangent.

to ∞. For the proposed method, the origin of ray (**u**) is the measured point whose association with any partition zone is to be determined.

To determine ray-line intersection, consider a ray $\mathbf{P}_1(s_1) = \mathbf{u}_1 + s_1\mathbf{v}_1$ and a line segment $\mathbf{P}_2(s_2) = \mathbf{u}_2 + s_2\mathbf{v}_2$, as shown in Figure 6.3(a) and (b). Solution to the two equations for intersection point ($\mathbf{P}_1(s_1) = \mathbf{P}_2(s_2)$) results in,

$$\left.\begin{aligned} \begin{bmatrix} s_1 \\ s_2 \end{bmatrix} &= \begin{bmatrix} \mathbf{v}_1 & -\mathbf{v}_2 \end{bmatrix}^{-1} \begin{bmatrix} \mathbf{u}_2 - \mathbf{u}_1 \end{bmatrix} \\ s_1 &> 0 \\ 0 < s_2 &< \mathrm{L} \end{aligned}\right\} \qquad 6.2$$

The square matrix $([\mathbf{v}_1 \quad -\mathbf{v}_2])$ to be singular implies that the ray and the line segment are parallel to each other. Also notice that, the configuration in Figure 6.3(b) does not satisfies inequalities $0 < s_2 < \mathrm{L}$, hence there is no intersection between the ray and the line segment. Moreover, the computation can be reduced by, setting the direction of ray parallel to line segment of the MSP (as shown in Figure 6.3(c)), because then intersections only need to be checked with the two angle bisectors at the ends of the line segment of the MSP.

6.2.2. Ray-Arc intersection

Determining Ray-Arc intersection contains two steps. In the first step, intersection between the ray and the circle, of which the arc is a segment, is determined; then in the second step, it is checked whether the intersection occurs on the arc segment or not.

Step-1: For a given center (**c**) and radius (*r*) (Figure 6.4), a circle can be defined as $(\mathbf{P}-\mathbf{c})\cdot(\mathbf{P}-\mathbf{c})=r^2$. Where **P** is any point on the circle. The intersection between a ray ($\mathbf{P}_1(s_1)=\mathbf{u}_1+s_1\mathbf{v}_1$) and the circle can be determined by [34, 35],

$$(\mathbf{u}_1+s_1\mathbf{v}_1-\mathbf{c})\cdot(\mathbf{u}_1+s_1\mathbf{v}_1-\mathbf{c})=r^2,$$

or in form of a quadratic equation,

$$s_1{}^2(\mathbf{v}_1\cdot\mathbf{v}_1)+2s_1(\mathbf{u}_1-\mathbf{c})\cdot\mathbf{v}_1+(\mathbf{u}_1-\mathbf{c})\cdot(\mathbf{u}_1-\mathbf{c})-r^2=0. \quad 6.3$$

Equating the Eqn. 6.3 with $Ax^2 + Bx + C = 0$, the value of the discriminant,

$$\Delta=\mathrm{B}^2-4\mathrm{AC}=4\big((\mathbf{u}_1-\mathbf{c})\cdot\mathbf{v}_1\big)^2-4(\mathbf{v}_1\cdot\mathbf{v}_1)\big((\mathbf{u}_1-\mathbf{c})\cdot(\mathbf{u}_1-\mathbf{c})-r^2\big), \quad 6.4$$

forms three possible cases relating the ray with the circle.

Case-1: If $\Delta < 0$, then there is no intersection.

Case-2: If $\Delta = 0$, then the ray is tangent to the circle. That means the point is outside the circle. For the proposed method, it can be considered as no intersection or twice intersections.

Case-3: If $\Delta > 0$, then the ray intersects the circle.

Further, if both the values of the solution,

$$s_1=\frac{-B\pm\sqrt{\Delta}}{2A}=\frac{-B\pm\sqrt{B^2-4AC}}{2A},$$

are positive, the ray intersects the circle twice; that implies that the point is outside the circle. On the other hand, if only one value is positive then there is only one intersection point and the point is inside the circle.

Step-2: Once the intersection between a ray and a circle is determined, then it is checked whether the intersection occurs *on* the arc-segment, which is a part of the partition zone. For that, consider the arc evolves in counterclockwise direction around its center. For example, as shown in Figure 6.4(a), the arc starts from the point **A** – progress in the counterclockwise direction – and ends at point **B**. Hence, the chord of the arc can be defined from point **A** to point **B**. This configuration ensures that the arc is on the right-hand side of the chord vector. Moreover, if the intersection point **P** is on right-hand side of the chord vector then the ray intersects the arc. For the intersection point **P**, if the condition

$$(\mathbf{B}-\mathbf{P})\times(\mathbf{A}-\mathbf{P})>0$$

satisfies, then the intersection occurs on the arc-segment.

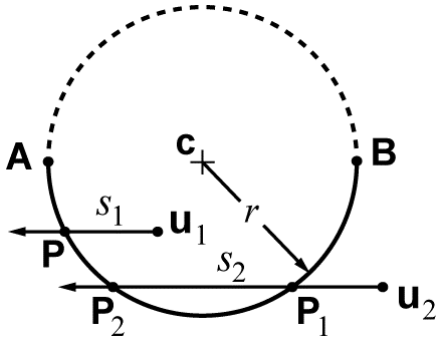

Figure 6.4 Rays $\mathbf{P}(s_1)$ and $\mathbf{P}(s_2)$ intersect an arc segment of a partition zone with center **c** and radius *r*. The arc segment progresses in the counterclockwise direction, from **A** to **B**.

6.3. Line-profile with concavity – Example

The sample concave profile (raised boss) used to demonstrate the partitioning method is shown in Figure 6.5. The concave part (arc segment) of the profile resembles one side of a turbine blade. Practically, small radiuses of 0.5 mm at upper left and lower right corners of the profile help to smooth out the cusp formed due to the geometric configuration. The shape of the boss is controlled by the line-profile tolerance ⌓ = 0.2 relative to Datums A, B and C. The specification establishes two parallel curves forming boundaries of the tolerance-zone at each

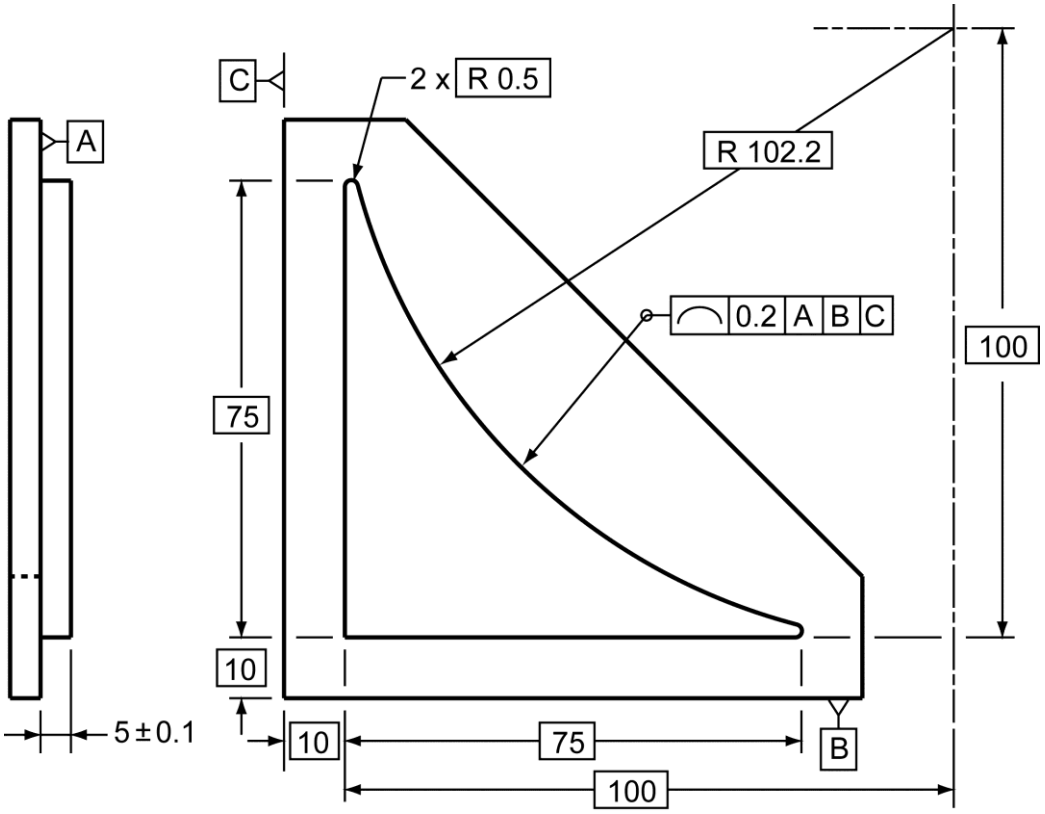

Figure 6.5 Specification for a sample concave raised profile. The concave part of the profile resembles the shape of a turbine blade. Its shape is controlled by the profile tolerance ⌓ = 0.2 mm relative to Datums A, B and C.

cross section of the profile. One is 0.1 mm larger along every line normal to the profile surface, and the other is smaller, according to the ASME standard [1]. For clarity, the exaggerated tolerance-zone for the line-profile is shown in Figure 6.6(a), and the detail of tolerance zone at two corners is shown in Figure 6.6(b). The dashed arc in Figure 6.6(b) represents combined MSP at the two corners, the two heavy arcs and two dotted arcs are tolerance zones at the two ends. Radiuses at each end form arc spanning approximately 174º.

It is helpful to view the displacements e_x, and e_y, and θ of the profile to be the same as those of a moveable lamina on which the middle-sized profile (MSP) is etched. For two such locations of a lamina, there is a unique point, here called the *invariant point*, that does not displace. For line-profiles, it is the point to

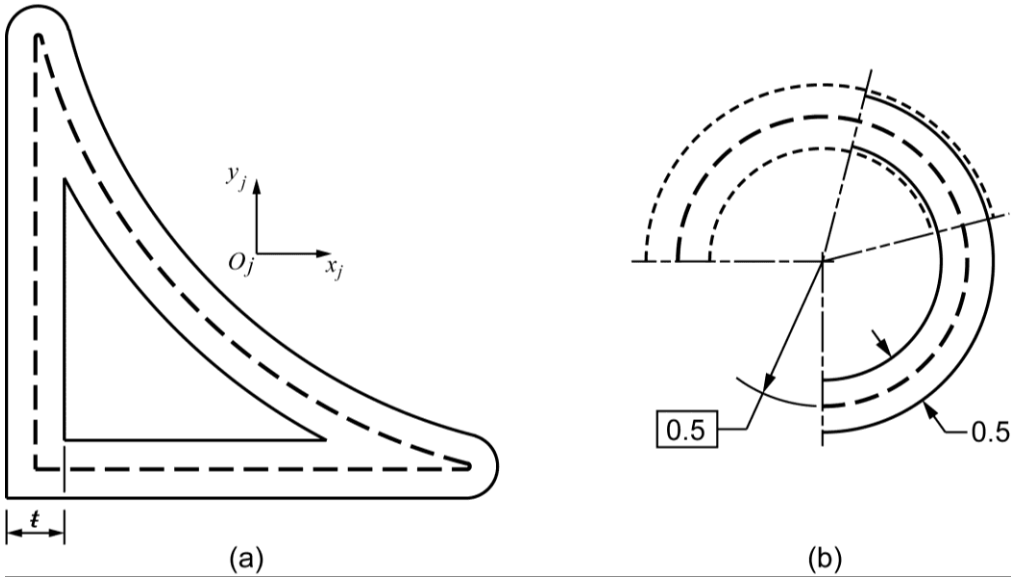

Figure 6.6 (a) Exaggerated tolerance-zone of the line-profile with profile tolerance t = 0.2 mm; (b) Detailed representation of tolerance-zone at the two rounded corners of the line-profile.

which the eccentricities e_x and e_y apply in the associated T-Map. As suggested by Figure 3 and associated comments in [22], the invariant point lies at the mid-point of the line joining the two furthest separated rounded corners of the profile. This was the basis for locating the $O_jx_jy_j$-frame shown in Figure 6.6(a).

6.4. Minimum distance between an envelope and a measured point

Coordinates of a line and envelope equation for an arc segment are developed in §§4.1 and 5.3. As per the least-squares fit method using robotics proposed in §§4.3, the linear actuators are applied inward normal to the envelope tangents at measured points. Consequently, the envelope equation (Eq. 5.29) for a convex arc-segment is used in a way that the unit normals are inward to the line profile. This subsection derives minimum distance between a measured point and an arc-segment that forms concave profile; for example, arc segment with radius of 102.2 mm in Figure 6.5.

As described in §§4.3, the reference envelope is formed such that all the measured points are inside it. For an arc segment of an envelope, which forms concave profile, Eq. 5.29 should be used in sense that the unit normals are pointing outward to the arc-segment. Also, as shown in Figure 6.7, determining the shortest distance between a measured point and arc-segment is now maximization problem (as oppose of minimization problem in §§5.4); i.e. here, farthest distance from the measured point and the arc tangent need to be determined. Hence, for arc segment that forms concavity of the profile, the Eqs. 5.33 modifies to,

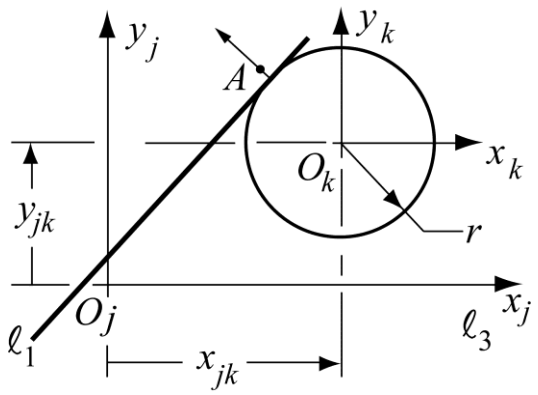

Figure 6.7 The measured point lies outside the arc-segment that forms concave profile. The unit outward normal is used to specify arc-tangent.

$$\left.\begin{aligned} 2\lambda &= -\sqrt{\left(x_j - x_{jk}\right)^2 + \left(y_j - y_{jk}\right)^2}, \\ p_j &= \left(x_{jk} - x_j\right)/2\lambda, \\ q_j &= \left(y_{jk} - y_j\right)/2\lambda, \quad \text{and} \\ d &= -r + \left(x_j - x_{jk}\right)p_j + \left(y_j - y_{jk}\right)q_j, \end{aligned}\right\} \qquad 6.5$$

where the negative sign is used for the square root, for the maximization problem. Also, in sense of outward unit normals, the term r becomes negative.

6.5. An example of least-squares for a concave line profile

As an example, the part specified in Figure 6.5, was manufactured by Austin Pezella, a graduate student in Design Automation Lab. He then measured the coordinates of points on the profile shape with respect to Datums A, B and C. The measured points, middle-sized profile and reference envelope are shown in Figure 6.8. The coordinates of the measured points (shown in Table 6.1) are center of the stylus, of diameter 6 mm, used for measurements. Consequently, the

reference envelope considered here is 3.5 mm (i.e. Δs = 3.5 mm) outside of the theoretical profile to make sure that all the measured points are inside it.

The MSP and the reference envelope are used to form the partition zones for the concave line-profile in Figure 6.5. The measured points are 3 mm (stylus radius) further from the middle-sized profile; hence they lie between the MSP and the reference envelope. Then, the association between each measured point and a profile segment is formed, if the point lies inside the partition zone associated to the segment (§§6.2). In Figure 6.5, five Partition zones are distinguished by thin dotted lines segments (angle bisectors). Moreover, Table 6.1 shows association between the measured points and the partition zones. The shortest distances and

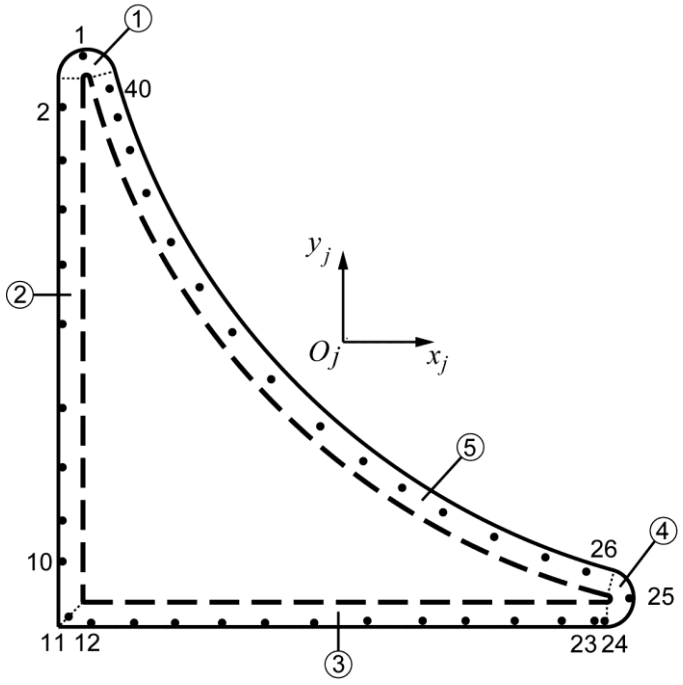

Figure 6.8 The measured point around the sample profile, the reference envelope and middle-sized profile. Angle bisectors in dotted lines are shown to distinguish partition zones (circled numbers).

the line coordinates (shown in Table 6.1) of linear actuators are calculated for each measured point (using Eqs. 5.30, 5.33 and 6.5) to form the matrix equation of least-squares Eq. 4.10. The Moore Penrose solution of [$\boldsymbol{K'}$] produces the least-squares result

$$[\$] = [\delta\theta \;\; \delta x \;\; \delta y \;\; (\Delta s - \Delta F)]^{\mathsf{T}}$$

$$= [0.00147 \;\; -0.33231 \;\; -0.06121 \;\; 2.71490]^{\mathsf{T}}.$$

The solution profile is displaced from its origin O_j by $\delta x = -0.33231$ and $\delta y = -0.06121$. It is rotated by $\delta\theta = 0.00147$ rad = 0.0842º. The size adjustment is $\Delta F = 3.5 - 2.71490 = 0.7851$ mm larger than the middle sized profile. Note that this value puts the least-squares profile well outside the tolerance zone specification in Figure 6.5. It is not known whether the large ΔF value is a result of difficulty in calibrating the milling machine used to make the profile or in calibrating the CMM used to make the measurements.

Table 6.1 Coordinates of measured points around manufactured concave line-profile

Point	Coordinates of measured points		Segment	L'_i	M'_i	R'_i mm	d'_i mm
	x_i mm	y_i mm					
1*	10.046	88.107	1	0.125	-0.992	32.084	0.365
2	6.891	80.664	2	1.000	0.000	-33.164	0.391
3	6.901	72.990	2	1.000	0.000	-25.490	0.401
4	6.915	66.193	2	1.000	0.000	-18.693	0.415
5	6.927	58.261	2	1.000	0.000	-10.761	0.427
6	6.939	49.637	2	1.000	0.000	-2.137	0.439
7	7.000	37.830	2	1.000	0.000	9.670	0.499

8	7.021	29.171	2	1.000	0.000	18.329	0.520
9	7.039	21.492	2	1.000	0.000	26.008	0.538
10	7.064	15.794	2	1.000	0.000	31.706	0.564
11	8.014	7.888	2	0.000	1.000	-39.486	1.388
12	11.053	7.092	3	0.000	1.000	-36.447	0.592
13	17.170	7.098	3	0.000	1.000	-30.330	0.598
14	23.164	7.100	3	0.000	1.000	-24.336	0.600
15	29.755	7.110	3	0.000	1.000	-17.745	0.610
16	35.982	7.121	3	0.000	1.000	-11.518	0.621
17	43.058	7.135	3	0.000	1.000	-4.442	0.635
18	50.669	7.151	3	0.000	1.000	3.169	0.651
19	58.480	7.167	3	0.000	1.000	10.980	0.667
20	64.685	7.208	3	0.000	1.000	17.185	0.708
21	71.596	7.222	3	0.000	1.000	24.096	0.722
22	78.315	7.243	3	0.000	1.000	30.815	0.743
23	83.061	7.294	3	0.000	1.000	35.561	0.794
24	84.394	7.342	3	0.000	1.000	36.894	0.842
25*	88.019	10.640	4	-0.999	-0.040	-38.445	0.478
26	81.975	14.395	5	-0.281	-0.960	-42.395	0.913
27	76.047	16.298	5	-0.341	-0.940	-37.469	0.949
28	68.776	19.228	5	-0.414	-0.911	-31.063	0.979
29	61.446	22.875	5	-0.487	-0.874	-24.169	1.026
30	55.532	26.419	5	-0.546	-0.838	-18.239	1.047
31	50.119	30.174	5	-0.600	-0.800	-12.492	1.074
32	43.988	35.132	5	-0.661	-0.750	-5.545	1.099
33	36.945	41.942	5	-0.732	-0.682	3.128	1.129
34	31.339	48.472	5	-0.788	-0.616	10.722	1.151
35	26.547	55.081	5	-0.835	-0.550	17.851	1.187
36	22.626	61.512	5	-0.874	-0.485	24.321	1.212
37	19.109	68.417	5	-0.909	-0.416	30.833	1.236
38	16.514	74.615	5	-0.935	-0.354	36.328	1.243
39	14.894	79.224	5	-0.951	-0.308	40.222	1.246
40	13.623	83.407	5	-0.964	-0.266	43.625	1.263

6.5.1. Weighted least-squares fit

One aspect of good measurement is to have uniformly distributed measurements i.e. one that 'span' well the profile shape, so that the substitute feature is not influenced by a more dense cluster of measured points [15]. For a profile, as in Figure 6.5, it is possible to have very few measured points on sharply rounded corners, such as the two in Figure 6.5 rounded with radius of 0.5 mm. In this case of measurement, only one point is measured on each corner. Serial numbers of those two points (#1 and #25) are superscripted with * in Table 6.1, and also depicted in Figure 6.8.

As suggested in [15], higher weights assigned to the measurements corresponding the sparser measurements can be used to compensate for non-uniform measurement. For experiment to know influence of the weight, we applied doubled the weight for the measured points at each of these two corners. In other words, now we have total 42 measured points (as compared to 40 measurements in previous case) with the measurements #1 and #25 each repeated once. Following the same procedure as earlier, the least-squares solution is,

$$[\$] = [\delta\theta \;\; \delta x \;\; \delta y \;\; (\Delta s - \Delta F)]^{T}$$

$$= [0.00172 \;\; -0.31421 \;\; -0.04154 \;\; 2.74019]^{T}.$$

Based on the location and direction of the linear actuators at the points, the results of location and orientation of the least-squares profile are influenced. Appropriate application of weight can help to reduce effect of non-uniform measurements.

CHAPTER 7

CONCLUSION

The method described in this thesis is an alternative to the one proposed in [18]: both techniques provide a rigid body transformation that locates a set of points that have been measured on a profile relative to a specified tolerance-zone. In [18] a minimum-zone capture of the points is computed, whereas here the least-squares fit of the points is utilized. However, in this paper another variable is added to the computed results, the size of the profile, so identifying a corresponding point (*i*-Map) within the T-Map as shown in Figure 4.7. Although the least-squares fit is just one of several possible fits to measured points, it is an important one because it recognizes (a) the inter-penetration of mating surfaces (asperities), which violate computed minimum-zone boundaries, and (b) the potential existence of other points further from the intended feature than any of the measured ones. Any one such point could noticeably change a computed minimum zone, but it would have little effect on a least-squares computation based on a large number of measured points. And, of course, a minimum-zone may be constructed from the least-squares solution by forming parallel inner and outer boundaries to it to just capture all the points.

The results of this thesis show that the T-Maps model may have broader application than modeling tolerances for analyses required in design. There also is potential for exploiting its inherent geometry in the setting of manufacturing. For instance, with appropriate transformation of the data, inspection information from one or more manufactured parts could be represented geometrically as an

inspection-Map (*i*-Map) within the T-Map. The measurements from one profile yields one *i*-Map point in the 4-D space of the T-Map, but a sequence of *i*-Map points, produced from measurements on a succession of parts, would yield a path of points internal to the T-Map. The relationship of this *i*-Map to the designer's intent could be represented visually as one object within another, and the position and trend of the *i*-Map path could potentially provide suggestions for changes in manufacturing machine settings. And, since all such geometric relationships in a higher dimensional geometry may be expressed in several 2-D sections or 3-D visualizations on a computer screen, a machine operator would never need to encounter higher dimensional geometry at all.

7.1. Future work

The methods proposed in this thesis for finding the least-squares line-profile from an array of measured points around it apply to *any* line-profile. It may be formed from a combination of line-segments, circular arc-segments, and/or free-form segments. It may contain C^1- and C^2-discontinuities. The profile also may contain double tangents, i.e. have one or more concavities, such as with most turbomachine blades. However, there are two other aspects of this thesis which, at this time, limit the *i*-Map method. First, methods for constructing the T-Maps (design specifications) for line-profiles are not general, and they do not yet include free-form shapes.

REFERENCES

[1] American National Standard ASME Y14.5M. (2009). *Dimensioning and Tolerancing*, The American Society of Mechanical Engineers, NY.

[2] American National Standard ASME Y14.5M. (1994). *Dimensioning and Tolerancing*, The American Society of Mechanical Engineers, NY.

[3] Mani N, Shah JJ, Davidson JK. *Standardization of CMM fitting algorithms and development of inspection maps for use in statistical process control*. ASME 2011 International Manufacturing Science and Engineering Conference, Volume 2, Corvallis, Oregon, USA, June 13–17, 2011. Paper #MSEC2011-50152.

[4] International Organization for Standardization ISO 1660. (1987). *Technical drawings—Dimensioning and toleran-cing of profiles*.

[5] Hopp, TH. Computational Metrology, *ASME Manufacturing Review*, December 1993.

[6] Nassef AO, ElMaraghy HA. Determination of Best Objective Function for Evaluating Geometric Deviations, *International Journal of Advanced Manufacturing Technology* 1999;**15**:90-95.

[7] Srinivasan, V. Computational metrology for the design and manufacture of product geometry: A classification and synthesis, *Journal of Computing and Information Science In Engineering* 2007;**7 (1)**: 3-9.

[8] Shakarji CM, Clement A. *Reference Algorithms for Chebyshev and One-sided Data Fitting for Coordinate Metrology*. CIRP Annals-Manufacturing Technology 2004;**53 (1)**;pp 439-442.

[9] Rodger G., Flack D., and McCarthy M. (2007), *A review of industrial capabilities to measure free-form surfaces*, NPL Report DEPC-EM 014.

[10] Murthy TSR, Abdin SZ. Minimum zone evaluation of surfaces, *International Journal of Machine Tool Design and Research*, 1979;**20**:123-136.

[11] Carr K, Ferreira P. Verification of form tolerances part I: Basic issues, flatness, and straightness. *Precision Engineering* 1995;**17**: 131-43.

[12] Carr K, Ferreira P. Verification of form tolerances part II: Cylindricity and straightness of a median line. *Precision Engineering* 1995;**17**: 144-56.

[13] Madsen K., Nielsen NB, and Tingleff O.. "Methods for nonlinear least squares problems." *Technical Report*. Informatics and Mathematical Modeling, Technical University of Denmark, 2004.

[14] Barari A, ElMaraghy HA, Knopf GK. Evaluation of Geometric Deviations in Sculptured Surfaces Using Probability Density Estimation. In *Models for Computer-Aided Tolerancing in Design and Manufacturing* (ed. J. K. Davidson), (Proc., 9th CIRP Int'l Seminar on CAT, April 10-12, 2005, Tempe, AZ, USA). Springer, Dordrecht, Netherlands;2007:45-54.

[15] Shakarji CM, Srinivasan V, (2012). *Fitting weighted total least-squares planes and parallel planes to support tolerancing Standards*. CD-Rom Proceedings of the 32nd ASME Computer and Information in Engineering Conf. Chicago, IL, August 12-15.

[16] Polini W, Prisco U, Giorleo G. A new Algorithm to Assess Revolute Surface through Theory of Surface Continuous Symmetry. In *Models for Computer-Aided Tolerancing in Design and Manufacturing* (ed. J. K. Davidson), (Proc., 9th CIRP Int'l Seminar on CAT, April 10-12, 2005, Tempe, AZ, USA). Springer, Dordrecht, Netherlands;2007:157-166.

[17] Choi W, Kurfess TR. Dimensional measurement data analysis, part 1: A zone fitting algorithm. *J Manuf Sci Eng* 1999;**121**:238-45.

[18] Choi W, Kurfess TR. Dimensional measurement data analysis, part 2: Minimum zone evaluation. *J. Manuf. Sci. Eng* 1999;**121**:246-50.

[19] Lipman Y, Cohen-Or D and Levin D. Error bounds and optimal neighborhoods for MSL approximation. *Proceedings of the 4th Eurographics symposium on Geometry processing* 2006;71-80.

[20] Lipman Y, Levin D. Approximating piecewise-smooth functions, *IMA Journal of Numerical Analysis* 2010;**30**:1159-1183.

[21] Davidson J.K, Shah J.J. (2002). Goemtric tolerances: a new application for line geometry and screws. *IMechE J. of Mechanical Eng. Science, Part C*;**216**:95-104.

[22] Davidson J.K. and Shah J.J. Modeling of geometric variations for line-profiles, *Journal of Computing and Information Science In Engineering* 2012;**12 (4)**: 10 pp.

[23] Davidson, J.K., Savaliya, S.B. and Shah, J.J., (2012). Least-squares fit of measured points for square line-profiles., In *CDRom Proc., 12th CIRP Conference on Computer Aided Tolerancing*, Univ. of Huddersfield, Huddersfield, UK, April 18-19, 10 pp.

[24] Davidson, J.K., Savaliya, S.B., He, Y., and Shah, J.J., (2012). *Methods of robotics and the pseudoinverse to obtain the least-squares fit of measured points on line-profiles*. CD-Rom Proceedings of the 17th ASME Design for Mfg. and the Life Cycle Conf. Chicago, IL, August 12-15.

[25] Choi SC. *Introductory applied statistics in science*, Prentice-Hall, Englewood Cliffs, NJ 1978, p. 23-35.

[26] Ben-Israel A, Greville TNE. *Generelized inverse: Theory and application 2nd edition*, Springer, New York, 2003.

[27] Coxeter HSM. *Introduction to geometry*. 2nd ed. Wiley Classic Library; 1969.

[28] Davidson JK, Hunt KH, *Robots and screw theory. Application of kinematics and statics to robotics.* Oxford University Press, Oxford, 2004.

[29] Hunt, K.H. (1979). Kinematic geometry of mechanisms. Clarendon Press, Oxford. Reprinted with corrections in 1990.

[30] Hain, K. (1967). *Applied kinematics*. 2nd ed. McGraw-Hill.

[31] McCarthy, J.M. (1990). *An introduction to theoretical kinematics*, MIT Press, Cambridge, MA.

[32] NIST Algorithm testing data. http://www.nist.gov/pml/div683/grp01/cst-algorithmtesting.cfm

[33] Farin G. (2002). *Curves and surfaces for CAGD*, Morgan-Kaufmann.

[34] Shirley P., Morley R. K. (2003), *Realistic Ray Tracing,* 2nd ed., A K Peters.

[35] D. Eberly, Intersection of linear and circular components in 2D, http://www.magicsoftware.com/ , 2000